Impact Damage Resistance of Shape Memory Alloy Hybrid Composite Structures

Hongyu Jia

Dissertation submitted to the Faculty of the
Virginia Polytechnic Institute and State University
In partial fulfillment of the requirements for the degree of

Doctor of Philosophy
in
Mechanical Engineering

Dr. D. J. Inman and Dr. C. A. Rogers
(Chairs)

Dr. R. G. Kirk
Dr. J. R. Mahan
Dr. K. L. Reifsnider
Dr. H. H. Robertshaw

May 26, 1998
Blacksburg, VA
Key words: Shape Memory Alloy, Composites, Impact, Damage, Super-elastic.

Impact Damage Resistance of Shape Memory Alloy Hybrid Composite Structures

Hongyu Jia

(ABSTRACT)

The strain energy absorption of shape memory alloy (SMA) bars and beams under tension and bending loading was studied. A theoretical model is presented that can give quantitative relations between the martensite fraction, the applied load, and the strain energy absorbed in the shape memory alloy (SMA). It was found analytically that the super-elastic SMA demonstrates a high strain energy absorption capability. The closed-form solution of the strain energy absorption capability of SMA bars is a simple and useful tool in the design of energy absorption applications of super-elastic SMA.

The nonlinear equations for SMA hybrid composite plates, which can be used for low velocity impact or quasi-static contact loading, are derived. The governing equations include the transverse shear deformation to the first-order, large deformation of the plates, and SMA/epoxy lamina. The equations are derived in the general form with general boundary conditions and general stack of angle ply. The equations can be simplified to special forms in the specific applications.

A theoretical study of the impact force and the strain energy absorption of an SMA/graphite/epoxy composite beam under a low-velocity impact has been performed. The contact deformation, the global bending deformation, the transverse shear deformation, and the martensitic phase transformation of the super-elastic SMA fibers are studied. The energy absorbed by the SMA hybrid composite is calculated for each task of the absorption mechanisms: contact deformation, global bending deformation, and

transverse shear deformation. The basic relationship between the energy absorption mechanisms and the extent of martensitic phase transformation is obtained.

A nonlinear beam model and a new failure analysis method are developed to predict the load-deflection characteristics of a Graphite/Bismaleimide composite beam under quasi-static loading by a steel cylinder. The model considers the large deflection of the beam, contact deformation of the beam, stiffness degradation due to the matrix cracks, delamination, and fiber breakage. The model captures the characteristics of an SMA composite beam with strong nonlinearity in geometry and materials. The model also simulates the stress/strain induced martensite phase transformation during this failure process.

The analysis methods and models developed in this dissertation are the first reported research in modeling SMA composite under low velocity impact and quasi-static loading. The models and methods developed here can be used for further study and design of SMA composites for low velocity impact or quasi-static loading in failure process.

ACKNOWLEDGEMENTS

I would like to express my gratitude to all the people who have been supportive of my endeavor towards my Ph.D. study.

I would like to thank my advisor, Dr. Craig A. Rogers, for giving me the opportunity to pursue my Ph.D. degree in this novel area at Virginia Tech. Thank you for your support, encouragement and guidance throughout my study.

I would like to thank my advisor, Dr. Daniel J. Inman for taking me as his student and guiding me through my study. I would like to express my thanks to you, for taking time away from your busy schedules to advise me.

I would like to thank Dr. R. Gordon Kirk, for taking time away from his busy schedules to serve on my committee. Thank you for your support and encouragement.

I would like to thank Dr. Robert J. Mahan, especially for his support during my difficult time. Your help encouraged me to continue to make progress in my study. I owe you my sincere thanks for all the help that you gave me.

I would like to thank Dr. Kenneth L. Reifsnider, for his productive suggestions and taking time away from his busy schedules to serve on my committee. Thank you for enlightening me with your knowledge.

I would like to thank Dr. Harry H. Robertshaw, for taking time away from his busy schedules to serve on my committee.

I also wish to thank many the people at CIMSS. I thank Dr. Fred Lalande for his help and management in this project when he was at CIMSS. I thank Dr. Victor Giurgiutiu for his interesting in this research and discussion.

I also wish to thank Beth, Fanping, Claire and the administrative staff at CIMSS for their help and providing a pleasant study and work environment at CIMSS.

My thanks also go to all the professors who supervised me or taught me at Virginia Tech and at University of Central Florida. Thank them for giving me the high quality education.

I also thank the Army Research Office (ARO) for their providing the funding for this research (ARO-URI Grant No. DAAL03-92-G-0180).

The support of my family has been encouraging me to pursue my Ph.D. study. Without their support I could not have achieved thus far. To my parents I thank them for their supporting me for so many years. I wish to make both of them proud. I thank my wife for her support, understanding and love. You have been a constant source of strength throughout my study whenever I need.

TABLE OF CONTENTS

NOMENCLATURE

σ_o	Stress at which martensitic transformation starts.
ε_o	Strain at which martensitic transformation starts.
E_1	Young's modulus of SMA in austenitic region.
E_2	Young's modulus of SMA in martensitic region.
h_e	Thickness of austenitite core of SMA beam.
U	Strain energy.
M_s	Martensite start temperature.
M_f	Martensite finish temperature.
A_s	Austenite start temperature.
A_f	Austenite finish temperature.
u_1, u_2, u_3	Displacements of the structures in x, y, z direction, respectively.
u, v, w	Displacements of the mid-plane in *x*, *y* and *z* direction, respectively.
ϕ_x, ϕ_y	Shear deformations in x-z and y-z planes, respectively.
E_{c11}	Module of SMA/epoxy lamina in 1 direction.
E_{c22}	Module of SMA/epoxy lamina in 2 direction.
E_{c33}	Module of SMA/epoxy lamina in 3 direction.
G_{c12}	Shear module of SMA/epoxy lamina in 1-2 plane.
G_{c13}	Shear module of SMA/epoxy lamina in 1-3 plane.
G_{c23}	Shear module of SMA/epoxy lamina in 2-3 plane.
ν_{c12}, ν_{c13}, ν_{c23}	Poisson's ratio of SMA/epoxy lamina in 1-2, 1-3, 2-3 planes, respectively.
k_{SMA}	SMA fiber volume fraction in the SMA/epoxy lamina.
E_m	Young's modulus of epoxy matrix in the SMA/epoxy lamina.
G_m	Shear modulus of epoxy matrix in the SMA/epoxy lamina.

ν_m	Poisson's ratio of epoxy matrix in the SMA/epoxy lamina.
k_m	Volume fraction of epoxy matrix in the SMA/epoxy lamina.
N_i	In-plane resultant forces.
M_1, M_2	Moments due to bending.
M_6	Moment due to twisting.
Q_i	Transverse shear forces.
$[A]$, $[B]$, $[D]$	Stiffness matrices.
Π	Total potential energy of composite laminate.
R	local radius of steel cylinder impactor.
υ_s	Poisson's ratio of steel cylinder impactor.
E_s	Young's modulus of steel cylinder impactor.
E_{yy}	Modulus of the impacted composite ply in the direction transverse to fibers.

LIST OF TABLES

LIST OF FIGURES

Chapter One

Introduction and Literature Review

1.1 Introduction

Composite materials are used extensively in aerospace and other industries. With high specific modulus, high specific strength, and the capability to be designed and fabricated with greater flexibility, composite materials have advantages compared to traditional materials. However, It is well known that fiber-reinforced polymeric composites are vulnerable to transverse loads such as low-velocity impact, which can result in extensive delaminations and multiple matrix cracking. Such internal damage can cause significant reduction of the load-carrying capacity of composite structures.

Although composite materials have become increasingly popular in a variety of applications, they are still cautiously used in areas where they are subjected to transverse loads such as low-velocity impact. Indeed, one of graphite/epoxy's main weaknesses is its poor resistance to impact damage due to the lack of plastic deformation mechanisms for absorbing impact energy. First, graphite has a high modulus, a high strength, and a low strain to failure or, in other words, the graphite fibers are brittle. Second, the epoxy is also brittle after curing due to the crosslinks in the matrix. These brittle properties make the graphite/epoxy very susceptible to impact, even at very low velocities. Impact damage will significantly reduce the integrity of the structure, affecting the performance and life of the composite structures.

Many researchers have been studying these topics in order to understand the damage mechanism, improve the impact damage resistance and load-carrying capacity of composite structures. Extensive experimental studies as well as modeling and analysis have been conducted in these areas.

1.2 Review of Impact on Composites

1.2.1 Impact force, and Response of Composite Structures

Due to the significance of the problem, extensive experimental investigation has been conducted on determining the impact force and response of composite structures. The impact force and deflection of the composite beam or plates are studied experimentally. The impact force or contact force was measured by including a force transducer in the impactor, by using an accelerometer mounted on the impactor or by measuring the target response using strain gauges. Experimental modal analysis by Tracy, et al. [1] in 1985 showed that low-velocity impact damage has only minor effects on the dynamic properties of laminated plates. This study confirms that the effect of damage can be neglected when modeling the low-velocity impact dynamics at low impact energy level.

In low-velocity impact with low impact energy level, composite structures are usually assumed to have no damage. Contact and global deformations are dominant. Quasi-static or dynamic (impulse) approach, contact mechanics and structural mechanics can be applied to these problems. Analytical and finite element method solutions can be obtained.

Modeling the impact on thin composite structures involves contact modeling of the impactor on the composite structures. The contact deformation, defined as the difference between the displacement of the impactor and that of the back face of the composite laminate, can be of the same order or larger than the displacement of the composite laminate [2]. The relationship between the contact deformation and the contact force is generally modeled by using Hertz contact laws or modified Hertz contact laws. One of the popular modified Hertz contact laws was proposed by Sun and Chattopadhyay [3] in 1975, which is for contact between a rigid sphere or cylinder and a composite laminate. Exact elasticity solutions for the contact of general composite laminates are not available. Thus, contact laws used in the modeling are Hertz law and modified Hertz laws. The Hertz law considers only the contact deformation for

composite plates supported at the outer boundary, thus, it overestimates the impact force. The modified Hertz law includes the flexural displacement of composite plate in addition to contact deformation, it gives the closer prediction of the impact force.

To understand the impact on composite structures, researchers first focused on modeling the impact responses of the composite structures to the impactor, without any damage. There are three methods to model these problems.

Spring-Mass Models

Dropweight impact on composite plates can be modeled as one or two degrees of freedom system [4]. The spring constant K represents the stiffness of the composite plate at the impact point. They obtained very good results compared to experimental data. Because the mass of the plate is negligible compared to that of the impactor and the contact time is relatively long, dynamic effects of the plate can be neglected. It was shown that the simple models are accurate enough when the mass of the composite beam is small compared to that of the impactor. Sjoblom, et al. [5] in 1988 used a two degrees of freedom model, with one spring constant representing the stiffness of the composite plate and the other nonlinear spring for the contact stiffness between the composite plate and the impactor.

Energy-Balance Models

These models are useful in the cases that the maximum contact force and the contact duration are of the main interest. The maximum contact force and contact duration can be determined more efficiently by using energy-balance models. The kinetic energy of the impactor is stored in the composite beam as the strain energy, such as, strain energy in bending, strain energy due to the contact. Thus, the maximum contact force can be determined from the energy balance equation [6].

Assumed Force Models

In order to study the dynamic response of the composite structures to the impact, researchers assumed certain kinds of the contact force and the form of its distribution over

the contact area. These assumptions are useful and efficient for studying the overall dynamic response of the composite structures under the impact. However, these models are not accurate enough to do the damage analysis based on these assumptions. The linear composite plate theories are usually used in modeling the impact responses of rectangular, circular and cantilever composite plates under low velocity impact.

1.2.2 Impact Damage of Composite Structures

Since the early 1980's many researchers were conducting research on characterizing the damage pattern and modes of composite structures under transverse load, such as low-velocity impact. The experiments were carried out using dropweight test, cylinder indentation, etc.

When conventional structural materials such as steel and aluminum under low-velocity impact are used, the energy is typically absorbed through elastic and plastic deformation. Although this deformation is permanent, it usually does not significantly reduce the load carrying capability of the structures.

Graphite composites have very little or no plastic deformation during low-velocity impact because of its low strain to failure of the fiber and brittleness of the epoxy matrix. Therefore, the impact energy is absorbed through various fracture processes. It is well known that composites dissipate impact energy through matrix cracking, delamination, and fiber breakage. This results in several possible ways to improve the damage tolerance of composites.

The extent of damage imposed by low-velocity impact may be affected by the geometry and laminate configuration of the composite structures. In most cases, particularly with low-velocity impact, the damage is internal and difficult to detect by visual inspection.

Damage Pattern

Due to the complicated phenomenon and the difficulty in modeling, most of the research in the impact damage on composite structures is experimental. Usually, the experiments are conducted using a dropweight tester, in which the projectile is large and its velocity is low, or a gas gun system with a small mass that is propelled at a higher velocity. It is generally agreed that low velocity impact results in global deformations, whereas with higher velocity, the deformation is confined within local region surrounding the impact point. Damage observed during low velocity impact was similar to that induced during quasi-static tests. The damage induced by low-velocity impact is usually believed to be matrix cracking, delamination, and fiber breakage.

Many studies were directed towards understanding damage patterns and determining the damage development sequence. The impact-induced damage, mainly the matrix cracking and delamination, were not generally understood until in late 1980's [7]. The damage zone is now recognized as "peanut-shaped" with its major axis oriented in the direction of fiber orientation of the lower ply for that interface.

Material Properties Effect

Elber [8] in 1985 indicated that matrix properties govern the damage initiation and determine the extent of impact damage. Fiber properties, on the other hand, control the penetration resistance.

a) Effect of Matrix:

It is generally recognized that an increase in strain to failure of the matrix will result in improved residual strength of the composite after impact, due to the better resistance to delamination and matrix cracking.

b) Effect of Fiber:

Higher fiber failure strains, with the same elastic modulus, will result in higher energy absorption, especially since the strain energy absorbed by the matrix represents a

large portion of the total strain energy. For the same impact energy, higher capability to absorb energy results in less fiber breakage and a higher residual tensile strength.

A comprehensive treatment and review of dynamic properties, damage detection and characterization, damage tolerance of fiber-reinforced composites are given by Sierakowski and Chaturvedi in their book "Dynamic Loading and Characterization of Fiber-Reinforced Composites" [9].

Modeling

In low-velocity impact, composite structures have damage but no complete failure or penetration. Quasi-static or dynamic approach, failure criteria and fracture mechanics can be applied. Analytical and finite element methods have been developed for analyzing the damage initiation, matrix cracking, delamination, and fiber breakage. Recently, a large amount of work has been reported in this area. However, these methods are still under developing since the failure modes and damage are very complicated and have not been fully understood yet. Most of the work simplifies the process by considering only the most important factors.

Damage development in a composite laminate under impact is complex, since several failure modes are present, and they usually interact with each other. Impact damage usually follows some very complex distributions, and it may not be possible to reconstruct the entire sequence of events leading to a given damage state. Also, it not enough to only use fracture mechanics approach or failure criteria to predict the damage development during the impact. For predicting the damage initiation (first matrix crack), the approach includes the determination of impact force, and stresses, applying the suitable failure criterion. Although it is complex, it still can be attacked by using composite plate or beam theory, contact mechanics, failure theory of composites, fracture mechanics, etc., since the composite structures still have their integrated shape. The impact damage initiates from matrix cracks that induce interface delaminations. A

significant effort was directed toward developing methods for accurately determining the stress distribution in the contact zone and for developing failure criteria for predicting matrix cracking and delaminations. These problems were not solved until the early 1990's. An exact solution was obtained by Matsumoto, et al. [10] in 1992 for the static stress distribution in rectangular simply supported plates subjected to uniform pressure distributed over a small rectangular patch.

Modeling of this induced damage was conducted in early 1990's by Chang and his co-workers [11-13]. Modeling of the damage area induced by the low-velocity impact was focused on determining the impact load for initializing the damage on the composite and relationship between the load and damage area has been established [11, 12]. It was shown that failure was initiated by matrix cracking that was then followed by delaminations starting from the crack tips. Hashin's failure criterion was used by Chang to predict matrix cracks [13]. Some empirical relations of in-plane shear strength were also proposed in order to solve the equations. Some assumptions are made that the damaged element cannot sustain any transverse tensile stress and out of plane shear stress. Delaminations are initiated in the form of mode I cracks and lead to further cracks.

While predicting the damage initiation is important, the final state of damage is what is needed to estimate the residual properties of the composite. A detailed prediction of the damage state is not possible, since the delamination is the major cause of the strength reduction, particularly under compression. So it is important to predict the size of the delaminataion. Sun and Jih [14] in 1992 showed that the strain energy release rate computed from static and dynamic analysis was in good agreement with experiment.

1.2.3 Complete Failure, and Penetration of Composite Structures

Characterization of Failure Pattern

Since the middle of 1980's the damage characteristics of the composite structures under the transverse load (dynamic penetration or quasi-static punch through) by blunt,

hemisphere, or cylinder objects were studied [15-17]). Most of the research in penetration of the composite structures was experimental. A few experimental studies have measured the residual velocity of various laminates under a range of striking velocities [18-20].

For the impact resulting in complete penetration of the laminate composite, the damage induced by penetration impact is very localized around the impact point. The energy losses during penetration are strongly affected by the shape of projectile since the failure modes can be significantly different. It is believed that the global deformation of the laminates and the size of delamination are very small, local deformation and fiber failure constituted the major energy absorption mechanism. It is generally accepted that fiber failure, matrix cracking, delamination and friction between the projectile and the target are the major failure modes during impact process.

Another important kind of experiment is the composite beam or plate under cylinder or line impact load or quasi-static punch. Due to the characteristics of two-dimensional problems, it is very useful to determine the failure mechanism of composite structures under low velocity impact or quasi-static load resulting in the complete failure.

Modeling

The impact or quasi-static loading energy may be so large that it results in the complete punch through or penetration of composite structures. Modeling and analysis of complete failure or penetration of composite structure remains a great challenge to researchers [21]. Very few reports in this area have been found in the literature. Due to the geometric discontinuity, highly geometric and material nonlinearities of the composite structures in the complete failure or penetration process, it is very difficult to apply conventional plate or beam theories and the corresponding numerical methods. Also, the failure process of composite structures is problem-dependent. It varies with different shape and materials of impactors as well as the composite structures. Thus, researchers

focus on developing the phenomenological models and the semi-analytical models by making appropriate assumptions based on the experimental observation [21-23]. Zhu, et al. [18] in 1992 proposed a phenomenological model for Kevlar-29-polyester laminates penetrated by a conical faced projectile which used a finite-difference scheme to capture the assumed local and global deformation modes of the composite plate during penetration. Lee and Sun [24] in 1993 proposed a model based on the static punch curve to characterize the penetration process of graphite-epoxy laminates. This model was then used to predict the energy needed to completely fail the composite laminates and compared with results from dynamic impact tests. Greif, et al. [25] in 1993 studied the successive failure modes in graphite epoxy beams. Kim, et al. [26] in 1996 proposed a model for predicting the behavior of composite beam under the line loading resulting the complete failure.

The modeling and analysis of complete failure or penetration of composite structures is at its beginning, and many aspects of this process have not been understood yet. Analysis of the geometric discontinuity, very large deflection of the composite structures with contact deformation, and material degradation of composite structures during this process is still the challenging task to researchers since there is no general theory available to handle such kind of problem. Phenomenological models, empirical relations and the semi-analytical models are proposed to attack these geometric and material nonlinear problems [18], [21-23]. A comprehensive review of the research in the area of impact on composite materials was given by Abrate [21], [27].

1.2.4 Improving Damage Resistance of Composite Structures

There is an increasing demand in the aerospace and other industries for high-performance composite structures with high strength, high modulus, low weight, and good damage resistance properties. While investigating the damage patterns and mechanisms of

graphite/epoxy composites, researchers started to look for various methods to improve the damage resistance of composite structures.

Toughening the Composite Structures

The load carrying capacity of Graphite/Epoxy composite structures is limited by its low strain to failure, or its low energy absorption capability. Toughened matrix composite structures have better flexibility, toughness, and energy absorption capability. To improve the damage resistance of composite structures requires improvement of the toughness of the composite structures. In order to keep the high load-carrying properties while improving the toughness of composite structures, many approaches have been proposed: fiber and matrix toughening, interface toughening, through-the-thickness reinforcements, and hybridizing.

Fiber toughening is the use of graphite fibers developed with a higher strain to failure. The impact resistance of the composite made from this kind of fiber has been reported with moderate success [28].

Several different approaches have been taken to make the matrix material tougher. Although the stiffness of the composite is slightly reduced, its toughness is improved. One of the ways to do this is by addition of rubber or thermoplastics. Replacing thermoset epoxy with the thermoplastic matrix Polyetheretherketone (PEEK) produces a higher resistance to impact. Instead of conventional thermoset matrices, high performance thermoplastic matrices, such as PEEK and related molecules, and the thermoplastic polyimides have been introduced. These thermoplastic matrices have significantly better toughness than those of thermoset matrices. More and more new materials for composites are being developed. These new materials offer more options for design engineers.

Impact-induced delamination occurs to graphite composites at relatively low interlaminar strength, so interface toughening by use of adhesive layers results in better damage resistance. Matrix cracking and delamination can significantly reduce the load

carrying capacity of the composite structures by as much as 50 % [29]. Increasing the matrix toughness will reduce matrix cracking and delamination. Therefore, it is among the most important improvements in damage resistance of composite structures.

Another effective way to reduce the amount of delamination caused by low-velocity impact is with through-the-thickness reinforcements, such as braiding, three dimensional weaving, and stitching. Although significant delamination reductions are achieved, these techniques are costly and degrade the in-plane properties due to fiber impalement.

Hybridizing graphite composites with additional tough high strain-to-failure fibers gives better damage resistance of composite structures [30,31]. Fibers used in hybridizing include: S-Glass, aramid, known as Kevlar, and Spectra.

SMA Hybrid Composites

One of the ways to make hybrid composites is to embed super-elastic shape memory alloy fibers in composites. Super-elastic shape memory alloy has a remarkably high strain-to-failure. This super-elastic alloy has a recoverable elastic strain up to 8%. The high strain capability of SMA fibers is primarily due to a stress-induced martensitic phase transformation creating a plateau region in the stress-strain curve. This property enables super-elastic shape memory alloy fibers to absorb much more strain energy than other fibers before their failure. Thus, embedding super-elastic shape memory alloy fibers in the composites could make the composites tougher and increase the damage impact resistance of composite structures.

Toughening composites by embedding super-elastic nickel titanium alloy fibers known as shape memory alloy was investigated experimentally at Center for Intelligent Material Systems and Structures in the Mechanical Engineering Department, Virginia Tech [32-35]. The super-elastic SMA hybrid composite specimens have been tested for damage resistance. It has been demonstrated experimentally that the addition of small amounts of super-elastic SMA fibers to graphite composites can improve its low-velocity

impact damage resistance. From the experimental results of low-velocity impact and quasi-static punch, we can see that super-elastic SMA fiber is a promising material for improving the damage resistance of composite materials.

1.2.5 The Need for Analysis of Damage in SMA Composites

The previous research on impact of SMA hybrid composites was largely experimental. The strain energy absorption of super-elastic SMA and the enhanced performance of SMA hybrid-toughened composites for damage resistance have not yet been understood. In order to utilize the super-elastic SMA's strain energy absorption capability in SMA hybrid composites and understand the mechanical behavior of SMA hybrid composites during the failure process, we need to develop models for analysis of this process. Therefore, this research focuses on the modeling efforts, and studying the strain energy absorption of super-elastic SMA, SMA hybrid composites, and the failure process of SMA hybrid composites. To the best of our knowledge, the experimental research as well as the analysis and modeling of super-elastic SMA, SMA hybrid composites for strain energy absorption and failure process of SMA hybrid composites at CIMSS are the only reported research in this area.

In order to perform the analysis on SMA composites, we need to understand the constitutive relations of SMA and incorporate appropriate constitutive equations of SMA in the SMA composites. Therefore, a review of constitutive relations of SMA is given in the following section.

1.3 Review of Shape Memory Alloys and Their Constitutive Equations

1.3.1 Shape Memory Alloys

Since the discovery of the shape memory effect in 1932, increasing attention has been brought to this material, particularly in 1962 when Nitinol was developed [36]. The principal characteristic of shape memory alloys (SMAs) is the ability to "memorize"

their original configuration after they have been deformed by heating the SMA above the characteristic transition temperatures. This phenomenon is caused by a phase transformation of the SMA microstructure from martensite to austenite when the transition temperature is reached. A typical relation between temperature and martensite phase concentration is shown in Fig. 1.1, where the four transition temperatures: M_f (martensite finish), M_s (martensite start), A_f (austenite finish), and A_s (austenite start), are represented. The recoverable strain resulting from this phase transformation can reach as much as 8%.

These unique properties allow SMA to be used in many innovative engineering applications such as couplings [37,38] and actuators [39]. SMA has also been used in hybrid composites in a variety of applications [40].

In order to fully utilize the potential of SMAs in engineering applications, it is necessary to have a comprehensive understanding of SMA mechanical behavior. However, the stress-strain relationship of SMA is not as simple as for common materials, as can be seen in the typical stress-strain curve for a SMA (Fig. 1.2). Indeed, the phase transformation of the SMA will have a significant variation in its material properties at working temperatures and will not behave like other engineering materials. Therefore, the constitutive models relating the stress and strain of common materials cannot be applied to SMA.

As mentioned earlier, a good understanding of the mechanical behavior of SMA is essential for the development of further applications, and thus an accurate constitutive model for SMA is necessary. Various approaches have been taken by researchers thus far to develop constitutive models: macroscopic, microscopic, and mixed. In the macroscopic approach, the constitutive model describes the material behavior based on experimental data. For the microscopic approach, the constitutive model attempts to predict and describe the material behavior based on fundamental physical concepts, such as the micro-

structure of the crystal lattice. Finally, the mixed approach uses both microscopic and macroscopic concepts for better modeling.

In this section, a review of the constitutive modeling of shape memory alloy research will be presented. The various models proposed by many researchers have been classified into five different types of models: ferroelectrics models, internal variable models, plasticity models, hysteresis models, and non-isothermal models. The goal of this review is to shed some light on the current status of this research area by reporting what constitutive models are available, and the differences between the models.

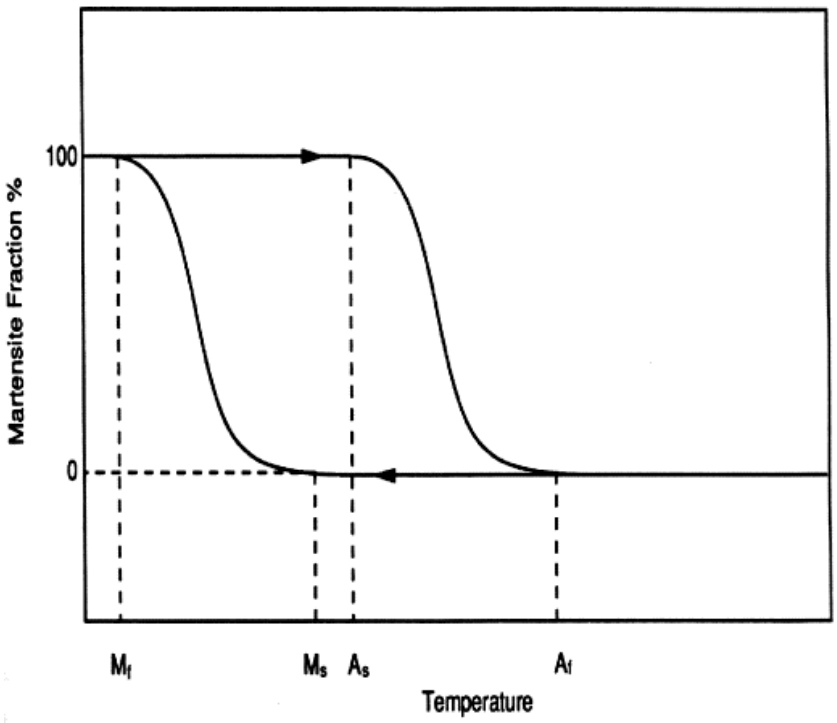

Figure 1.1 The phase transformation with temperature [41].

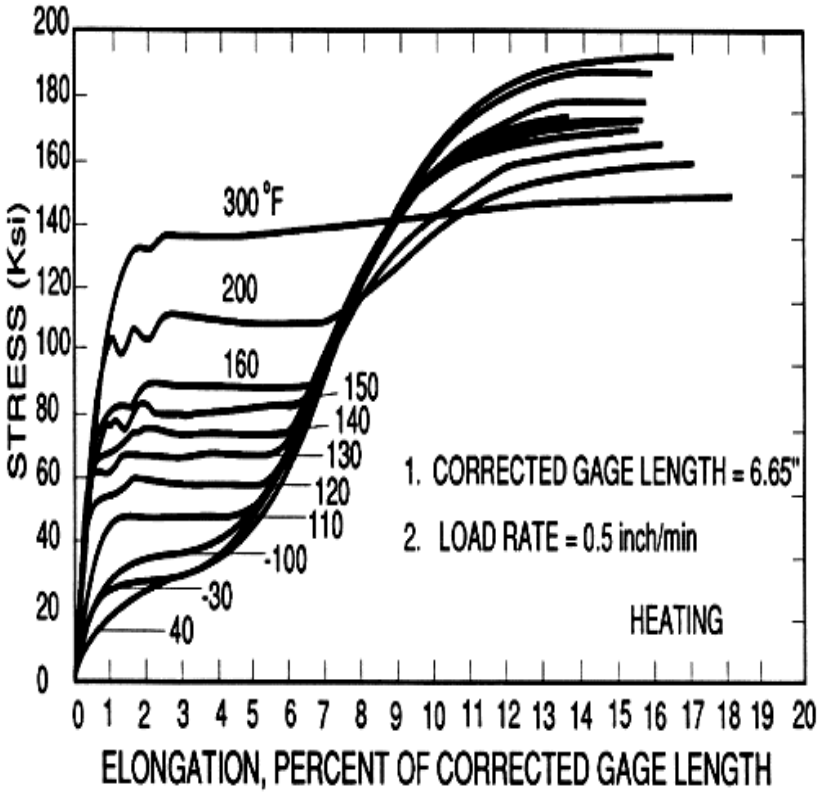

Figure 1.2 The strain-stress relation varies with temperature [42].

1.3.2 Constitutive Modeling of Shape Memory Alloys

Shape memory alloys are increasingly used in many engineering fields. The principal characteristic of shape memory alloys is their ability to memorize their original configuration after they have been deformed, by heating the alloys above the characteristic transition temperature. During this process, a large recoverable strain on the order of 8% can be obtained, making SMAs excellent actuators. Shape memory effect gives SMA many applications, such as shape control of structures, buckling control of structures, and medical devices, etc. The super-elastic effect also makes SMAs very useful in many applications, such as SMA springs, SMA hybrid composites for impact damage resistance.

In order to fully utilize the potential of SMAs, it is necessary to have a good understanding of their mechanical behavior under thermal and mechanical loading. The constitutive equations of SMA are much more complicated that most of the common engineering materials. SMAs have very unusual behaviors that we have not encountered before. This attracts many researchers to study in this field. For this reason, the constitutive modeling of SMA has been, and still is, the focus of many researchers. Several models based on various theories have been proposed thus far. Considering the various theories used, the proposed constitutive models can be classified into five categories: ferroelectrics models, internal variable models, plasticity models, hysteresis models, and nonisothermal models. A review of the SMA constitutive models is presented here [43].

Ferroelectrics Model

Müller, et al. [44-47] proposed a model based on thermodynamics, statistical physics and free energy in ferroelectrics and ferromagnetics. They extended these relations to the constitutive relation of SMA. The effects of temperature were described as the fluctuation of energy of the particles in the potential well, which is defined by the

depth of the potential well. Two coexisting phases of SMA were assumed in the model. Each of the coexisting phases has its own free energy. This model gives a very good understanding of the transformation and the related material behavior. However, it is complex and difficult to use in engineering design, other than to evaluate the properties of microstructures in various processes. Falk [48] modified the free energy-force-temperature relation in Müller's model and obtained a much simpler explicit relation. The model can be used to study the change of elastic modulus, shape memory effect, temperature and stress-induced phase transformation, as well as hysteresis loop under uniaxial stress.

Hoffman, et al. [49, 50]) then proposed a model based on a generalized free energy equation. The free energy was assumed as a function of the absolute temperature and a high order of strain. A one-dimensional differential equation which governs the SMA undergoing a thermomechanical process was derived. The numerical results showed that this model can describe the martensitic transformation of SMA. The model relies on numerical simulation, which can make it tedious to use in some applications.

Internal Variable Model

The second type of constitutive model is derived from the concept of the Helmholtz free energy, which can be derived from thermodynamic principles. The Helmholtz free energy is a function of the general state variable, Λ. The state variables for shape memory alloys are defined as strain, temperature, and martensite fraction (ξ). Thus, the general state variable can be defined as

$$\Lambda \equiv (\bar{\varepsilon}, T, \xi). \tag{1.1}$$

Based on Equation 1.1, the constitutive relation can be derived by using the first and second laws of thermodynamics [51]:

$$\bar{\sigma} = \rho_0 \frac{f\Phi}{f\bar{\varepsilon}} = \sigma(\bar{\varepsilon}, T, \xi) \ . \tag{1.2}$$

From equation 1.2, the rate form of the constitutive equation, which describes the change in stress is the function of changes in strain, temperature and martensite fraction can be derived as

$$\dot{\bar{\sigma}} = D\dot{\bar{\varepsilon}} + \Theta\dot{T} + \Omega\dot{\xi}, \tag{1.3}$$

where D is the Young's modulus, Θ is the thermoelastic tensor, and Ω is the transformation tensor, which defines the change of strain during the phase transformation. If the equation of free energy is given, the equilibrium state of phases can be obtained by minimizing the free energy. Thus, the relation among the martensite fraction, the applied stress and the temperature can be obtained. However, it is impractical to obtain such an equation. So instead of deriving the equation of free energy, the martensite fraction (ξ) is assumed to be a function of stress and temperature and experimental data are used to fit the martensitic transformation or austenitic transformation relations. Considering the different functions of the martensite transformation fraction, many researchers developed different internal variable models.

A one-dimensional SMA of length, *L,* which undergoes either martensite transformation or austensite transformation was studied by Tanaka, et al. [52-57]. In this work, the martensite transformation fraction was assumed to be an exponential function of stress and temperature according to transformation kinetics:

$$\xi_{M\to A} = \exp[A_a(T - A_s) + B_a\sigma] \tag{1.4}$$

and

$$\xi_{A\to M} = 1 - \exp[A_m(T - M_s) + B_m\sigma]\ ,$$

where A_a, A_m, B_a and B_m are material constants in terms of the transition temperatures, A_s, A_f, M_s, and M_f. This model can be used to predict and describe the stress-strain relations, superelastic effect and the energy dissipation of the pseudoelastic effect. However, it is not easy to use this model in engineering design and computations, because the phase transformation is piecewise, and the calculation may sometimes be very complex according to Liang [41].

Following Tanaka, Liang, et al. [51] proposed and developed another one-dimensional internal variable constitutive model. Instead of using the martensite transformation fraction as an exponential function of stress and temperature, a cosine function of martensite fraction (ξ) was proposed to correlate the experimental data:

$$\xi_{M\to A} = 0.5\xi_M\{\cos[a_A(T - A_s) + b_A\sigma] + 1\} \tag{1.5}$$

and

$$\xi_{A\to M} = 0.5(1 - \xi_A)\cos[a_M(T - M_f) + b_M\sigma] + 0.5(1 + \xi_A)\ ;$$

This model can predict and describe the stress-strain relations, superelastic effect and the energy dissipation of super-elastic effect for a certain of range of temperatures. The free recovery, restrained recovery and controlled recovery can also be described by this model. Only basic measurable material constants are needed in this model. Therefore, this model can be easily used in engineering design and computations. In Fig. 1.3, the results of the free strain recovery using the methods of Tanaka, et al. and Liang, et al. are compared to experimental data.

This one-dimensional model was later extended to a three-dimensional SMA model [39]. The three-dimensional model can be applied in studying the complex structures made of shape memory alloys. Experimental results are needed to compare with the numerical results. The model was also extended to a model that is capable of predicting the two-way shape memory effect [58].

Brinson [59] developed another cosine model based on that of Liang, et al. In this model, the martensite fraction internal variable, for the first time, is separated into stress-induced and temperature-induced components:

$$\xi = \xi_S + \xi_T , \tag{1.6}$$

where ξ_T is the martensite fraction of SMA which is induced by temperature with multiple variants, and ξ_S is the martensite fraction of SMA which is oriented by stress into a single martensite variant. By separating these two components, the model can predict and describe stress-induced martensitic transformation at temperatures above A_s with accompanying super-elastic behaviors, and predict and describe the shape memory effect with applied stress at all temperatures. Thus, Brinson's model can be used at all temperatures, and produces a better description of martensitic transformation in shape memory alloys. Brinson's model also gave us a new idea in modeling martensitic transformation of SMA to correlate the new findings in the experiments. Non-constant material functions which account for the change in material properties were also introduced in Brinson's model. The predicted stress-strain curves of the Brinson's model are shown in Fig 1.4. By using common and measurable material properties, Brinson's model can be easily used in engineering design and for computations of the stress-strain relations and the super-elastic effects of SMA.

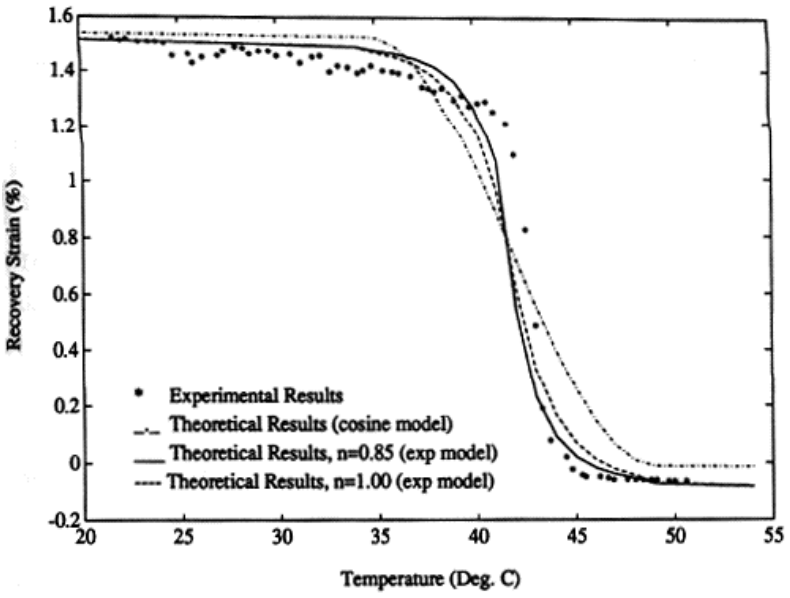

Figure 1.3 Comparison between cosine model and experiment [41].

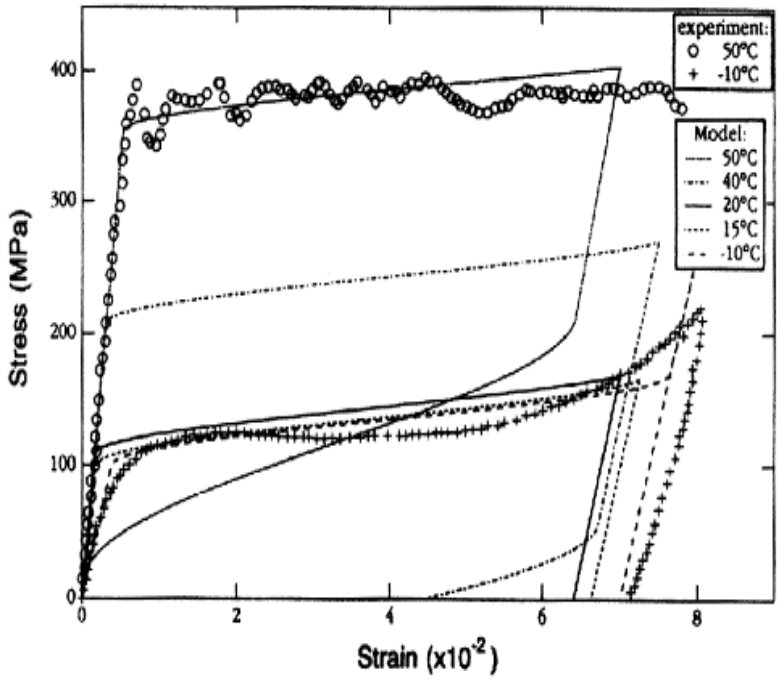

Figure 1.4 The Brinson's stress-strain relation of SMA [60,61].

Barret [62-63] considered the difference between the tensile and compressive properties of SMA, and proposed a model using the martensite fraction, ξ, as the internal variable. This model, based on a linear transformation relation, also separates the stress and temperature-induced transformation strains. In addition, the phase change hardening and the tension-compression history were considered. Thus, for tension and compression processes, this model gives better predictions than the other models. Different stress rate factors for tensile and compressive processes were used in the constitutive rate equation of both the one-dimensional and the three-dimensional models:

$$\dot{\varepsilon} = \frac{\dot{\sigma}}{E} + (\alpha + \beta)\dot{T}. \tag{1.7}$$

In equation 1.7, the dot indicates a rate term, ε is the strain, E is the elastic modulus, α is the secant coefficient of thermal expansion, and T is the temperature. The material properties are assumed to be independent of temperature. The model can predict tension-compression transformation, phase change hardening and hysteresis with partial transformation. This model works for the elastic deformation process.

Boyd, et al. [64] proposed a one-dimensional model based on Tanaka's exponential model. In this model, the tensile stress was replaced with Von Mises' stress, as in the theory of plasticity, because of the inelastic process. The first and second laws of thermodynamics were applied to obtain the evolution relations for internal state variables in the inelastic process. An additional assumption required by the inelastic process was needed in this model: the energy was assumed to be a general function of martensite fraction, ξ. This assumption was introduced by using Edelen's dissipation potential theory in the expression of mixing free energy. Bo, et al. [65] then generalized their model by introducing the threshold value as a function of state variables instead of a

constant, and by assuming some parameters as a function of ξ. With these modifications, the model unified the models proposed by Tanaka, Liang, et al., and Boyd, et al..

Plasticity Model

Kafka [66, 67] extended the modeling of the inelastic process in heterogeneous materials [68] to the constitutive relations of SMA. The constitutive equation of the isothermal deformation process in a heterogeneous material consists of an elastic and an elastic-plastic continuous domain. This model was modified to represent the shape memory effect and the superelasticity present in SMA. The effect of temperature changes was modeled by a simple linear relation between the thermal expansion of SMA under the deviatoric stress and strain process. This one-dimensional model can predict the shape memory effect and super-elasticity of SMA.

Brandon, et al. [69] proposed a model based on the experiments of single crystals of SMA conducted by Müller and Xu [47]. The model accounts for both elastic and plastic modes inside the hysteresis loop. The model represents a wider range of physical phenomena than the traditional plasticity theory. It can predict transformations between elastic and plastic phases through a dependence on the time history of strain and phase fractions. It can give the constitutive relation of SMA which has yield curves at all points within the hysteresis loop. This model works well for single crystal SMA in a smooth transition process from elastic to plastic mode.

Hysteresis Model

Graesser and Cozzarelli [70, 71] proposed a one-dimensional constitutive model based on the hysteresis modeling of damping materials. The stress-induced micromechanical phase transformation in SMA, which causes inelastic deformation and gives rise to a large energy-absorbing capacity is modeled. The inelastic strain rate is expressed as a function of stress, phase fractions, and other internal variables:

$$\dot{\sigma} = E[\dot{\varepsilon} - \left|\dot{\varepsilon}\right|\left|\frac{\sigma-\beta}{Y}\right|^{n-1}\left(\frac{\sigma-\beta}{Y}\right)]$$

and

$$\beta = E\alpha[\varepsilon - \frac{\sigma}{E} + f_T|\varepsilon|^c erf(a\varepsilon)] \quad , \tag{1.8}$$

where β is one-dimensional backstress, Y is the threshold stress to start stress-induced phase transformations, α is the constant which determines the slope of the inelastic region, n is a constant representing the sharpness of transition from elastic to inelastic behavior, f_T is a constant identifying the type and size of hysteresis, a is a constant which determines the amount of elastic recovery during unloading, and c is a constant controlling the slope of the unloading stress plateau.

The modeling is analogous to inelastic formulations for creep and viscoplasticity containing backstress. The model can represent elastic and inelastic states and the differences between loading and unloading in SMA. It can also predict superelasticity and the martensite twinning hysteresis of SMA. A uniform temperature field of SMA was assumed in this model. Using this hysteresis model, two kinds of SMA hysteresis at different temperatures are shown in Fig. 1.5 and Fig. 1.6.

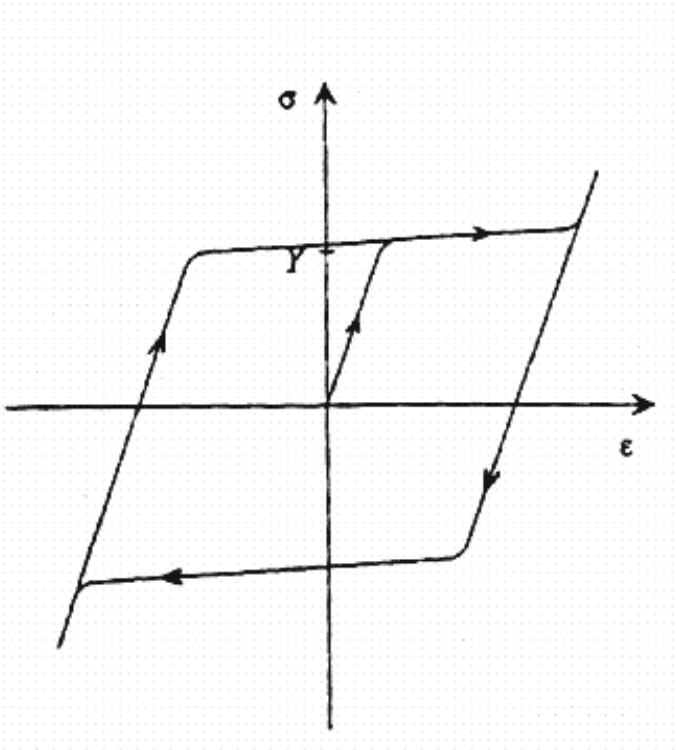

Figure 1.5 Twinning hysteresis of SMA (at temperature below M_f [72]).

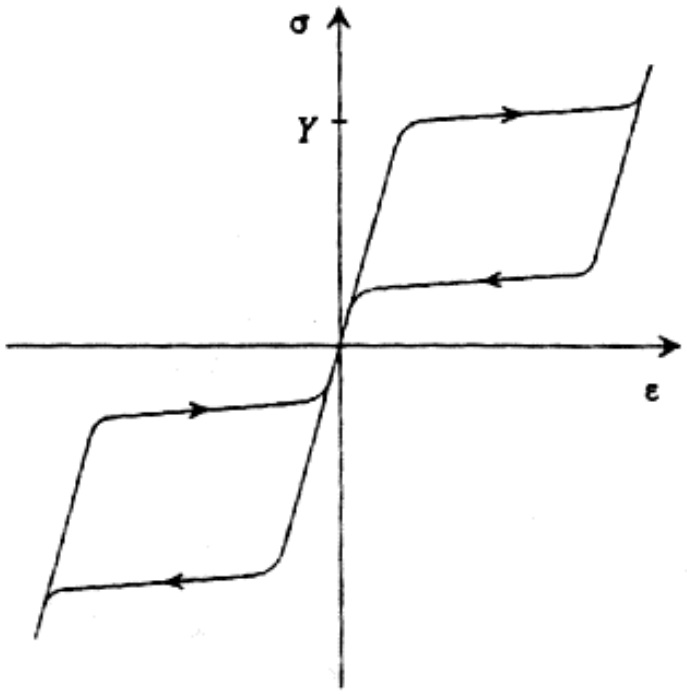

Figure 1.6 Superelasticity of SMA (at temperatures above A_f [72]).

Graesser and Cozzarelli [72] also extended their one-dimensional model to a three-dimensional model. This rate-dependent three-dimensional model accounts for uniaxial loading, shear loading, and non-proportional biaxial loading. This nonlinear model is relatively simple because only two evolutionary equations are required to model inelastic strain and a generalized back-stress at a material point. Therefore, only one internal variable was used. As in the case of the one-dimensional model, the three-dimensional model can represent elastic and inelastic state and the difference between loading and unloading in SMA. It can also predict superelasticity and martensite twinning hysteresis of SMA. Experimental data are still needed to compare with the numerical results.

Non-isothermal Model

Ivshin, et al. [73] and Pence, et al. [74] proposed a model which considers the connection between the complete transformation phenomena and the arrested loading or unloading. Also, the model considers the transition from isothermal to adiabatic loading in a heat-convective environment. This model has only one variant of any phase, and hence will not capture certain phenomena in twinning that are usually associated with the shape memory effect. It can predict the stress-strain relation of SMA in adiabatic loading through the loading in a heat convective-environment.

Abeyaratne, et al. [75] proposed a model which considers high loading rate effects on SMA. At low loading rates, an isothermal relation can be used to describe the behavior of materials. However, at high loading rates, the heat generated by the phase transformation has a significant effect on the material behavior. Indeed, the temperature field in the SMA material is non-uniform and the phase boundary of the heat moves as a moving heat source, in which the strength and velocity of the heat are not known. The local heat in SMA can also cause thermal hardening in the SMA. Thus, the mechanical behavior of SMA at high loading rates has a coupled thermo-mechanical response. To take into account these thermal and rate effects, an internally self-consistent model based on

classical continuum thermodynamics was developed, resulting in a nonlinear relation with coupling between thermal and mechanical effects:

$$\frac{k}{\rho c}\theta_{xx} = [1 + \frac{\mu\alpha^2}{\rho c}\theta]\theta_t + \frac{\alpha}{\rho c}\dot{\sigma}\theta + \left(\frac{\zeta}{c}\right)(\theta - \theta_0). \tag{1.9}$$

By solving the moving boundary problem, the stress-strain relationship of SMA at high loading rates was predicted. The predicted stress-strain curves at different strain rates are shown in Fig. 1.7.

Boyd, et al. [76] proposed a model which is based on the free energy function and dissipation potential. The closed-form equations of the damping capacity and the efficiency of converting heat into work were derived. It was found that significantly more work is required to complete the adiabatic transformation than the isothermal transformation. This is due to the loading rate effect. When SMA is loaded at a low loading rate, the process is assumed to be isothermal and no temperature rise due to the external work done on SMA. However, when SMA is loaded at high loading rates, there is irreversible heat generated by external work. The heat dissipates in SMA and environment. This heat causes temperature rise in SMA, thus the process is considered to be adiabatic. So, to make an SMA specimen deform at a high loading rate for the same amount of deformation as it deforms at a low loading rate, more work is needed to produce such deformation according to the first law of thermodynamics. The extra work is actually converted to heat in SMA.

Their model accounts for non-proportional loading, simultaneous transformation and reorientation, adiabatic deformation, and combined isotropic and kinematic hardening. Experimental results are still needed to compare with analytical results.

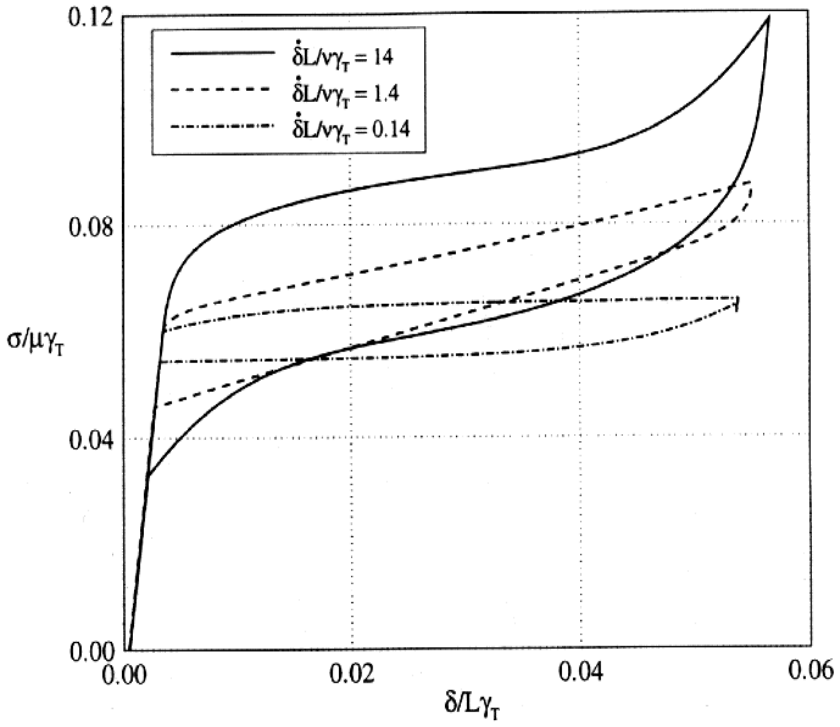

Figure 1.7 Stress-strain relation of SMA at different elongation rates [75].

Table 1.1 Comparison of five types of SMA constitutive models.

Models	Dimension	σ-ε	Superelastic	Elastic	Inelastic	Isothermal	Loading
Ferroelectric	1-D	nonlinear	yes	yes	no	yes	Tension
Internal variable	1-D, 3-D	nonlinear	yes	yes	no	yes	Tension compression
Plasticity	1-D, 3-D	nonlinear	yes	yes	yes	yes	multiaxial
Hysteresis	1-D, 3-D	nonlinear	yes	yes	yes	yes	multiaxial
Non-isothermal	1-D	nonlinear	yes	yes	no	no	tension

1.3.3 Summary

The constitutive models presented can predict and describe the stress-strain relation (linear and nonlinear), the superelastic effect, the energy dissipation of the superelastic effect, the tensile and compressive effects, as well as the one-way and two-way shape memory effects in shape memory alloys for one-dimensional isothermal loading. The models can also predict the superelasticity and martensite twinning hysteresis of SMA.

Three-dimensional constitutive models that can account for uniaxial loading, shear loading, and non-proportional biaxial loading, and elastic and inelastic states, as well as the differences between loading and unloading, have also been proposed. However, experimental data is needed to confirm the theoretical predictions made by the three-dimensional models.

The research on the non-isothermal loading, high loading rate is just beginning. There are only a few publications in this area. Again, experimental investigation is needed to confirm the theoretical predictions of the non-isothermal models.

A comparison of five different types of constitutive models is summarized in Table 1.1. The strengths of each type of constitutive model are:

- Ferroelectric models are good for studying the transformation process in the SMA material, but are difficult to use in engineering applications.
- Internal variable models use the martensite fraction, ξ, as an internal variable in the transformation process, which makes it more physically tractable and easy to understand. Most of the internal variable models prove to be simple, easy to use and of good accuracy. The use of these models has to be confined within the elastic and isothermal processes.
- Plasticity models can be used in elastic and inelastic processes although they are usually used in smooth transition processes.

- Hysteresis models work well in inelastic processes, although they are more phenomenological than physical.
- Non-isothermal models are especially suitable for adiabatic process, such as high loading rates.

1.4 The Goals of This Research

The research on impact and quasi-static contact loading of SMA hybrid composites was experimental and the first reported work, the mechanical behavior and damage mechanism of SMA composites, as well as strain energy absorption and phase transformation of SMA in composites, have not been understood yet. Thus, this research is aimed at developing the models and methods to analyze the phenomena in the experiment, and to provide the understanding for SMA composites under impact and quasi-static loading. This understanding and these models and methods can be used for future applications of SMA composites under impact and quasi-static loading.

Because this research is the first reported on the analysis and modeling of SMA composites under impact and quasi-static loading, we need to start the research from some fundamental issues, such as strain energy absorption in SMA, basic governing equations of SMA composite laminates, and strain energy absorption of SMA composites. After we have understood these fundamentals, we can develop the model for predicting the mechanical behavior, damage mechanism, SMA phase transformation in SMA composites under quasi-static contact loading in failure process.

Based on the above strategy, this dissertation is organized as follows:

In Chapter 2, the study of strain energy absorption in SMA is presented. The basic relationship among the strain energy absorption, martensite phase transformation, and external load will be developed. Then in Chapter 3, the basic nonlinear governing equations of SMA composite laminates are derived. These equations account for the large deformation and shear deformation of SMA composite laminates with general stack of

angle ply and general boundary conditions, and can be used for impact and contact loading. Then in Chapter 4, the strain energy absorption of SMA composite beam, global deformation, and local contact deformation are analyzed. Numerical study illustrates the relationship among these factors. With the understanding and methods developed in Chapters 2, 3, and 4, we develop a model and a new method to analyze the damage mechanism, failure process, and SMA phase transformation in SMA composite under quasi-static contact loading by a steel cylinder up to complete failure. This process involves matrix cracking, delamination, fiber breakage, and stress/strain induced martensite phase transformation of SMA. This is a strongly nonlinear problem in both geometry and material. Due to these strong nonlinearities and discontinuities, conventional methods from nonlinear plate or beam theory are not applicable. A new method is proposed to treat this problem. The results predicted by the proposed model and method are compared with experimental results. Good agreement between the predicted value and the experiment data are found.

Chapter Two

Theoretical Study of Strain Energy Absorption of Shape Memory Alloys

2.1 Introduction

A shape memory alloys (SMA) is able to recover its original configuration after it has been deformed by heating the alloy above its characteristic transition temperature. This unique property of martensitic SMA is often referred to as the shape memory effect (SME). Shape memory alloys can also be formulated to be stable in the austenitic phase, and can be transformed to the martensitic phase by applying stress/strain, which is known as the stress/strain-induced martensitic phase transformation. The austenitic SMA behaves super-elastically and can be loaded to large strain without any plastic deformation. This super-elastic formulation of the alloy has a remarkable recoverable elastic strain up to 8%, and an unusual high strain to failure exceeding 15%. The super-elastic property is caused by the reversible stress-induced martensitic phase transformation that creates a large plateau in the stress-strain relation. Another unique property of austenitic SMA is the high strain energy absorption capability. Indeed, materials with a large area under the stress-strain curve have a high strain energy absorption capability. When compared to other materials, the super-elastic SMA performs exceptionally well. Thus, SMAs are available with two very distinctive characteristics depending on their formulation: the martensitic SMA has a shape memory effect, while the austenitic SMA is super-elastic.

The super-elasticity of SMA can be used to improve the impact damage tolerance of composite materials. Because super-elastic SMA can absorb more strain energy than graphite fibers [32-35]) proposed to embed super-elastic SMA fibers in graphite/epoxy composites to enhance the impact damage resistance. Through experimental investigation, it was found that the addition of small amounts of super-elastic SMA fibers to graphite composites can improve the low-velocity impact damage resistance. Thus, the SMA hybrid composite is able to elastically store more impact energy before fiber failure by increasing the maximum strain energy capabilities of the fibers in the composite.

As the first step to further understand the strain energy absorption of super-elastic SMA, and to fully utilize the energy absorption capability of super-elastic SMA, theoretical relationship for evaluating the strain energy absorption of SMA is needed. For this purpose, a simple model to evaluate the energy absorption capability of super-elastic shape memory alloy under bending and tension loading will be developed. Since most SMA products are available in a one dimensional form, such as fibers, bars, and ribbons, a one dimensional analysis will be made. The model is developed to quantitatively evaluate the strain energy absorption of the SMA and to predict the threshold loads needed to initiate and complete the stress-induced martensitic phase transformation. This model will provide a simple tool to quantitatively evaluate the energy absorption capability of shape memory alloys under bending and tension loading.

The mechanical behaviors of shape memory alloys (SMAs) can be separated into two major categories: the shape memory effect and super-elastic effect. When the austenitic finish temperature A_f is below the working temperature, shape memory alloys behave super-elastically. The super-elastic SMA undergoes a stress-induced martensitic transformation that will result in a large recoverable strain. Thus, the super-elastic effect makes SMA an excellent candidate for energy absorption. This research presents simple theoretical equations for quantitatively evaluating the strain energy absorption capacity of shape memory alloy beams in stress/strain induced martensitic transformation due to pure bending in the loading process. The equations are developed by using Euler-Bernoulli beam theory. These equations describe the two phase transformation regions co-existing in the shape memory beam. The two regions are changing and interacting each other under the loading process. The threshold moment and force for initiating martensitic transformation and threshold moment and force for completing martensitic transformation are obtained. The formula of strain energy absorption capacity of SMA beam during loading is developed. The energy absorption capacity of SMA beam in uniaxial loading is also given by this model. The case studies are made for a super-elastic SMA beam and a martensite SMA beam by using these theoretical relations. The numerical results show that super-elastic SMA beam has significantly more energy absorption capability than that of martensite SMA beam. The comparison was also made between the bending case and tension case. The results show that the tension case has more energy absorption capability

that the bending case due to the uniform distribution of stress through the across section of SMA beam. The theoretical relations provide an useful tool for quantitatively evaluating the strain energy absorption capability of SMA beam. They can be easily used in analysis and design of super-elastic SMA for energy absorption applications.

Statement of Problem

In this section, the theoretical relations quantitatively evaluating the strain-energy absorption of a SMA beam under bending will be derived first, followed by the relation of a SMA bar under tension. For this purpose, a rectangular SMA beam of length L, width b, and thickness h will be used. Since SMA fibers, bars, and ribbons are usually thin and long ($b<<L$, $h<<L$), the Euler-Bernoulli beam theory will be used to develop the bending model. For the tension model, the rod theory will be used. Among the various SMA constitutive model available [43] the one-dimensional internal variable constitutive model developed by Brinson [59] will be used. A typical stress-strain relation obtained from Brinson's model is shown in Figure 2.1, both for the super-elastic SMA and the martensitic SMA.

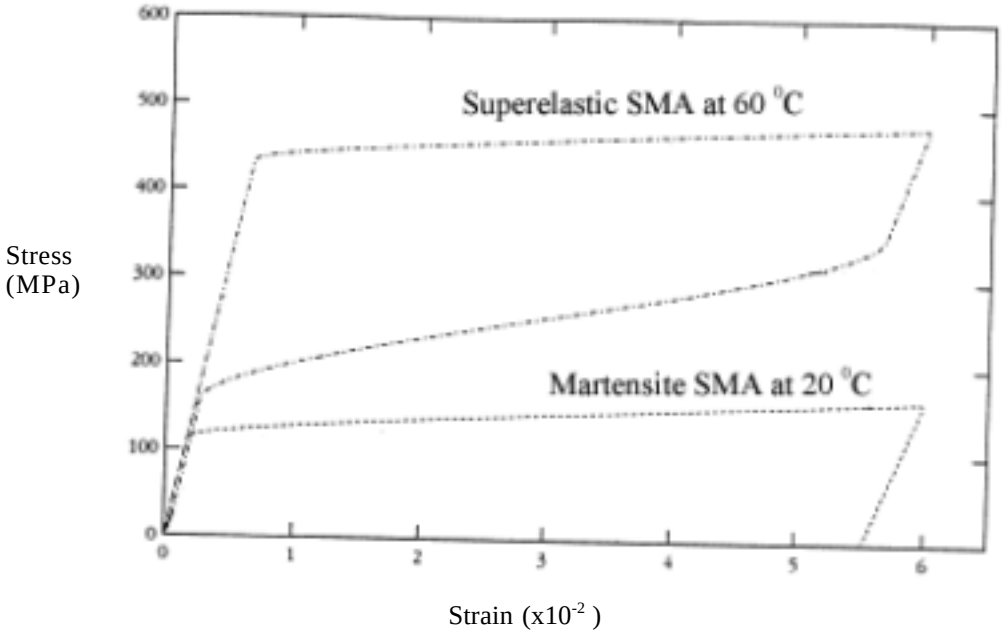

Figure 2.1 Stress-strain relation of super-elastic and martensitic SMA [59].

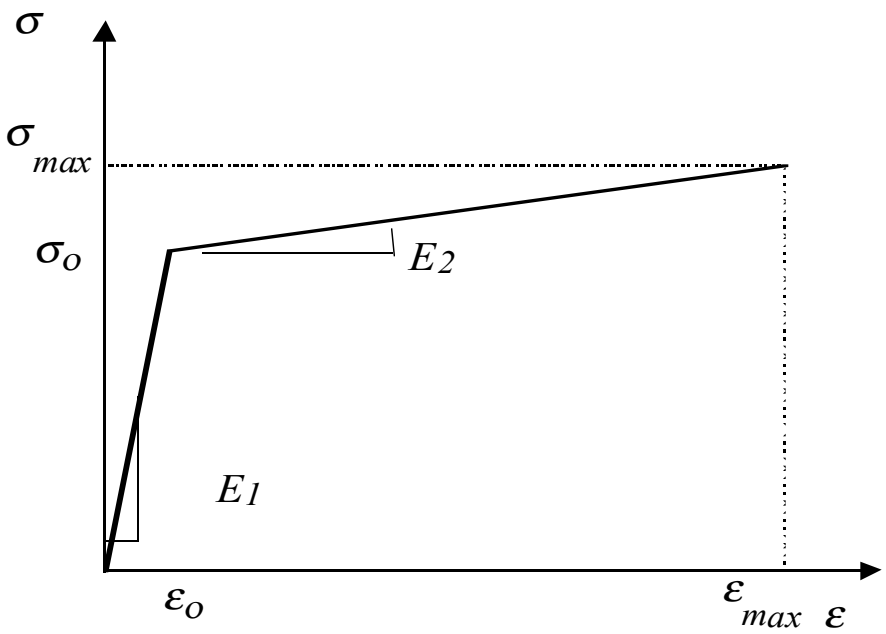

Figure 2.2 Piecewise linear model.

In order to simplify the strain-energy model derived in this section, a linearization of the one dimensional constitutive equations is made. This linearization results in a piecewise linear equation (strain hardening constitutive equation). Even though nonlinear stress-strain relation and numerical integration can be used to get more accurate results, the piecewise linear approximation will give acceptable results for studying the strain energy absorption of SMA, since it captures the physical essence of energy absorption capability of SMA. The piecewise linear stress-strain relation used in this paper is schematically shown in Fig.2.2, where σ_o and ε_o are stress and strain at which martensitic transformation starts, ε_{max} is the maximum recoverable strain with σ_{max} being the corresponding stress, and E_1 and E_2 are the Young's before and after the strss-induced martensitic phase transformation is initiated, respectively. These parameters are obtained by drawing two straight lines on the stress-strain curve in Fig.2.1, and taking the corresponding values for the simplified piecewise linear stress-strain curve. In this modeling approach, the martensitic fraction ξ is 0 at (σ_o , ε_o,) and 1 at (ε_{max}, σ_{max}).

Another assumption made in section is the identical SMA stress-strain relation in tension and in compression. This assumption was shown to be valid for one dimensional SMA based on experimental results [41]. Thus, based on Fig. 2.2, the one dimensional piecewise linear stress-strain relation in tension is:

$$\begin{aligned} \sigma_A &= E_1\varepsilon && 0 < \varepsilon < \varepsilon_o \\ \sigma_M &= \sigma_o + E_2(\varepsilon - \varepsilon_o) && \varepsilon_o \le \varepsilon \le \varepsilon_{\max} \end{aligned} \quad , \qquad (2.1a)$$

and the one dimensional piecewise linear stress-strain relation in compression is:

$$\begin{aligned} \sigma_A &= E_1\varepsilon && -\varepsilon_o < \varepsilon < 0 \\ \sigma_M &= -\sigma_o + E_2(\varepsilon + \varepsilon_o) && -\varepsilon_{\max} \le \varepsilon \le \varepsilon_o \end{aligned} \quad . \qquad (2.1b)$$

2.2 SMA Beam in Bending

In this section, the strain-energy absorption of a SMA beam in bending is modeled. As the SMA beam is increasingly loaded, the strain distribution through the beam's thickness remains linear, as shown in Fig. 2.3. However, the stress distribution in the SMA beam is not linear, but piecewise linear due to the changing material properties from martensite to austenite along the beam's thickness. Thus, the loading process of the SMA beam in pure bending can be separated in three stages. In loading stage 1, the SMA beam is austenite throughout its thickness until the stress at the outer fibers of the beam reaches σ_o, and the corresponding the stress distribution is shown in Fig. 2.4a. As more load is applied, a stress-induced martensitic phase transformation starts occurring at the outer fibers of the SMA beam, and the stress-induced martensite region progresses towards the beam's neutral axis as the applied moment continues to increase, as shown in Fig. 2.4b. In this second loading stage, the SMA beam will consist of martensite outer layers, with an austenite core. Loading stage 2 ends as the stress and strain of the beam's outer fibers reach ε_{max} and σ_{max}, respectively, as shown in Fig. 2.4c. From this point further, a plastic deformation will be present in the beam, which is the third loading stage. In this section, the plastic deformation (stage 3) will not be included in the strain energy absorption modeling, only considering the elastic deformation of the SMA.

As the beam is loaded through its three stages, the strain energy will be absorbed through different mechanisms. In loading stage 1, the strain energy is stored elastically in the austenite ($0<\varepsilon<\varepsilon_o$); in loading stage 2, the strain energy is stored elastically both in the austenite and in the stress-induced martensite ($\varepsilon_o<\varepsilon<\varepsilon_{max}$); and in loading stage 3, the strain energy is stored elastically in the austenite and in the stress-induced martensite, and plastically in the martensite ($\varepsilon>\varepsilon_{max}$). The strain energy stored in the beam at the point where the outer fibers of the beam reach ε_{max} and σ_{max} is defined as strain energy absorption capability of the SMA beam.

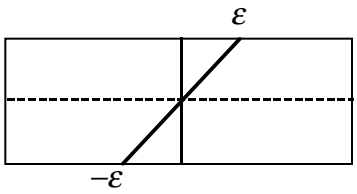

Figure 2.3. Strain distribution in the SMA beam.

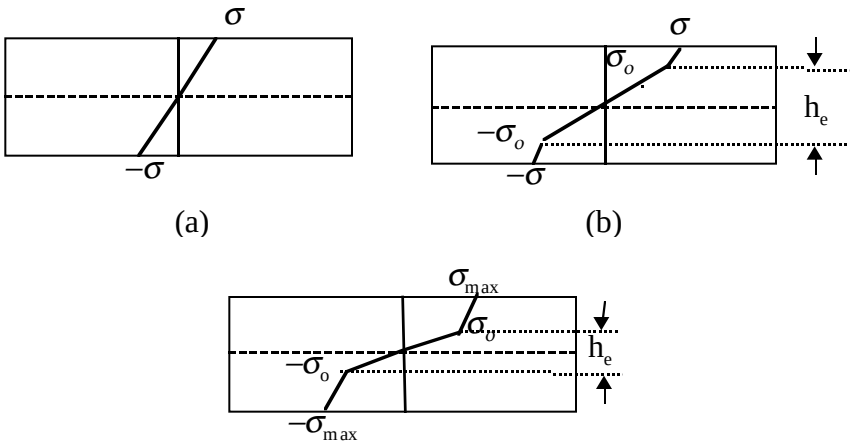

Figure 2.4. Stress distribution at the various stages of loading:

(a) Stage 1 - 100% austenite;

(b) Stage 2 - austenite and martensite;

(c) End of stage 2, and beginning of stage 3.

Loading stage 1: In the first loading stage, the modeling is straightforward since the stress distribution is linear through the thickness of the beam, as shown in Fig. 2.4a. Starting with the common expression of the stress of a beam under bending:

$$\sigma = \frac{My}{I}, \tag{2.2}$$

where $I = bh^3/12$, M is the moment applied, and y is the distance to the neutral axis, the expression of the moment needed to initiate the martensitic phase transformation, M_i, is:

$$M_i = \frac{\sigma_o bh^2}{6}. \tag{2.3}$$

The strain energy absorbed by the SMA beam is simply obtained by integrating along the length of the beam:

$$U = 2\int_o^{L/2} \frac{M^2}{2E_1 I}\, dx. \tag{2.4}$$

and, the maximum strain energy that can be absorbed before the stress-induced martensite phase transformation is:

$$U_i = \frac{6L}{E_1 bh^3} M_i^2. \tag{2.5}$$

Loading stage 2: In the second loading stage, the applied moment range from the initiating martensitic transformation moment M_i and completing martensitic transformation moment M_f ($M_i < M < M_f$). As discussed earlier, the stress distribution across the section is piecewise linear (Fig. 2.4b). Since the SMA beam has two distinct regions, the total moment applied on the beam is a linear superposition of the moment carried by the austenitite core, M_A, and the moment carried by martensitite outer layers, M_M:

$$M = M_A + M_M \tag{2.6}$$

where the moment on the austenitite core and the martensite outer layers are:

$$M_A = 2\int_o^{\frac{h_c}{2}} y\sigma_A b\, dy \tag{2.7a}$$

$$M_M = 2\int_{\frac{h_e}{2}}^{\frac{h}{2}} y\sigma_M b dy, \tag{2.7b}$$

repectively. In equation 2.7, h_e is the thickness of the austenitite core. The linear stress distributions in the austenitite core and in the martensite regions are:

$$\sigma_A = \frac{2y}{h_e}\sigma_o \; 0 \le y \le \frac{h_e}{2} \tag{2.8a}$$

$$\sigma_M = \left[1 + \frac{E_2}{E_1}\left(\frac{2y}{h_e} - 1\right)\right]\sigma_o \qquad \frac{h_e}{2} \le y \le \frac{h}{2}, \tag{2.8b}$$

respectively, where the stress expressions were obtained by incorporating the beam's linear strain expression

$$\varepsilon = 2\frac{\varepsilon_o}{h_e} y \tag{2.9}$$

in equation 2.1. Then, by combining equations 2.6-2.8, the expression of the moment carried by the SMA beam is obtained as a function of the austenite core thickness h_e:

$$M = \left[\frac{h_e^2}{6} + \frac{E_2}{E_1}\frac{h^3 - h_e^3}{6h_e} + \left(1 - \frac{E_2}{E_1}\right)\frac{h^2 - h_e^2}{4}\right] b\sigma_o \tag{2.10}$$

The strain energy absorbed by the beam is obtained by integrating the energies stored in the austenite and the martensite along the length of the beam:

$$U = \int_v u dv = 4b\int_o^{\frac{L}{2}} dx\left[\frac{1}{2}\int_o^{\frac{h_e}{2}} \sigma_A \varepsilon dy + \int_{\frac{h_e}{2}}^{\frac{h}{2}}\left(\int_{\varepsilon_o}^{\varepsilon} \sigma_M d\varepsilon\right)dy\right], \tag{2.11}$$

Substituting equations 2.1 and 2.9 into equation 2.11, the expression of the strain energy as a function of the austenite core thickness is obtained:

$$U = bL\sigma_o\varepsilon_o\left[\frac{h_e}{6} + (h - h_e)\left(\frac{E_2}{2E_1} - 1\right) + \left(1 - \frac{E_2}{E_1}\right)\frac{h^2 - h_e^2}{2h_e} + \frac{E_2}{E_1}\frac{h^3 - h_e^3}{6h_e^2}\right] \tag{2.12}$$

Finally, the stress induced martensite fraction in the SMA is obtained by incorporating equation 2.8b in the general expression derived by Brinson:

$$\xi_s = \tfrac{1}{2} Cos\left\{ \frac{\pi}{\sigma_s^{cr} - \sigma_f^{cr}} \left[\sigma_o \left(1 + \frac{E_2}{E_1} \left(\frac{2y}{h_e} - 1 \right) \right) \right] - \sigma_f^{cr} - C_M \left(T - M_s \right) \right\} + \tfrac{1}{2}. \tag{2.13}$$

2.3 SMA Bar in Tension

The strain energy absorption model for an SMA rod under tension is presented here. The theoretical model is straightforward since the strain distribution through the thickness of the SMA rod is uniform. The loading process will have the same three stages as for the bending case, but the stress-induced martensitic phase transformation is uniform in the rod. Since the approach used is the same as for the bending model, but much simpler, only the final results will be presented. The maximum strain energy that can be absorbed before the stress-induced martensite phase transformation (stage 1) is:

$$U_i = bLh \frac{\sigma_o^2}{2E_1}, \tag{2.14}$$

and the expression of strain energy during loading stage 2 is:

$$U = bLH \left[\frac{\sigma^2}{2E_1} + \frac{\left(\sigma - \sigma_o \right)}{2E_2} + \frac{\sigma_o \left(\sigma - \sigma_o \right)}{E_2} \right], \tag{2.15}$$

where σ is the stress applied to the SMA bar.

Table 2.1. Properties of the Shape Memory Alloy.

Property	Value
Martensite Start Temperature, M_s	18.4°C
Martensite Finish Temperature, M_f	9°C
Austenite Start Temperature, A_s	34.5°C
Austenite Finish Temperature, A_f	49°C
Transformation constant, C_M	0.008 GPa/°C
Transformation constant, C_A	0.0138 GPa/°C
Transformation constant, σ_s^{cr}	0.1 GPa
Transformation constant, σ_f^{cr}	0.17 GPa
Austenite Modulus, D_A	67 GPa
Martensite Modulus, D_M	26.3 GPa

Table 2.2. Parameters of piecewise-linear SMA constitutive model.

Property	Superelastic SMA	Martensitic SMA
Young's Modulus, E_1	67193MPa	67000MPa
Young's Modulus, E_2	907MPa	678MPa
Transformation start strain, ε_o	0.647%	0.185%
Transformation start stress, σ_o	434.8MPa	112.8MPa
Transformation finish strain, ε_{max}	8.18%	8.8%
Transformation finish stress, σ_{max}	503MPa	182MPa

2.4 Numerical Results

The developed model will be used to evaluate the strain energy absorption capability of super-elastic SMA and martensitic SMA. For this purpose, a case study of a superelastic SMA bar (A_f= 49 degrees Celsius, T = 60 degrees Celsius) and a martensitic SMA bar (A_f = 49 degrees Celsius, T = 20 degrees Celsius) with dimensions, length, L=100 mm, width, b=2 mm, and thickness, h=2 mm, loaded in bending and in tension, will be presented. The material properties of the SMA bar used in the calculations are given in Table 2.1. The corresponding parameters of the linearized SMA constitutive model of the superelastic SMA and the martensitic SMA are given in Table 2.2.

2.4.1 Bending Case

The relation between the strain energy absorbed and the SMA beam's austenite core thickness is presented in Fig. 2.5, which represents loading stage 2. As expected, the super-elastic SMA has better strain-energy absorption capabilities than the martensitic SMA: the maximum strain energy stored in the super-elastic SMA being at least twice the maximum strain energy stored in the martensitic SMA. An important thing to notice in Fig. 2.5 is the amount of strain energy stored in the beam in loading stage 1, which is the offset of the curves at h_e = 0.002m. For the superelastic SMA, 0.19J of strain energy is absorbed before any stress-induced martensite phase transformation occurs, while only 0.02J of strain energy was absorbed for the case of the martensitic SMA.

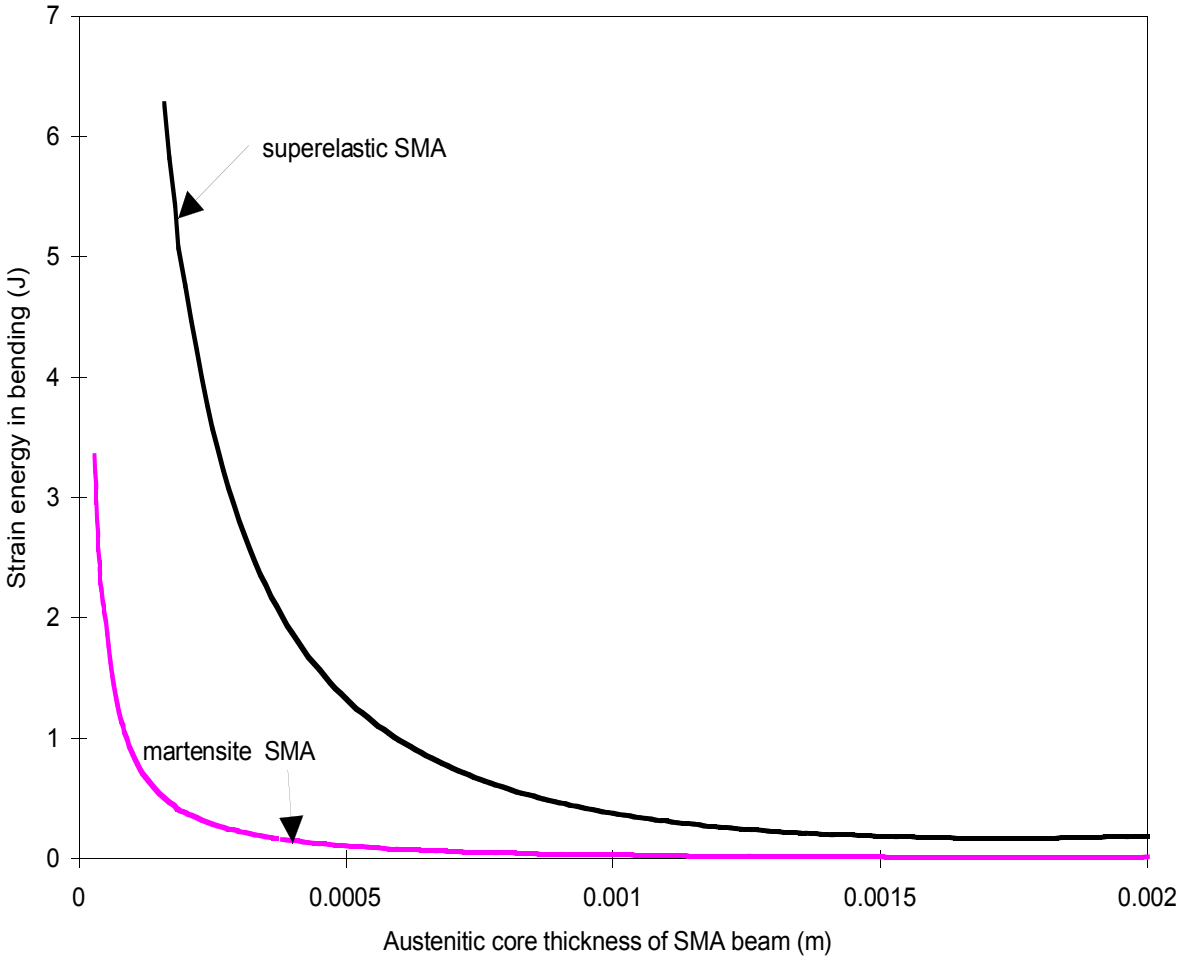

Figure 2.5. Strain energy vs Austenitic core thickness of SMA beam.

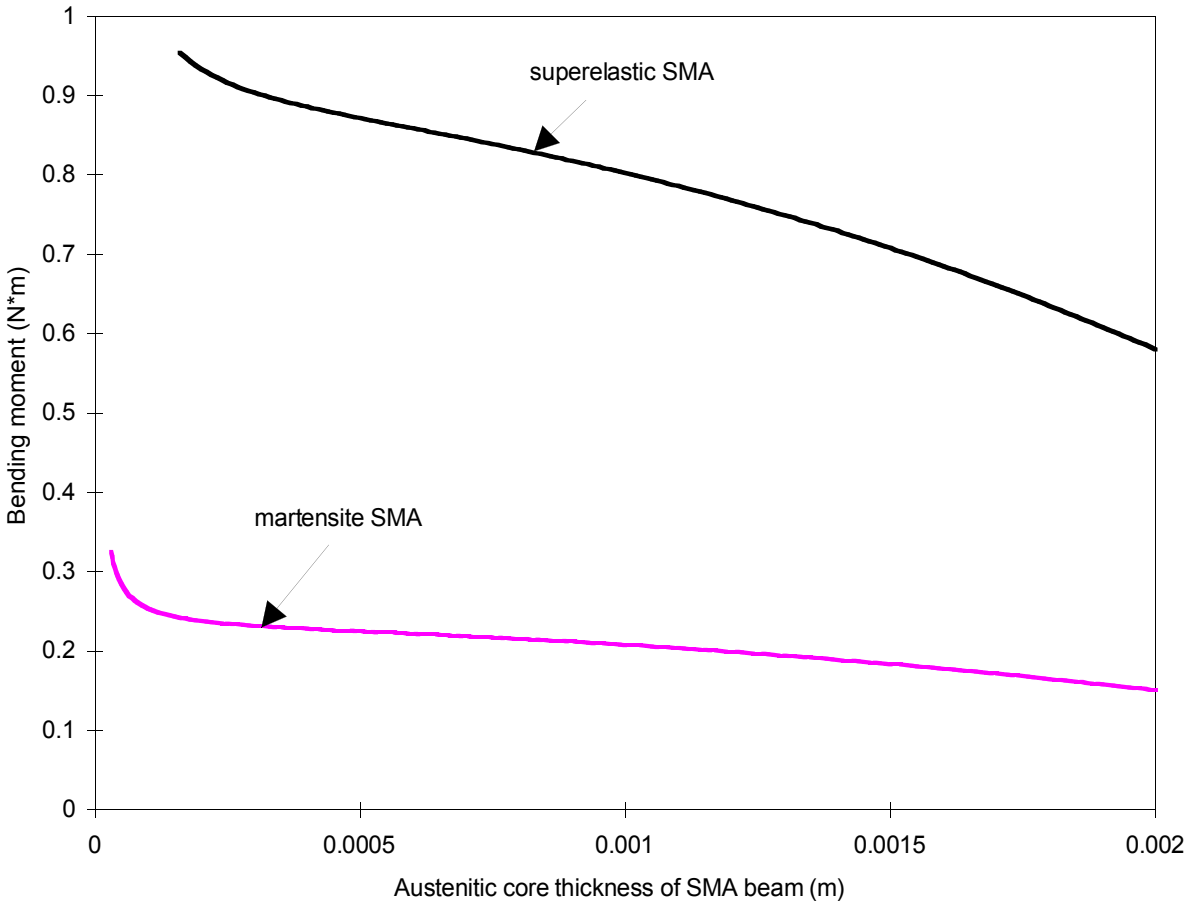

Figure 2.6. Bending moment vs Austenitic core thickness of SMA beam.

The next figure (Fig. 2.6) shows the relationship between the bending moment and austenite core thickness of SMA beam in bending. The bending moment needed to induced the martensite phase transformation in the superelastic SMA is much larger than the moment needed for the martensitic SMA (0.58 N.m vs. 0.17 N.m), mainly due to the larger value of σ_o. The other observation to be made is that the applied moment does not increase dramatically during the martensitic phase transformation, which is a property common to all shape memory alloys.

In Fig. 2.7, the relation between the martensite fraction at the surface of the SMA beam and the austenite core thickness is presented. The martensitic phase transformation increases slowly at the beginning, but rapidly as the austenite core thickness reaches one half the thickness of the SMA beam for the superelastic SMA, and one fourth the thickness of the SMA beam for the martensitic SMA.

In the next three figures (Figs 2.8-2.10), the data from the previous three figures (Figs 2.5-2.7) is combined to further understand the behavior of SMA undergoing a stress-induced martensitic phase transformation. First, Fig. 2.8 gives the relation between the strain energy absorbed and the martensite fraction at the surface of the SMA beam. It can be observed that the martensitic phase transformation absorbs most of strain energy in the structure and that the strain energy in bending increases nonlinearly with the martensite fraction. For the same martensite fraction, the superelastic SMA will absorb at least twice the strain energy of the martensitic SMA.

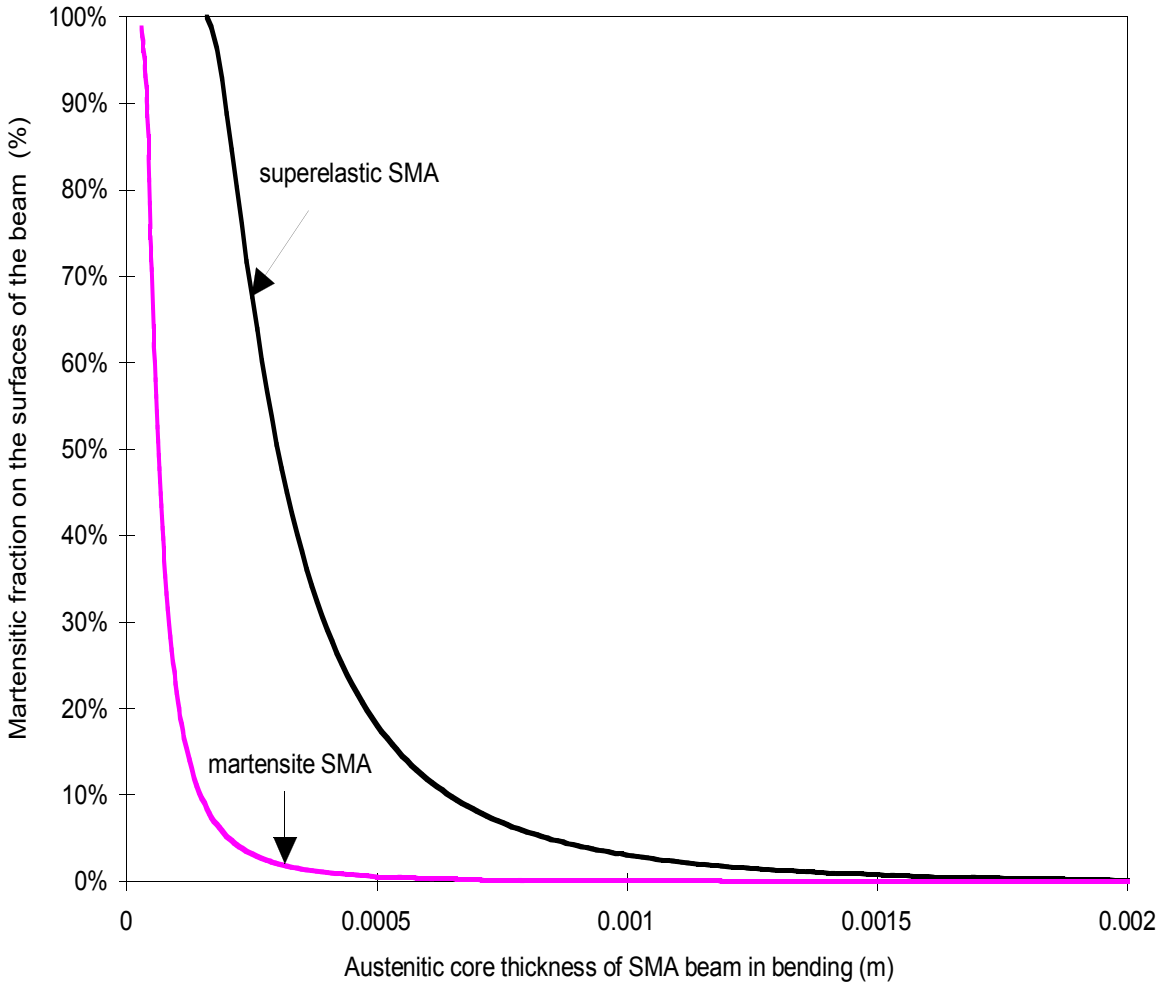

Figure 2.7. Martensitic fraction vs Austenitic core thickness of SMA beam.

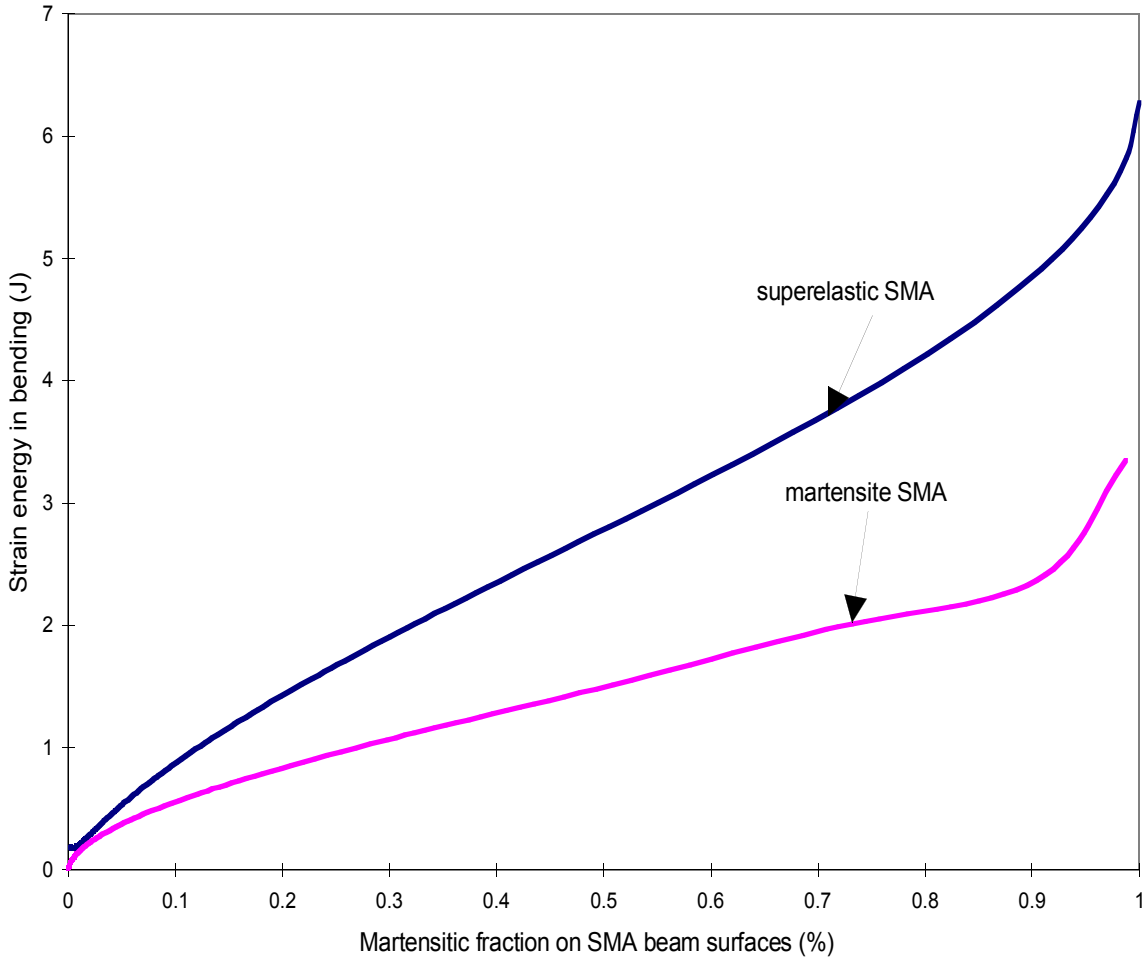

Figure 2.8. Strain energy vs Martensitic fraction.

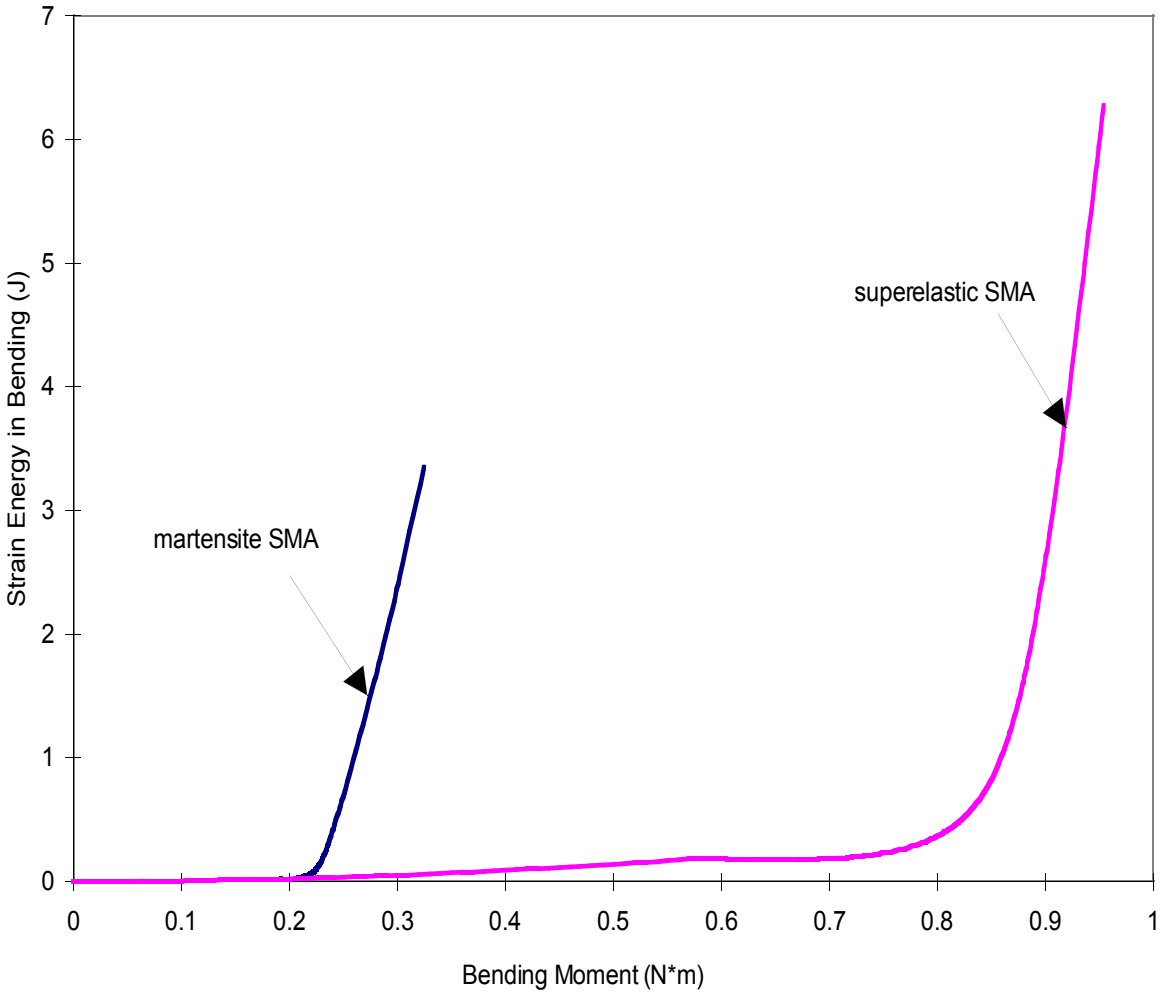

Figure 2.9. Strain energy vs bending moment.

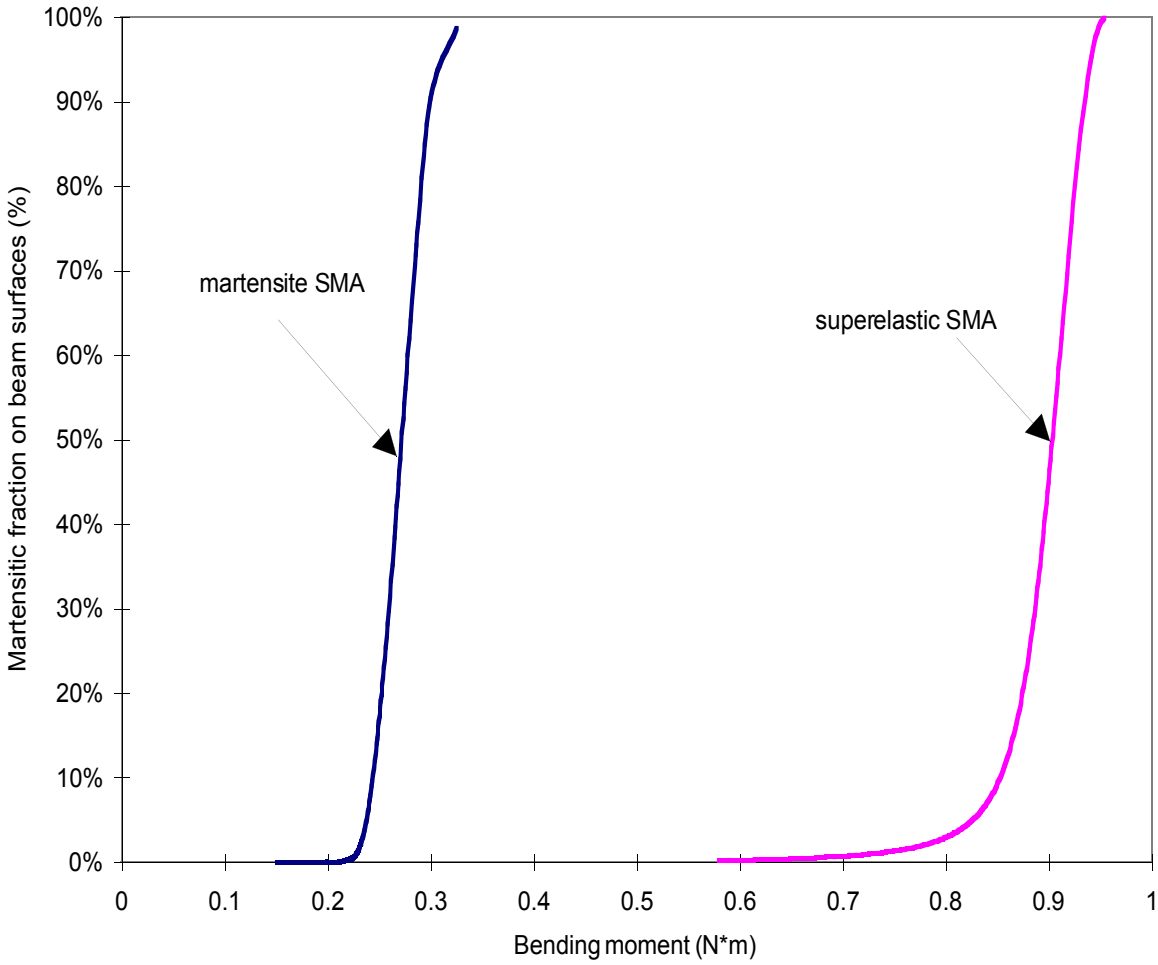

Figure 2.10. Martensitic fraction vs bending moment.

Fig. 2.9 shows the relationship between the strain energy absorption and the bending moment applied to the SMA beam. It can be seen that before the martensitic phase transformation starts, the strain energy increases very slowly with the applied bending moment, and thereafter, the strain energy increases rapidly with the applied bending moment. It is clear that super-elastic SMA can withstand more bending moment and absorb more strain energy than the martensitic SMA.

The results in Fig. 2.9 are confirmed by Fig. 2.10, which shows the relationship between the martensite fraction and the bending moment. Indeed, it can be observed that the martensite fraction increases rapidly with little moment increase after the bending moment exceeded the martensitic phase transformation threshold.

2.4.2 Tension Case

In this section, the results of the strain energy absorption capabilities of an SMA bar loaded in tension are presented. In Fig. 2.11, the strain energy absorbed in tension increases with the martensite fraction in a very similar way to the bending loading case presented in Fig. 2.8. However, the maximum strain energy absorbed is much higher for the tension loading (16 J) than for the bending loading (6.5 J) since the martensitic phase transformation occurs uniformly through the bar thickness, as opposed to only part of the beam thickness for the bending loading case. Again, the superelastic SMA absorbs more energy than the martensitic SMA for the same reasons mentioned earlier.

In the last figure (Fig. 2.12), the relationship between the strain energy due to tension and the stress of SMA bar is presented. Again, the similarities with the bending loading case can be observed: the super-elastic SMA can absorb more strain energy than the martensitic SMA and most of the strain-energy is absorbed after the martensitic phase transformation has been initiated.

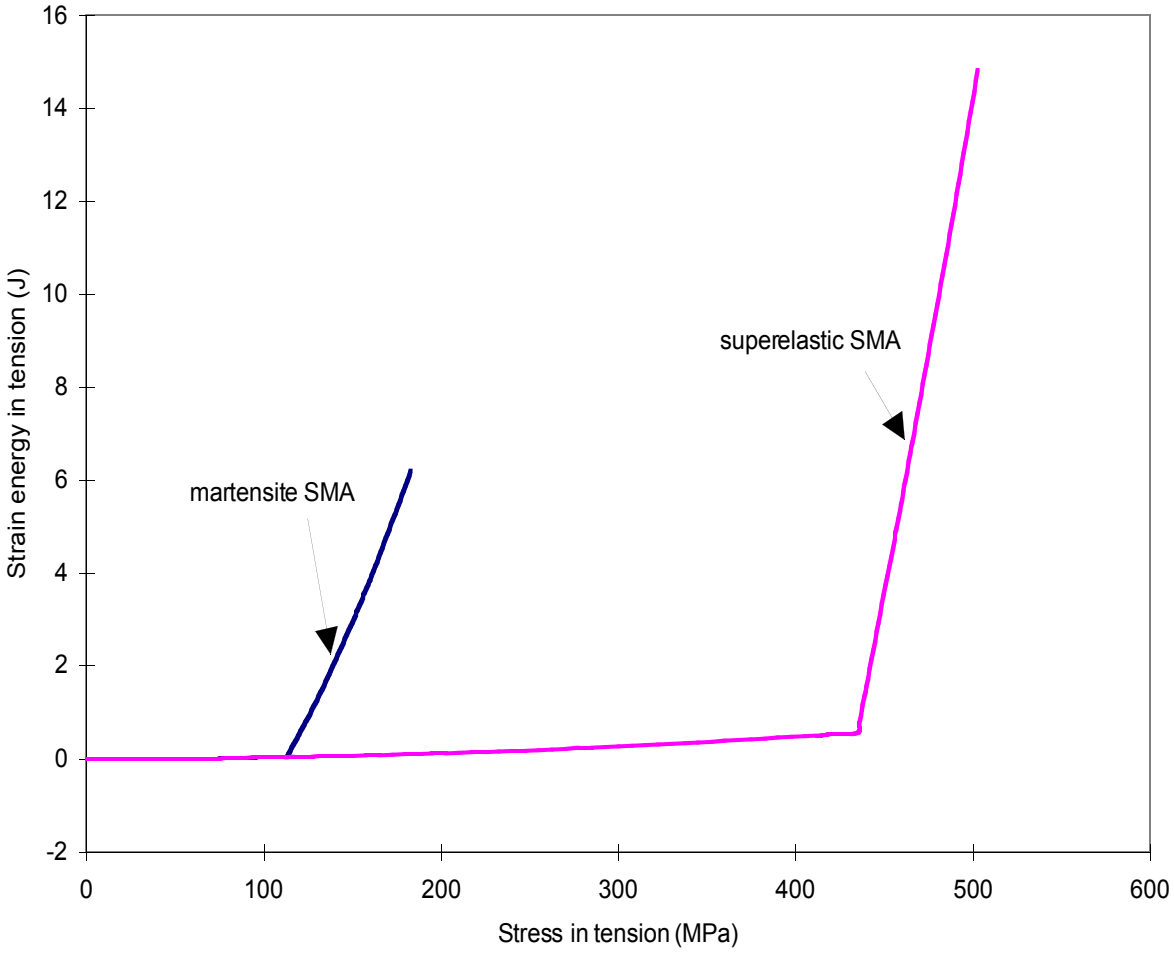

Figure 2.11. Strain energy vs stress in tension.

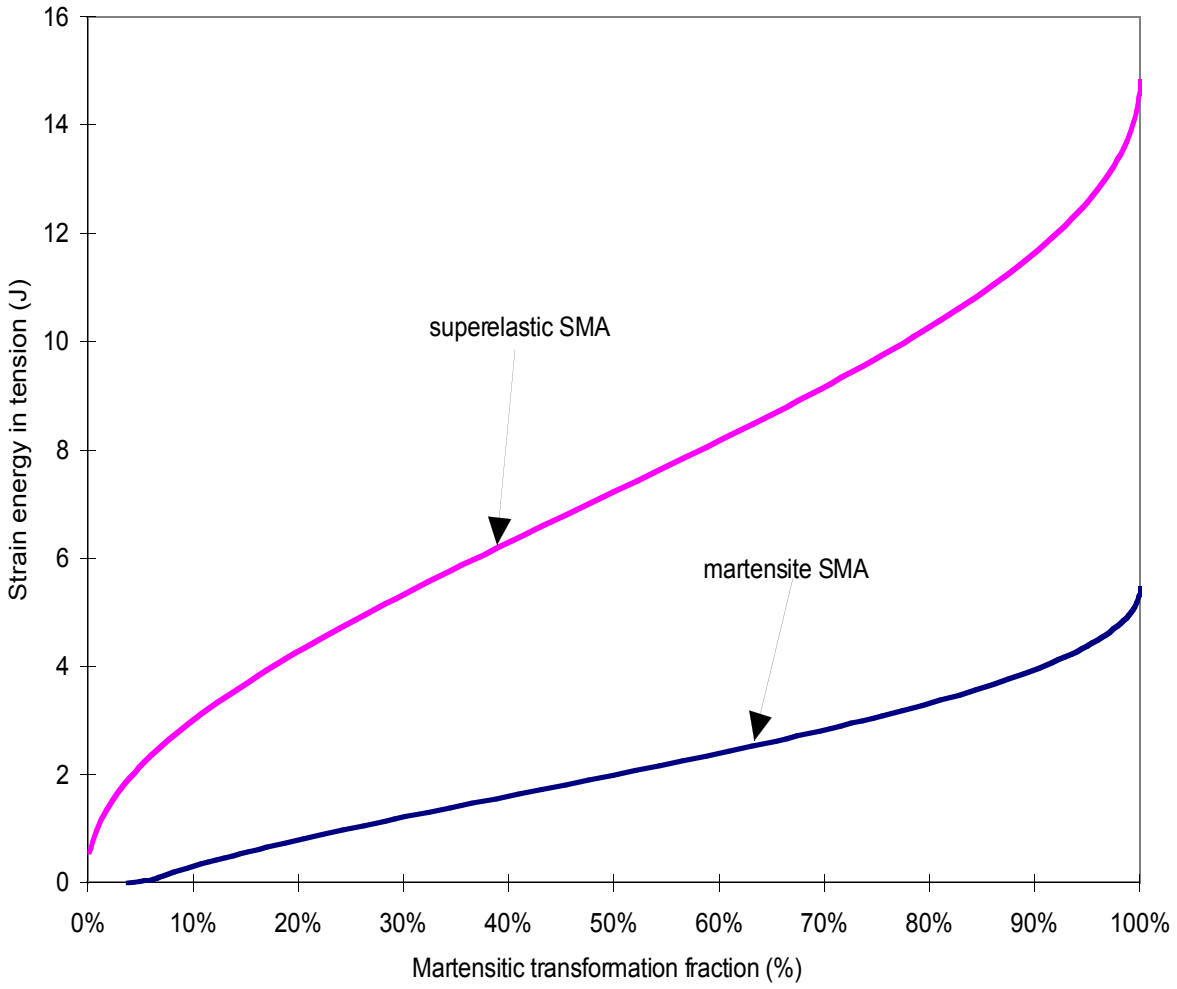

Figure 2.12. Strain energy vs Martensitic fraction in tension.

2.5 Conclusion and Summary

In this chapter, the strain energy absorption of shape memory alloy bars and beams under tension and bending loading was studied. This theoretical model can give quantitative relations between the martensite fraction, the applied load, and the strain energy absorbed in the SMA. The theoretical relations are only valid in the elastic range, stopping at the end of the martensitic phase transformation where the plastic deformation begins. As expected, the super-elastic SMA has demonstrated a high strain energy absorption capability. Also, the SMA shows a highly nonlinear relation between the martensite fraction, the applied load, and the strain energy absorbed in the SMA. The closed form solution of the strain energy absorption capability of SMA bars is a simple and useful tool in the design of energy absorption applications of super-elastic SMA. The model also gives, the threshold load for initiating and completing the martensitic phase transformation both for tension and bending loading. In this chapter, the advantage of using super-elastic SMA to absorb strain energy compared to martensitic SMA was demonstrated numerically. The results and conclusions obtained in this chapter are the first reported research in the strain energy absorption of super-elastic SMA, which is the contribution of this research.

Chapter Three

Nonlinear Equations for SMA Hybrid Composite Laminates

3.1 Introduction

To this date, the research on impact of SMA hybrid composites has been experimental. The increased energy absorption capabilities of the SMA hybrid composite were attributed to the martensite phase transformation in SMA. Super-elastic SMA fibers has good strain energy absorption capability. In order to understand the mechanisms in the SMA hybrid composite under low velocity impact or quasi-static contact loading, and the energy transfer between the impactor and the composite, analytical models are needed.

SMA hybrid composites have been studied for shape memory effects, actuators and shape control [77-79]. Such applications use the shape memory effect of SMA, which is the ability to recover its original shape upon heating above a certain phase transformation temperature. SMA has a phase transformation from martensite to austenite, starting at the austenite start temperature and ending at the austenite finish temperature. An SMA in the temperature which is below the martensitic start temperature, when plastically deformed and with the external stresses removed, will recover its original shape when heated. In all of the above, the shape memory and thermal effects are utilized. Such SMA hybrid composites are fabricated by embedding SMA fibers along the same direction with graphite fibers. To model the SMA hybrid composites, some researchers have proposed a few micromechanics constitutive models [80]. These models were proposed to study the temperature effects, not the super-elastic effects and the energy absorption mechanisms.

There is a linear shell theory of SMA composites [81] and linear plate theory of SMA composites [79]. However, the nonlinear plate theory of SMA composite which can be used for impact and contact analysis is not available yet.

The linear theory of small displacements of plates assumes infinitesimal displacements and provides accurate results only for very small displacements. The linear theory gives good results when the composite plates have small deflections under low velocity impact or quasi-static contact loading [11, 12].

However, when the deflections are the same order of magnitude as the thickness of the plate, the results are inaccurate. The impact response predicted by the linear theory can show poor correlation with experimental data under certain conditions, such as for a firmly clamped thin plate impacted by a relatively large impactor. In addition, plate deflection obtained from the experimental results were on the order of several laminate thickness which violated the assumptions of the linear theory. The geometrical nonlinearity accounting for the membrane stiffening effect has to be considered in order to have better predictions.

A general geometrical nonlinearity in the plate without shear deformation has been described by Chia [82] and whitney [83] and known as Von Karman nonlinear plate theory. A nonlinear laminated plate theory with shear deformation can be derived from the three-dimensional nonlinear theory of elasticity by combining Timoshenko-type theory and Von Karman nonlinear plate theory as described by Reddy [84, 85].

In order to make the equations general, we will derive the nonlinear equations for SMA hybrid composite plate, which can be used for low velocity impact or quasi-static contact loading, although the linear theory may give satisfactory results in some cases. Such nonlinear equations for SMA hybrid composites have not been found in the literature, thus, we will present these equations in this chapter. These equations are of general interests, other than the applications in the following chapters.

3.2 Statement of the Problem

In the present study, nonlinear SMA hybrid composite laminated equations with the first order shear deformation will be developed by using virtual work principle. The resulting plate equations are general in nature, and can be simplified according to the particular applications.

The following assumptions are made to develop the governing equations:

a. The strain–displacement relations are nonlinear. The second-order terms at the mid-plane are considered;
b. Through-the thickness strain, ε_{33} , is negligible, and the lateral displacement, w, is a function of in-plane coordinates, x and y, only.
c. The first order shear deformation is considered.
d. To avoid the lengthy computation, higher order shear deformation is neglected.

For SMA hybrid composite laminates under low velocity impact or quasi-static contact loading, It can classified into two categories. First, the load level is low, and the laminates have small deflection compared to their thickness, thus the linear theory applies. The other case is that the load level is large and the laminates undergo large deflections, thus the nonlinear theory has to be used.

It was found that the location and type of failure for a dynamically loaded composite laminate in low velocity impact or quasi-static loading were similar to those for a laminate loaded statically. A quasi-static model developed by Wen, et al. [86] in 1995 successfully predicted the dynamic response and failure of clamped metal beam subjected to the low velocity impact. For both of the cases in low velocity impact or quasi-static contact loading, dynamic effect is negligible [21], [27]. We will adopt their approach to formulate the nonlinear governing equations for SMA composite plates.

The nonlinear plate equations are derived basing on the shear deformation theory of plate developed by Reddy [85].

3.3 Displacement Field

A rectangular composite plate with dimensions length a, width b and the thickness h. The coordinates are chosen in such a way that x-y plane coincides with the mid-plane of the plate, and the z –axis is perpendicular to that plane as shown in Fig. 3.1.

Considering the first-order shear deformation which assumes that cross-section remain planar but not normal to the plate mid-plane during deformation, a linear variation of the displacements is assumed through the thickness for the shear deformation.

Thus, the displacement fields are

$$\begin{Bmatrix} u_1(x,y,z) \\ u_2(x,y,z) \\ u_3(x,y) \end{Bmatrix} = \begin{Bmatrix} u(x,y) + z\phi_x(x,y) \\ v(x,y) + z\phi_y(x,y) \\ w(x,y) \end{Bmatrix} \tag{3.1}$$

Where u_1, u_2, u_3 are the displacements in x, y, z direction, respectively. *u, v* and *w* are the displacements of the mid-plane of the plate in *x*, *y* and *z* direction respectively. ϕ_x and ϕ_y are the shear deformations (rotations) in x-z and y-z planes due to bending through the thickness of the plate.

3.4 Strain-Displacement Relations

The linear theory of plate is based on the assumptions that the deflection of the plate is small, and thus the displacements are infinitesimal. When the deflections are as large as the thickness of the plate, the results predicted by linear theory are inaccurate. The large deflection theory of plate was developed by Von Karman, and the assumptions are as follows:

The plate is thin. The thickness h is much smaller than the plate dimension. The magnitude of the deflection is of the same order as the thickness of the plate, but small compared with the plate dimensions.

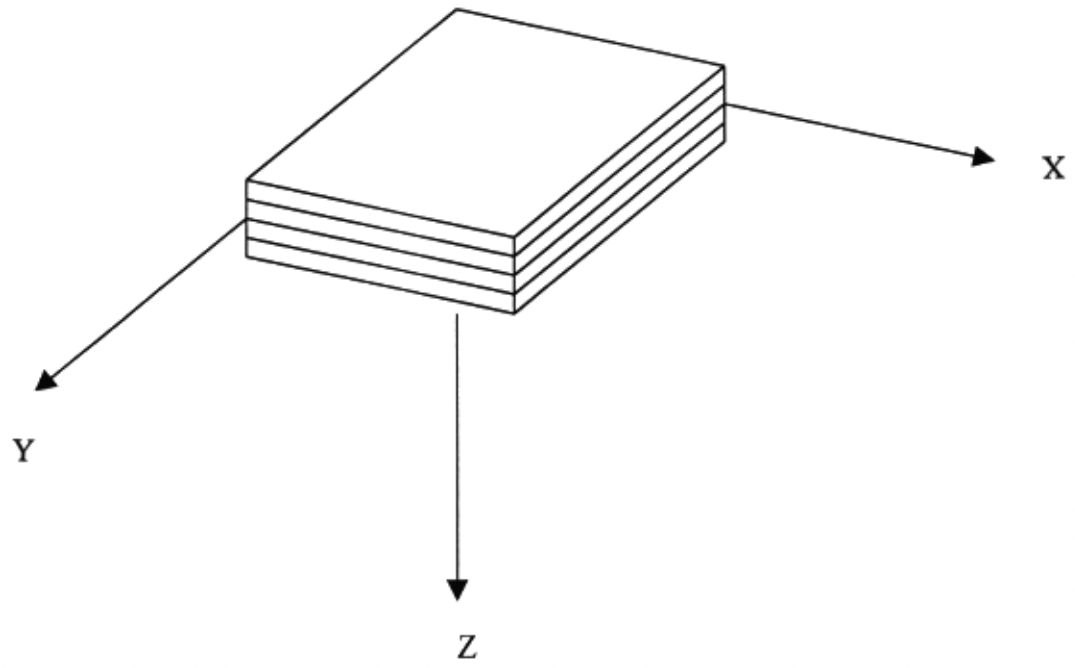

Figure 3.1 Coordinates of composite laminates.

Only the nonlinear terms that have w_x and w_y are retained. The higher order terms of u, v, ϕ_x, and ϕ_y are negligible in the Green' strain tensor.

Thus, the strains in the mid-plane of the plate are:

$$\begin{Bmatrix} \varepsilon_1^0 \\ \varepsilon_2^0 \\ \varepsilon_6^0 \end{Bmatrix} = \begin{Bmatrix} u_{,x} + \frac{1}{2}(w_{,x})^2 \\ v_{,y} + \frac{1}{2}(w_{,y})^2 \\ u_{,y} + v_{,x} + w_{,x} w_{,y} \end{Bmatrix} \tag{3.2}$$

These relations account for the geometric nonlinearity of the second order in the mid-plane.

The curvatures in the mid-plane of the plate are:

$$\begin{Bmatrix} k_1^0 \\ k_2^0 \\ k_6^0 \end{Bmatrix} = \begin{Bmatrix} \phi_{x,x} \\ \phi_{y,y} \\ \phi_{x,y} + \phi_{y,x} \end{Bmatrix} \tag{3.3}$$

From above two sets of equation, we have the strains in the plate through the thickness as follows:

$$\begin{Bmatrix} \varepsilon_1 \\ \varepsilon_2 \\ \varepsilon_6 \end{Bmatrix} = \begin{Bmatrix} \varepsilon_1^0 + zk_1^0 \\ \varepsilon_2^0 + zk_2^0 \\ \varepsilon_6^0 + zk_6^0 \end{Bmatrix} \tag{3.4}$$

and the shear strain

$$\begin{Bmatrix} \varepsilon_4^0 \\ \varepsilon_5^0 \end{Bmatrix} = \begin{Bmatrix} \phi_y + w_{,y} \\ \phi_x + w_{,x} \end{Bmatrix} \tag{3.5}$$

$$\begin{Bmatrix} \varepsilon_4 \\ \varepsilon_5 \end{Bmatrix} = \begin{Bmatrix} \varepsilon_4^0 \\ \varepsilon_5^0 \end{Bmatrix} \tag{3.6}$$

3.5 Constitutive Relations

The SMA composite laminate consists of N thin orthotropic layers perfectly bonded together. The ith ply is oriented at an angle θ_i with respect to the plate coordinate axes. The constitutive equations for this particular ply can be written in terms of the material principal directions as

$$\begin{Bmatrix} \overline{\sigma}_1 \\ \overline{\sigma}_2 \\ \overline{\sigma}_6 \end{Bmatrix}_i = \begin{bmatrix} \overline{Q}_{11} & \overline{Q}_{12} & 0 \\ \overline{Q}_{12} & \overline{Q}_{22} & 0 \\ 0 & 0 & \overline{Q}_{66} \end{bmatrix}_i \begin{Bmatrix} \overline{\varepsilon}_1 \\ \overline{\varepsilon}_2 \\ \overline{\varepsilon}_6 \end{Bmatrix}_i \tag{3.7}$$

and

$$\begin{Bmatrix} \overline{\sigma}_4 \\ \overline{\sigma}_5 \end{Bmatrix}_i = \begin{bmatrix} \overline{Q}_{44} & 0 \\ 0 & \overline{Q}_{55} \end{bmatrix}_i \begin{Bmatrix} \overline{\varepsilon}_4 \\ \overline{\varepsilon}_5 \end{Bmatrix}_i \tag{3.8}$$

where the plane-stress reduced stiffness coefficients in the material axes of the ply are given by Jones [87]. The ply stress-strain relations can be written in terms of the stresses and strains in the laminate coordinates as follows:

$$\begin{Bmatrix}\sigma_1\\ \sigma_2\\ \sigma_6\end{Bmatrix}_i = \begin{bmatrix}Q_{11} & Q_{12} & Q_{16}\\ Q_{12} & Q_{22} & Q_{26}\\ Q_{16} & Q_{26} & Q_{66}\end{bmatrix}_i \begin{Bmatrix}\varepsilon_1\\ \varepsilon_2\\ \varepsilon_6\end{Bmatrix}_i \tag{3.9}$$

and

$$\begin{Bmatrix}\sigma_4\\ \sigma_5\end{Bmatrix}_i = \begin{bmatrix}Q_{44} & Q_{45}\\ Q_{45} & Q_{55}\end{bmatrix}_i \begin{Bmatrix}\varepsilon_4\\ \varepsilon_5\end{Bmatrix}_i \tag{3.10}$$

where the transformed stiffness coefficients are given by Jones [87].

There are two kinds of ply (lamina) in the laminate. One is the SMA/matrix lamina, the other is host lamina. Due to the uniqueness of SMA/matrix, we give the constitutive equations of this lamina here.

SMA/Epoxy Lamina:

In this section, the SMA/Matrix such as SMA/Epoxy lamina will be considered in two aspects. (i) the SMA constitutive equations, and (ii) the elastic properties of the SMA/Matrix lamina. In this application, the SMA is super-elastic, i.e. it has 100% austenite when no load is applied.

We use the SMA constitutive equation in chapter two as the basic constitutive relations of SMA in SMA/Matrix lamina. This piece wise linear strain hardening relation can be easily used in the laminate equations. The other way is to use the constitutive equation by Brinson [59].

Therefore, there are two different phase of SMA during the loading. SMA fibers starts from 100% austenite reach the martensite start point at critical strain or stress and continue to change to martensite due to the stress-induced phase transformation.

Lamina Elastic Properties:

We use the method proposed by Saravanos, et al.[80] for the micromechanics modeling of SMA hybrid composites. According to this method, a representative cell is divided into a set of subregions, each one containing portions of an SMA fiber and the matrix. It is further assumed that the strain and stress in the various regions of the representative cell are constant, that the Poisson's effect on transverse deformations is negligible, and that the SMA fibers are packed in a square array formation. The analysis uses a mechanics of materials approach based on the equilibrium of stresses within each region and the compatibility of strains at the boundaries of each region. The mechanical properties in the third direction are the same as those in the second because they are obtained by assuming that the ply is transversely isotopic in the 2-3 plane. Therefore, a total of five independent elastic constants are required. Note that the SMA is an isotropic material.

The resultant equations for the elastic properties of the SMA/epoxy lamina are for the longitudinal modulus:

$$E_{c11} = k_{SMA}E_{SMA} + k_m E_m \tag{3.11}$$

the transverse modulus:

$$E_{c22} = E_{c33} = \frac{E_m}{1-\sqrt{k_{SMA}}\left(1-E_m/E_{SMA}\right)} \tag{3.12}$$

the shear modulus:

$$G_{c12} = G_{c13} = \frac{G_m}{1-\sqrt{k_{SMA}}\left(1-G_m/G_{SMA}\right)} \tag{3.13}$$

$$G_{c23} = \frac{G_m}{1-k_{SMA}\left(1-G_m/G_{SMA}\right)} \tag{3.14}$$

and the Poisson's ratio:

$$\nu_{c12} = \nu_{c13} = k_{SMA}\nu_{SMA} + k_m\nu_m \tag{3.15}$$

$$\nu_{c23} = k_{SMA}\nu_{SMA} + k_m\left(2\nu_m - \frac{\nu_{c12}}{E_{c11}}E_{c22}\right) \tag{3.16}$$

where E_{c11}, E_{c22}, E_{c33} are the module of SMA/epoxy lamina in 1, 2, 3 direction, respectively; G_{c12}, G_{c13}, G_{c23} are the shear module of SMA/epoxy lamina in 1-2, 1-3, 2-3 planes, respectively; and ν_{c12}, ν_{c13}, ν_{c23} are the Poisson's ratio of SMA/epoxy lamina in 1-2, 1-3, 2-3 planes, respectively. k_{SMA} is the SMA fiber volume fraction in the SMA/epoxy lamina. Finally, E_m, G_m, ν_m and k_m are the Young's modulus, shear modulus, Poisson's ratio, and volume fraction of epoxy matrix in the SMA/epoxy lamina, which is equal to 1- k_{SMA}.

With the material properties of SMA/epoxy lamina (Equations 3.11-3.16) as well as the material properties of graphite/epoxy lamina, the stiffness coefficients of the SMA composite laminates can be calculated.

3.6 Contact Constraints

For the laminated composite subjected the transverse impact or contact loading, the contact constraints needs to be specified to formulate the problem. In this chapter, we derive the equations assuming that the SMA hybrid composites have their structural integrity, so the conventional plate theory applies.

Here we consider the normal contact between the impactor and SMA composites. Thus, in order to prevent the contact surfaces from overlapping, an impenetrability condition must be specified and satisfied along the contact interfaces. This condition

requires that the shortest distance, the gap g, between two contact surfaces must be grearter than or equal to zero. The Kuhn-Tucker conditions for normal contact states

$$\begin{aligned} &\lambda_N \le 0; \\ &g(u_i) \ge 0; \\ &\lambda_N g(u_i) = 0. \end{aligned} \tag{3.17}$$

The first inequality states that upon contact, the contact must be less than or equal zero. The second inequality states that the shortest distance, the gap g, between two contact surfaces must be greater than or equal to zero. The equation states that the pressure is nonzero only when g = 0.

The contact we consider here are cylinder contact and sphere contact. For the specific problem, we will use cylinder contact relation or spheres contact relations, as demonstrated in the following chapters.

3.7 Virtual Work

The total potential energy consists of the strain energy of the SMA composite plate and the work done by the external impact or contact force denoted by F_c . The potential energy is

$$V = \frac{1}{2}\int_{-h/2}^{h/2}\int_A \left(\sigma_1\varepsilon_1 + \sigma_2\varepsilon_2 + \sigma_6\varepsilon_6 + \sigma_4\varepsilon_4 + \sigma_5\varepsilon_5\right) dA dZ \quad -\int_A F_c w dA \tag{3.18}$$

Substituting equations 3.9 and 3.10 into equation above and integrating over the thickness of the plate, we have the strain energy as follows:

$$U = \frac{1}{2}\int_A \left\{ N_1(u_{,x} + \frac{1}{2}w_{,x}^2) + N_2(v_{,y} + \frac{1}{2}w_{,y}^2) + N_6(u_{,y} + v_{,x} + w_{,x}w_{,y}) + M_1\phi_{x,x} + M_2\phi_{y,y} \right\} dA$$
$$+ \frac{1}{2}\int_A \left\{ M_6(\phi_{x,y} + \phi_{y,x}) + Q_2(\phi_y + w_{,y}) + Q_1(\phi_x + w_{,x}) \right\} dA$$

(3.19)

Potential energy as follows

$$V = \int_A F_c w dA \tag{3.20}$$

where N_i , M_i , Q_i are the stress resultants and defined as follows

$$(N_i, M_i) = \int_{-h/2}^{h/2} \sigma_i(1, z) dz, \quad (i = 1,2,6) \tag{3.21}$$

$$Q_2 = \int_{-h/2}^{h/2} \sigma_4 dz \tag{3.22}$$

$$Q_1 = \int_{-h/2}^{h/2} \sigma_5 dz \tag{3.23}$$

N_i are the in-plane resultant forces, M_1 and M_2 are moments due to bending, M_6 is the moment due to twisting, Q_i are the transverse shear forces.

The relations between above resultant forces and the total strains are as follows

$$\begin{Bmatrix} N_1 \\ N_2 \\ N_6 \\ M_1 \\ M_2 \\ M_6 \end{Bmatrix} = \begin{bmatrix} A_{11} & A_{12} & A_{16} & B_{11} & B_{12} & B_{16} \\ A_{12} & A_{22} & A_{26} & B_{12} & B_{22} & B_{26} \\ A_{16} & A_{26} & A_{66} & B_{16} & B_{26} & B_{66} \\ B_{11} & B_{12} & B_{16} & D_{11} & D_{12} & D_{16} \\ B_{12} & B_{22} & B_{26} & D_{12} & D_{22} & D_{26} \\ B_{16} & B_{26} & B_{66} & D_{16} & D_{26} & D_{66} \end{bmatrix} \begin{Bmatrix} \varepsilon_1^0 \\ \varepsilon_2^0 \\ \varepsilon_6^0 \\ k_1^0 \\ k_2^0 \\ k_6^0 \end{Bmatrix} \tag{3.24}$$

$$\begin{Bmatrix} Q_2 \\ Q_1 \end{Bmatrix} = \begin{bmatrix} A_{44} & A_{45} \\ A_{45} & A_{55} \end{bmatrix} \begin{Bmatrix} \varepsilon_4^0 \\ \varepsilon_5^0 \end{Bmatrix} \tag{3.25}$$

$$\begin{Bmatrix} N \\ M \end{Bmatrix} = \begin{bmatrix} A & B \\ B & D \end{bmatrix} \begin{Bmatrix} \varepsilon^0 \\ k \end{Bmatrix} \tag{3.26}$$

In which, {N} are in-plane resultant forces, {M} are resultant moments. [A], [B] and [D] are the stiffness matrices, and are given by:

$$\left(A_{ij}, B_{ij}, D_{ij}\right) = \int_{-h/2}^{h/2} (1, z, z^2) Q_{ij} dz, \ (i, j = 1, 2, 6) \tag{3.27}$$

$$(A_{ij}, D_{ij}) = \int_{-h/2}^{h/2} Q_{ij} (1, z^2) dz, \ (i, j = 4, 5) \tag{3.28}$$

Thus, the total potential energy of the laminated composite plate is:

$$\Pi = U + V \tag{3.29}$$

We use the principle of virtual work to derive the governing equations.

$$\delta\Pi = 0 \tag{3.30}$$

That is

$$\begin{aligned}
&\int_A \left\{ N_1(\delta u_{,x} + w_{,x}\delta w_{,x}) + N_2(\delta v_{,y} + w_{,y}\delta w_{,y}) + N_6(\delta u_{,y} + \delta v_{,x} + \delta w_{,x} w_{,y} + w_{,x}\delta w_{,y}) \right\} dA \\
&\quad + \int_A \left\{ M_1 \delta\phi_{x,x} + M_2 \delta\phi_{y,y} \right\} dA \\
&\quad + \int_A \left\{ M_6(\delta\phi_{x,y} + \delta\phi_{y,x}) + Q_2(\delta\phi_y + \delta w_{,y}) + Q_1(\delta\phi_x + \delta w_{,x}) \right\} dA - \int_A F_c \delta w dA = 0
\end{aligned} \tag{3.31}$$

3.8 Nonlinear Equations of SMA Composite Laminates

Integrating the terms in above equation by parts, assigning zero to each of the coefficients of δu , δv , δw , $\delta\phi_x$ and $\delta\phi_y$, we have the governing equations of SMA composite plate as follows

$$\delta u: \qquad N_{1,x} + N_{6,y} = 0 \tag{3.32}$$

$$\delta v: \qquad N_{6,x} + N_{2,y} = 0 \tag{3.33}$$

$$\delta w: \qquad \begin{aligned} &N_{1,x}w_{,x} + N_1 w_{,xx} + N_{6,x}w_{,y} + 2N_6 w_{,xy} \\ &+N_{6,y}w_{,x} + N_{2,y}w_{,y} + N_2 w_{,yy} \\ &+Q_{1,x} + Q_{2,y} - F_c = 0 \end{aligned} \tag{3.34}$$

$$\delta\phi_x: \qquad M_{1,x} + M_{6,y} - Q_1 = 0 \tag{3.35}$$

$$\delta\phi_y: \qquad M_{2,y} + M_{6,x} - Q_2 = 0 \tag{3.36}$$

The boundary conditions are as one set of the following forms, which are specified:

$$u_n = un_x + vn_y \text{ or} N_n = N_1 n_x^2 + N_2 n_y^2 + 2N_6 n_x n_y \tag{3.37}$$

$$u_{ns} = -un_y + vn_x \text{ or} N_{ns} = (N_2 - N_1) n_x n_y + N_6 (n_x^2 - n_y^2) \tag{3.38}$$

$$w \text{ or} Q_n = Q_1 n_x + Q_2 n_y \tag{3.39}$$

$$\phi_n \text{or} M_n = M_1 n_x^2 + M_2 n_y^2 + 2M_6 n_x n_y \tag{3.40}$$

$$\phi_{ns} \text{or} M_{ns} = (M_2 - M_1) n_x n_y + M_6 (n_x^2 - n_y^2) \tag{3.41}$$

The SMA hybrid composite plate with large deflection and contact loading can be described by above equations. The piece-wise linear constitutive equations of SMA may be used, and two kinds of contact, cylinder contact and sphere contact can be included with the contact laws. The equations are general which can be applied to the specific applications, such as different angle ply, symmetric or anti-symmetric with different boundary conditions, and different location of SMA lamina.

3.9 Conclusion and Summary

The nonlinear equations for SMA hybrid composite plate, which can be used for low velocity impact or quasi-static contact loading, are derived. The governing equations include the transverse shear deformation to the first order, large deformation of the plates, and SMA/matrix lamina. The equations are derived in the general form with general boundary conditions, general stack of angle ply. The equations can be simplified to special forms in the specific applications. Such nonlinear equations for SMA hybrid composites have not been found in the literature. It is the contribution of this research.

Chapter Four

Theoretical Study of Strain Energy Absorption of SMA Hybrid Composite Beam Under Low Velocity Impact

4.1 Introduction

The impact on composite structures has been studied since the 1970s. Many models were developed for all ranges of velocities, but a greater effort was made towards low-velocity impact, as summarized in chapter one. A comprehensive review of the impact on composites can be found in the literature [21], [27].

To predict the impact force of a impactor, the theoretical models available usually include the contact deformation α by using the Hertz contact equation. The contact deformation α is the measure of how close the centers of the beam and the projectile approach each other. The impact force P and the contact deformation are related by the Hertz contact law. During the contact, the impact force P acts over an area of contact between the impactor and beam. The area of contact depends on the force and module of the impactor and beam. Because the area of contact is small, it is generally assumed that the impact force is centrally concentrated.

Solving the problem of low-velocity impact on composite laminates involves a three-dimensional nonlinear analysis of a central mass attached to the laminate through a Hertizian spring. This approach is complex, costly and sometimes numerically intractable. To avoid this difficulty, many researchers developed simpler and more efficient models [21], [27]. Among these, the energy balance model has been proven to be a simple and efficient way for predicting the impact force and energy transfer at low velocities.

4.2 Objectives of This Study

The objectives of this chapter are to study the an SMA hybrid composite beam subjected to low-velocity impact while no damage occur in the beam, determine the impact force, the strain energy absorption, contact energy, and the effect of martensitic transformation of the SMA fibers on the energy absorption. This study is the first effort on analyzing the low velocity impact of SMA hybrid composites. It is of theoretical interest, and to lay the basis for the following chapter, which is the modeling of the damage and failure of SMA composites, and the effect of stress-induced martensitic transformation of the SMA on the behavior of SMA composites during the failure process.

4.3 Statement of the Problem

A steel spherical nose impactor of radius R_p, mass M_p, and velocity V_p impacting the center of a super-elastic SMA/graphite/epoxy hybrid composite beam of width b, length L, and thickness t_b under clamped-clamped boundary condition is studied [88]. The laminated composite beam is made up of cross-ply graphite/epoxy layers and two plies of super-elastic SMA/epoxy placed on the top and bottom surfaces of the graphite/epoxy beam. The bottom surface SMA/epoxy lamina is included to keep the SMA hybrid composite beam symmetric. The SMA fibers embedded in the epoxy matrix run along the length of the beam (Fig. 4.1). The plies are assumed to be perfectly bonded, without any delamination or voids in the composites. The velocity of the projectile is low, so the impact process is assumed to be quasi-static as proposed by Wen [86]. Also, the impact energy level is low so that there is no damage occur in the beam, or it is negligible. Thus, the analysis proposed in this chapter is belong to the first category of impact modeling summarized in Chapter 1.

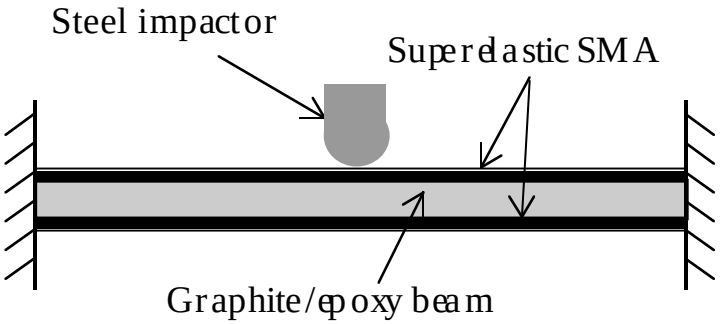

Figure 4.1 Schematic of the SMA composite beam under low velocity impact.

The method proposed in this chapter is developed based on the energy balance principle. The analysis will include three kinds of deformation in the composite beam occurring during low velocity impact: (i) contact deformation α, (ii) transverse deformation w, which is measured at the mid-surface, and (iii) transverse shear deformation ψ. Also, the martensitic transformation of the SMA fibers will be included in the energy balance to study its effect on the SMA/graphite/epoxy hybrid composite beam.

4.4 SMA Hybrid Composite Lamina

Following the method proposed in chapter three, we can easily develop a model for SMA/Epoxy lamina. In this section, the SMA constitutive equations will be presented, then the constitutive relations of SMA/epoxy lamina will be obtained.

SMA Constitutive Equation:

In this application, the SMA is super-elastic, i.e. it has 100% austenite when no load is applied. Two kinds of constitutive equations can be used, one is the piece-wise linear model proposed in chapter two, which is obtained from Brinson's model [59]. This model can significantly reduce the computation task. The other one is Brinson's model, which requires more computational efforts.

Using Brinson's model, we have the constitutive equation of the SMA for this particular application with the martensitic phase fraction ξ is:

$$\sigma = E_{SMA}(\xi)\varepsilon + \Omega(\xi)\xi \tag{4.1}$$

In equation 4.1, the Young's modulus function $E_{SMA}(\xi)$ is given by:

$$E_{SMA}(\xi) = E_a + \xi(E_m - E_a) \tag{4.2}$$

where E_m and E_a are the martensite and austenite modulus of the SMA, respectively, and the transformation tensor $\Omega(\xi)$ is given by:

$$\Omega(\xi) = -\varepsilon_L E_{SMA}(\xi) \tag{4.3}$$

where ε_L is the maximum residual strain. Martensitic transformation fraction ξ varies from 0 to100%.

Constitutive Relations of SMA Composite Lamina:

Using the results obtained in chapter three, we have a total of five independent elastic constants are required. Since the SMA is an isotropic material, $E_{SMA11}(\xi) = E_{SMA22}(\xi) = E_{SMA}(\xi)$; $G_{SMA12}(\xi) = G_{SMA23}(\xi) = G_{SMA}(\xi) = \frac{E_{SMA}(\xi)}{2(1+\nu_{SMA})}$ and $\nu_{SMA12} = \nu_{SMA23} = \nu_{SMA}$, where $E_{SMA}(\xi)$ is obtained from equation 4.2.

The resultant equations for the elastic properties of the SMA/epoxy lamina are for the longitudinal modulus:

$$E_{c11} = k_{SMA}E_{SMA} + k_m E_m \tag{4.4}$$

the transverse modulus:

$$E_{c22} = E_{c33} = \frac{E_m}{1-\sqrt{k_{SMA}}\left(1-E_m/E_{SMA}\right)} \tag{4.5}$$

the shear modulus:

$$G_{c12} = G_{c13} = \frac{G_m}{1 - \sqrt{k_{SMA}}\left(1 - G_m / G_{SMA}\right)} \tag{4.6}$$

$$G_{c23} = \frac{G_m}{1 - k_{SMA}\left(1 - G_m / G_{SMA}\right)} \tag{4.7}$$

and the Poisson's ratio:

$$\nu_{c12} = \nu_{c13} = k_{SMA}\nu_{SMA} + k_m\nu_m \tag{4.8}$$

$$\nu_{c23} = k_{SMA}\nu_{SMA} + k_m\left(2\nu_m - \frac{\nu_{c12}}{E_{c11}}E_{c22}\right) \tag{4.9}$$

where E_{c11}, E_{c22}, E_{c33} are the module of SMA/epoxy lamina in 1, 2, 3 direction, respectively; G_{c12}, G_{c13}, G_{c23} are the shear module of SMA/epoxy lamina in 1-2, 1-3, 2-3 planes, respectively; and ν_{c12}, ν_{c13}, ν_{c23} are the Poisson's ratio of SMA/epoxy lamina in 1-2, 1-3, 2-3 planes, respectively. k_{SMA} is the SMA fiber volume fraction in the SMA/epoxy lamina. Finally, E_m, G_m, ν_m and k_m are the Young's modulus, shear modulus, Poisson's ratio, and volume fraction of epoxy matrix in the SMA/epoxy lamina, which is equal to 1- k_{SMA}.

4.5 Formulation of SMA Hybrid Composite Beam

Following the method proposed in chapter three, the governing equations of the SMA hybrid composite beam will be briefly derived. Due to the assumption that the impact energy level is low, and the deflection of the beam is small, the linear theory of

the beam is used here. The Timoshenko beam theory will be used to include the first-order shear deformation, i.e., the interlaminar shear strains are not neglected. Thus, the displacement fields of the SMA hybrid composite beam are as follows:

$$\begin{aligned} u &= z\psi_x(x) \\ v &= 0 \\ w &= w(x) \end{aligned} \tag{4.10}$$

where u is the in-plane displacement along the beam centroid, v is the displacement along the width of the beam, w is the transverse displacement through the thickness of the beam, and ψ_x is the transverse shear deformation of the beam.

The strain-displacement relations can be obtained from equation 4.10. The in-plane and transverse shear strains are given by equation 4.11 and equation 4.12, respectively:

$$\begin{Bmatrix} \varepsilon_x \\ \varepsilon_y \\ \gamma_{xy} \end{Bmatrix} = \begin{Bmatrix} z\kappa_x \\ 0 \\ 0 \end{Bmatrix} \tag{4.11}$$

$$\begin{Bmatrix} \gamma_{xz} \\ \gamma_{yz} \end{Bmatrix} = \begin{Bmatrix} \psi_x + w_{,x} \\ 0 \end{Bmatrix} \tag{4.12}$$

and the midplane curvatures are given by:

$$\begin{Bmatrix} \kappa_x \\ \kappa_y \\ \kappa_{xy} \end{Bmatrix} = \begin{Bmatrix} \psi_{x,x} \\ 0 \\ 0 \end{Bmatrix} \tag{4.13}$$

The SMA hybrid composite beam constitutive equation based on the first-order shear deformation theory can be expressed as:

$$\begin{Bmatrix} N \\ M \end{Bmatrix} = \begin{bmatrix} A & B \\ B & D \end{bmatrix} \begin{Bmatrix} \varepsilon \\ \kappa \end{Bmatrix} \tag{4.14}$$

and

$$\begin{Bmatrix} Q_y \\ Q_x \end{Bmatrix} = \begin{bmatrix} A_{44} & A_{45} \\ A_{45} & A_{55} \end{bmatrix} \begin{Bmatrix} \gamma_{yz} \\ \gamma_{xz} \end{Bmatrix} \tag{4.15}$$

where $\{N, M, Q\}$ are the resultant in-plane force vector, resultant bending moment vector, and resultant shear force vector, respectively, $\{\varepsilon\}$ is the midplane strain vector, and $\{\kappa\}$ is the curvature vector. For cross-ply SMA/graphite/epoxy laminated composite beam with the displacement field defined by equation 4.10, the resultant shear forces are:

$$\begin{aligned} Q_x &= A_{55}\gamma_{xz} \\ Q_y &= A_{45}\gamma_{xz} \end{aligned} \tag{4.16}$$

The laminate stiffness coefficients of the SMA hybrid composite beam are defined by:

$$\left(A_{ij}, B_{ij}, D_{ij}\right) = \int_{-h/2}^{h/2} \overline{Q}_{ij}(1, z, z^2)\, dz \quad (i,j=1,2,6) \tag{4.17}$$

and the additional stiffness coefficients involving transverse shear are defined by:

$$\left(A_{44}, A_{45}, A_{55}\right) = \int_{-h/2}^{h/2} \left(k_1^2 \overline{Q}_{44}, k_1 k_2 \overline{Q}_{45}, k_2^2 \overline{Q}_{55}\right) dz \tag{4.18}$$

where $\overline{Q}_{ij}$ are the transformed material constants and k_1 and k_2 are the shear correction factors for the transverse shear strains γ_{yz} and γ_{xz}, respectively [89].

The solution of a Timoshenko beam clamped at both ends and subjected to a concentrated load in the middle will be made using the relation between Timoshenko beam and Euler-Bernoulli beam developed by Wang [90]. This relation provides a simple way to obtain the bending solutions of the Timoshenko beam from the Euler-Bernoulli solutions without performing a complicated analysis. For the identical beam with clamped-clamped boundary condition, the Timoshenko beam solution and Euler-Bernoulli solution are related as the following:

$$\psi_x = w_{,x}^E + \frac{6\left(M_L^E - M_0^E\right) L\Omega}{D_{11}(1+12\Omega)} \left(\frac{x}{L}\right)\left(\frac{x}{L} - 1\right) \tag{4.19}$$

$$\begin{aligned} w = w^E &+ \frac{\left(M^E - M_0^E\right) L^2 \Omega}{D_{11}} \\ &+ \frac{3\left(M_L^E - M_0^E\right) L^2 \Omega}{D_{11}(1+12\Omega)} \left(\frac{x}{L}\right)\left(\frac{2x^2}{3L^2} - 4\Omega - \frac{x}{L}\right) \end{aligned} \tag{4.20}$$

where ψ_x and w are the shear deformation and lateral displacement of the Timoshenko beam solution, respectively. The terms with an E superscript refer to the Euler-Bernoulli solution: w^E is the lateral displacement, M^E is the bending moment, and M_0^E and M_L^E are the bending moments at the clamped ends (x = 0 and x = L), respectively. Ω is the non-dimensional shear parameter defined as:

$$\Omega = \frac{D_{11}}{G_b K_s L^2 t_b b} \tag{4.21}$$

where D_{11}, G_b, L, t_b, and b are the bending stiffness, shear modulus, length, thickness, and width of the cross-ply laminated composite beam, respectively. To simplify the calculations, G_b is assumed to be equal to the shear modulus of the graphite/epoxy laminate G_{13}. K_S is the shear correction coefficient, which accounts for the difference between the constant state of shear stress in the Timoshenko beam theory and the parabolic variation of the actual shear stress through the beam thickness. The values of K_S can be calculated approximately by [89]:

$$K_S = \frac{12 + 11\nu_b}{10(1 + \nu_b)} \tag{4.22}$$

where ν_b is the Poisson's ratio of the hybrid composite beam. Again, to simplify the calculations, ν_b is assumed to be equal to the Poisson's ratio of the graphite/epoxy laminate ν_{12}.

Thus, using Wang's approach, the solution of the Timoshenko beam clamped at both ends and subjected to a concentrated load in the middle is:

$$\psi_x = w^E_{,x} + \frac{3PL^2\Omega}{2D_{11}(1+12\Omega)}\left(\frac{x}{L}\right)\left(\frac{x}{L}-1\right) \tag{4.23}$$

$$w = w^E + \frac{PL^2\Omega}{2D_{11}}x + \frac{3PL^3\Omega}{4D_{11}(1+12\Omega)}\left(\frac{x}{L}\right)\left(\frac{2x^2}{3L^2}-4\Omega-\frac{x}{L}\right) \tag{4.24}$$

where the lateral displacement of the Euler-Bernoulli beam solution is:

$$w^E = \frac{P(4x^3-3x^2L)}{48D_{11}} \tag{4.25}$$

4.6 Contact Law

The relationship between the impact force P and contact deformation α is given by Hertzian contact law [91]:

$$P = n\alpha^{\frac{3}{2}} \tag{4.26}$$

where the contact deformation α is the distance between the center of the projectile's nose and the mid-surface of the beam and n is the modified constant of the Hertz contact law proposed by Sun, et al. [3]:

$$n = \tfrac{4}{3}\sqrt{R_p}\,\frac{1}{\left[\left(1-\nu_p\right)/E_p + 1/E_{c22}\right]} \tag{4.27}$$

where R_p, ν_p , E_p are the local radius, Poisson's ratio, and Young's modulus of the projectile, respectively. E_{c22} is the transverse modulus normal to the fiber direction in the surface ply facing the projectile.

4.7 Energy Balance Model

The energy balance model is based on the principle of conservation of energy between the impactor and the SMA hybrid composite beam. The kinetic energy of the impactor is equal to the sum of the energies due to contact, bending, and transverse shear deformations. In this paper, the energy losses from material damping, surface friction, and higher modes of vibration are neglected.

Energy Balance:

Based on the conservation of the total energy, the kinetic energy of the projectile is completely absorbed by the beam, and becomes the strain energy and contact energy of the beam [91]:

$$\tfrac{1}{2} M_p V_p^{\,2} = U + U_c \tag{4.28}$$

where M_p and V_p are the mass and velocity of the projectile, respectively, U and U_c are the beam's strain energy and contact energy, respectively. The following is the derivation of the expressions of the contact energy and the strain energy.

Contact Energy:

The contact energy is the integral of the product of the impact force and contact deformation:

$$U_c = \int_0^{\alpha} P d\alpha \tag{4.29}$$

Incorporating the contact law of equation 4.26 in equation 4.29, the contact energy is obtained:

$$U_c = \frac{2}{5} \frac{P^{5/3}}{n^{2/3}} \tag{4.30}$$

Strain Energy:

The strain energy of a composite beam using the Timoshenko theory is given by:

$$U = \frac{1}{2} \int \left(M_x \kappa_x + Q_x \gamma_{xz} \right) b dx \tag{4.31}$$

Using the derivation of the composite beam-governing equations, the strain energy can be expressed in terms of displacements as the following:

$$U = \frac{1}{2} \int_{vol} \left[D_{11} \psi_{x,x}^2 + A_{55} \left(\psi_x + 2 \psi_x w_{,x} + w_{,x}^2 \right) \right] b dx \tag{4.32}$$

With the solution of the Timoshenko beam theory equations 4.23 and 4.24, the strain energy of the composite beam is separated in two parts:

$$U = U_b + U_s \tag{4.33}$$

where U_b is the bending strain energy, which can be obtained from the Euler-Bernoulli beam solution:

$$U_b = \frac{bL^3P^2}{384D_{11}} \tag{4.34}$$

and U_s is the shear deformation energy:

$$\begin{aligned} U_s = {} & \frac{bL^3P^2}{D_{11}}\left(\frac{\Omega}{32(1+12\Omega)} - \frac{3\Omega^2}{8(1+12\Omega)^2}\right) \\ & + \frac{A_{55}bL^5P^2}{D_{11}^2}\left(\frac{1}{5120} - \frac{\Omega}{96} + \frac{\Omega^2}{8}\right) \\ & + \frac{A_{55}bL^5P^2}{D_{11}^2(1+12\Omega)}\left(\frac{21\Omega}{2560} - \frac{3\Omega^2}{16} - \frac{3\Omega^3}{2}\right) \\ & + \frac{A_{55}bL^5P^2}{D_{11}^2(1+12\Omega)^2}\left(\frac{3\Omega^2}{40} + \frac{9\Omega^3}{8} + \frac{9\Omega^4}{2}\right) \end{aligned} \tag{4.35}$$

4.8 Numerical Examples

To study the numerical relationship among above factors, the case of a 100 mm by 30 mm cross-ply SMA/AS4/3501/graphite/epoxy composite beam with a thickness of 2.685 mm in a symmetric $[0_{SMA}/90/0/90/0/90/0/90]_S$ stack sequence is analyzed. As described earlier, the SMA hybrid composite beam is clamped at both ends and a

spherical nose impactor 10 mm in diameter impacts the middle of the beam at velocities ranging from 0 m/s up to 6 m/s [91]. The numerical values used in this case study are presented in Tables 4.1-4.5.

Fig. 4.2 shows the relationship between the velocity of the impactor and the impact force on the SMA hybrid composite beam. It can be seen that the impact force applied to the beam increases nonlinearly with the increasing impact velocity of the steel impactor. This behavior agrees with the trends predicted by other researchers for common composite plates [92]. Also, it can been observed that the effect of the martensite fraction on the impact force is minor, but beneficial: an increase of martensite fraction will have the effect to reduce the impact force, for a given velocity of impactor.

The relationship between the impact velocity of the impactor and the energy absorption due to the contact deformation of the SMA hybrid composite beam is shown in Fig. 4.3. The graph shows the results for three levels of martensite fraction. The first observation to be made is the nonlinear increase of the contact energy with the increase of the impact velocity. Second, the contact energy is reduced with increasing martensite fraction, for a given impact velocity. This reduction in contact energy is simply caused by the SMA's increased compliance with increased martensite fraction, which results in the reduced contact force.

Fig. 4.4 shows the effect of the martensitic phase transformation on the total strain energy absorption of SMA composite beam. The model predicts that the total strain energy absorbed by the beam will increase with increasing martensite phase transformation. This observation is in agreement with the conclusions drawn from previous experiments [32-35].

Table 4.1 Properties of the SMA hybrid composite beam.

Length:	L	100 mm
Width:	b	30 mm
Thickness:	t_b	2.685 mm
Lay-up:		$[0_{SMA} / 90 / 0 / 90 / 0 / 90 / 0 / 90]_S$
Shear correction factors:	k_1	5/6
	k_2	5/6

Table 4.2 Properties of the steel projectile.

Elastic Modulus:	E_p	207 GPa
Poisson's ratio:	n_p	0.3
Radius:	R_p	5 mm
Mass:	M_p	160 g
Velocity:	V_p	0-6 m/s

Table 4.3 Properties of AS4/3501/graphite/epoxy.

Elastic modulus:	E_1	144.8 GPa
	E_2	9.65 GPa
Shear modulus:	G_{12}	4.14 GPa
	G_{23}	3.45 GPa
	G_{13}	4.14 GPa
Poisson's ratio:	n_{12}	0.3
Ply thickness:	t	0.144 mm

Table 4.4 Properties of SMA fibers.

Austenite modulus:	E_a	67 GPa
Martensite modulus:	E_m	26.3 GPa
Poisson's ratio:	n_{SMA}	0.33
Transformation temperatures:	M_f	9 degrees Celsius
	M_s	18.4 degrees Celsius
	A_s	34.5 degrees Celsius
	A_f	49 degrees Celsius
Transformation constants:	C_M	0.008 GPa/ degrees Celsius
	C_A	0.0138 GPa/ degrees Celsius
	σ_s^{cr}	0.1 GPa
	σ_f^{cr}	0.17 GPa
Volume fraction:	k_{SMA}	0.6

Table 4.5 Properties of the epoxy matrix.

Elastic Modulus:	E_m	2.8 GPa
Shear Modulus:	G_m	1.27 GPa
Poisson's ratio:	n_m	0.25
Volume fraction:	k_m	0.4

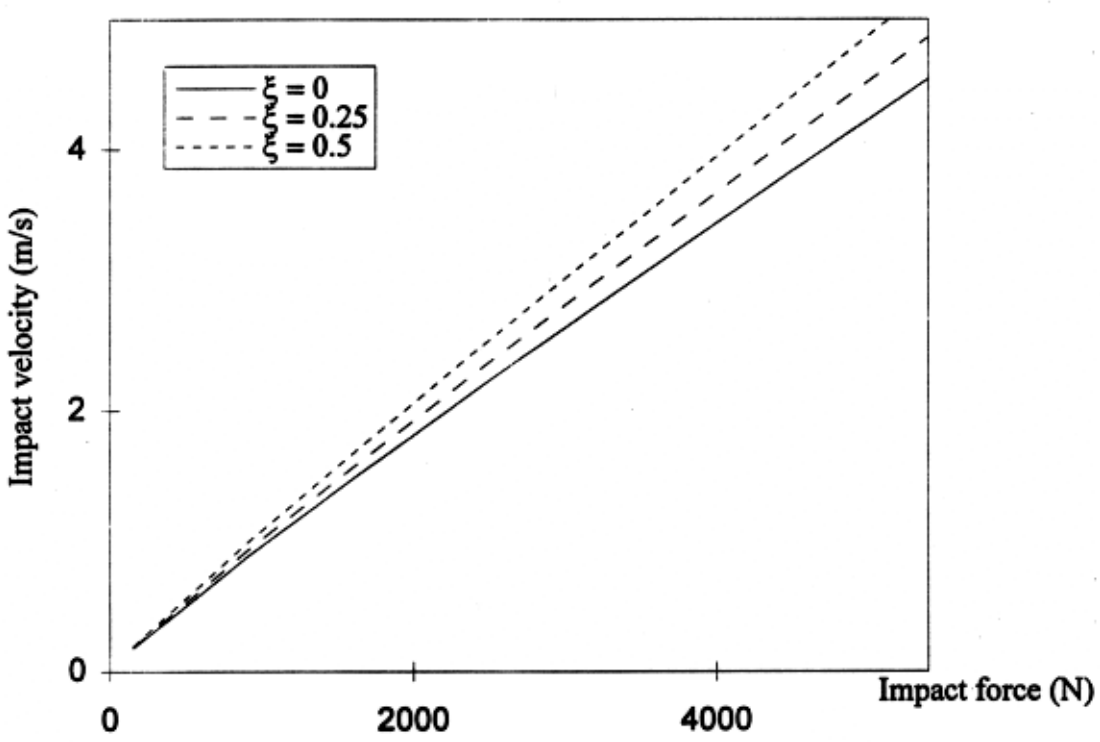

Figure 4.2 Impact velocity vs impact force.

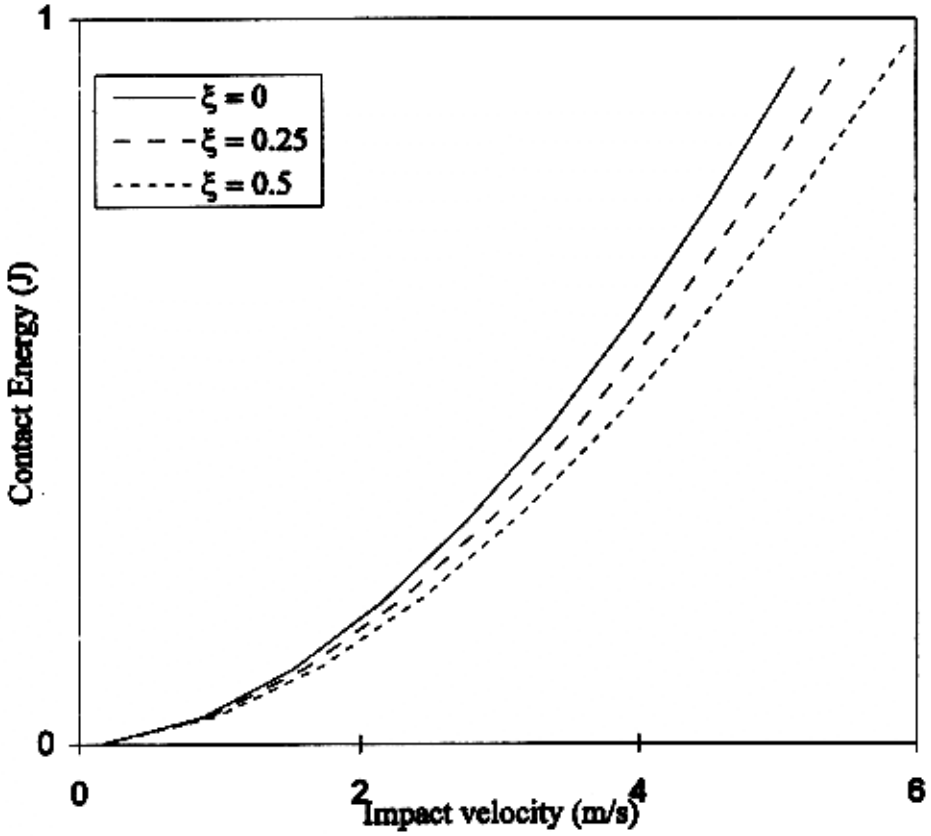

Figure 4.3 Contact energy vs impact velocity.

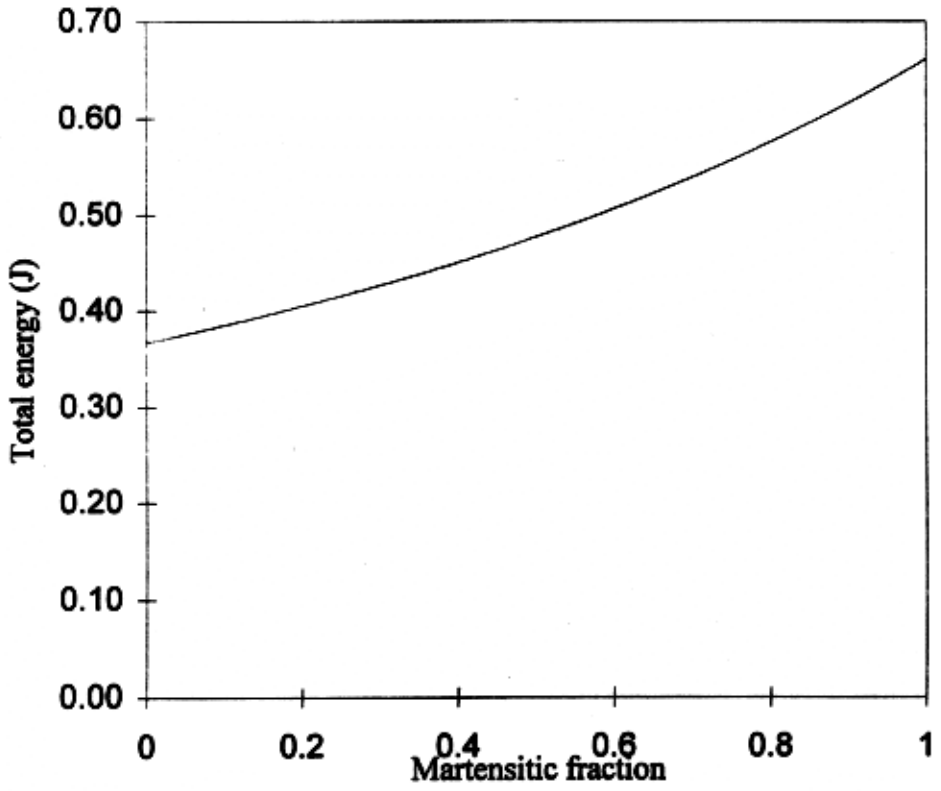

Figure 4.4 Total energy vs Martensitic fraction.

4.9 Conclusion and Summary

A theoretical study of the impact force and the strain energy absorption of an SMA/graphite/epoxy composite beam under a low-velocity impact has been performed. The contact deformation, the global bending deformation, the transverse shear deformation, and the martensitic phase transformation of the super-elastic SMA fibers are studied. Then, the energy absorbed by the SMA hybrid composite was calculated for each of the absorption mechanisms: contact deformation, global bending deformation, and transverse shear deformation. The basic relationship between the energy absorption mechanisms and the extent of martensitic phase transformation is studied.

It was found numerically that the total strain energy absorption of the SMA hybrid composite beam increases when the martensitic fraction of SMA increases. This observation agrees with the conclusions drawn from previous experiments [31-33]. This is an important numerical observation. The results in this chapter have built the basis for further study of SMA composite under impact. This is the first effort to perform the analysis on the impact of SMA hybrid composite, and the results encourage us to go further and pursuit the modeling of damage and failure of SMA composite in low velocity impact or quasi-static contact loading. Above conclusions and observation are the contributions of this research.

Chapter Five

Failure Analysis of SMA Graphite/Bismaleimide Composite Beams Under the Quasi-Static Load By A Steel Cylinder

5.1 Introduction

Although composites have high strength and stiffness at a low weight, they have limited applications. Composites are usually brittle because of the matrices and fibers and do not have good damage tolerance to impact compared to ductile materials. This is a concern in the applications where the composite structures are subjected to impact, such as aircraft and automobile structures. Impact from the environment during service, such as birds and runway with debris, are threats to the performance of composite structures.

Unlike metallic materials, graphite composites do not undergo plastic deformation during impact. During impact, metallic structures absorb the impact energy through plastic deformation. Plastic deformation does not significantly reduce the load-carrying capability of the structures, although deformation is permanent. Graphite composites usually cannot effectively absorb impact energy while maintaining their load-carrying capacity. It is well reported that composite structures dissipate impact energy through the matrix cracking, delamination, and fiber failure [93], [94].

There has been extensive research on improving the impact resistance of composite structures as reviewed in Chapter 1. Among these, several techniques are effective. Matrix cracking and delamination are among the first modes of damage occurring in composite structures during impact. The matrix is relatively weak and brittle compared to the reinforcing fibers. One of these techniques is to improve the matrix toughness by introducing toughened polymer matrices to reduce matrix cracking and delamination [95], [96]. Matrix cracking and delamination at the initial stage of damage is a potential threat to the performance of composite structures, since they are usually undetectable by visual surface inspection. The fibers break after matrix cracking and

delamination have occurred. Another technique of improving the impact damage resistance of composite structures is to improve the strain-to-failure of the fibers, or embed toughened fibers in the host structures. By increasing the strain-to-failure, or strain energy absorption of fibers, the composite structures are capable of resisting higher impact energy before the fibers fail. One way of improving the impact energy-absorbing ability of composite materials is to add tough materials to the host composites, such as high strain-to-failure fibers, e.g. S-Glass, Kevlar, or Spectra. This technique leads to the hybrid composites. Developing hybrid composites, researchers combine fibers having high stiffness, such as graphite fibers, with fibers having high toughness, such as Kevlar and Sprectra fibers. A compromise between high structural performance and the toughness would result in composite structures with high load-carrying capacity and improved impact energy absorption. Hybridizing composites to improve impact energy absorption has been studied in detail [30], [32]. Most research is directed towards improving the impact energy-absorbing capabilities. Jang, et al. [30] showed that hybridizing graphite with 50% polyethylene increased the energy-absorbing ability by as much as 8.5 times. They also showed that Nylon and Polyester also offer large improvements in impact energy absorbing ability. Paine, et al. [32] and Kiesling, et al. [34] showed experimentally that SMA hybrid composites have better impact resistance than the conventional structural composites.

In order to understand the mechanism of impact resistance of SMA hybrid composites, a model has to be developed and failure analysis has to be performed. As a continued study in the modeling and analysis of impact and energy-absorption capability of SMA and SMA hybrid composites presented in Chapters 2, 3, and 4, the present chapter presents a nonlinear beam model and a new failure analysis method to analyze and predict the mechanical behavior of composite beams under quasi-static load by a cylinder. Part of the analysis in this chapter was presented in ARO Work Shop in 1997 [97].

5.2 Statement of the Problem

A four-layer graphite/bismaleimide composite clamped-clamped beam is impacted by a steel cylinder, as shown in Fig. 5.1. This is low-velocity impact or quasi-static contact loading. The load was applied from an MTS machine on the cylinder until the beam failed. The steel cylinder has a 5/8-in. diameter. The beam has dimensions 4 by 0.75 by 0.048 in. The composite beam has unidirectional lay-up with stack sequence [0/0]s. The load-deflection curve needs to be predicted by the proposed model, so that the energy needed to completely fail the composite beam can be obtained. The process involved matrix crack, delamination, and fiber failure. Thus, the stiffness degradation and failure criteria have to be proposed.

5.3 Experiment

In order to state the problem clearly, the experiments performed by Kiesling, et al. [34], [98] are briefly described here. The impact tests were designed to study the behavior of thin composite laminates with a thickness of 0.048 in. under the impact by a steel cylinder (quasi-static) resulting the complete penetration. The experiment was designed to investigate the behavior of SMA composites during the failure process, and the energy needed to completely penetrate the SMA composite beam.

A series of experiments was performed to investigate the properties of SMA fibers and their interaction with the graphite composites. Wang, et al [31] report that the load displacement curve of graphite laminates is virtually independent of the loading rate. Their observation was also obtained in the experiments by Kiesling, et al. [34]. Each test was designed to give statistically significant results by using at least three replications of each specimen. The specimens are simple lay-ups so that damage modes can be observed without complications, such as ply orientation or effect of specimen thickness. The visual inspection also can be performed during the test.

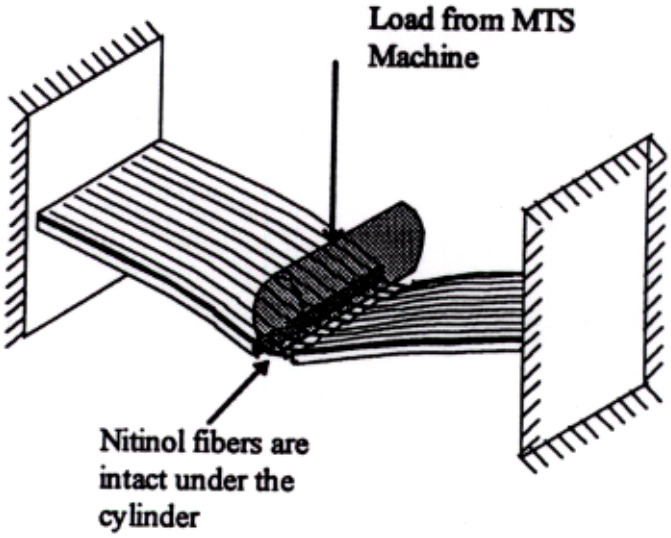

Figure 5.1 Graphite/Bis composite beam loaded by a steel cylinder [34], [98].

Fabrication of SMA Composite Specimen

All specimens were fabricated using a graphite/bismaleimide pre-preg from the BASF Corporation, now Cy-Tech Corporation. Each specimen was made of four layers of double-ply (0.012 in.) graphite/bismaleimide. SMA fibers of 0.012 in. diameter were manually embedded into the pre-preg in the directions of the fibers. The SMA fibers were spaced 0.0625 in. apart. This spacing does not significantly affect bonding between plies. This arrangement gives an approximate volume fraction of 13.8% SMA per ply. The unidirectional SMA layer was studied here. This gave a total volume fraction of approximately 3%. The specimens were thin beams cut from plates cured in a hot press. The hot press allows a maximum plate size of 12x12 in. A diamond saw was used to cut the specimens from these plates. The cure cycle for the composite recommended by the manufacturer is shown in Fig. 5.2. A vacuum is applied during the first 45 min of the cycle to remove the air from the lay-up. At 300^0F the vacuum is removed and a pressure of 80 psi is applied to the laminate. The pressure is held for the rest of the cure cycle.

Fig. 5.3 shows the set-up used to cure the composite specimen. The breather cloth provides an even pressure distribution over the composite during curing. The Teflon allows some excess resin to bleed away from the laminate and prevents the composite from bonding to the tool and pressure plate. The pressure plates are forced together by a hot press, which provides heat and keeps the plate sealed when the 80 psi of air pressure is applied. The tool and the pressure plate make the composite specimen flat.

Clamp Fixture for Specimen

The specimens were clamped in the steel fixture shown in Fig. 5.4. The fixture is similar to those used by Lagace, et al. [94]. The fixture can handle 8 in. long and 0.75 in. wide beams. The grips are 2 in. long giving a total gripped length of 4 in. The grips were coated with sandpaper to prevent the specimens from slipping. The eight bolts were torqued to 150 in-lbs in an alternating pattern to ensure that the specimen was evenly and securely clamped. No slippage was found in using this set-up.

Damage Evaluation

C-scans determine the damage area by passing sound waves through the specimen. The specimen is immersed in water to improve measurement. By measuring the reflection of the sound waves and variations in this reflection, it is possible to determine the location of damage in the composite. No damage or voids caused by cutting or curing were found by C-scans before the specimens were loaded.

Test Methods

Tests were performed by using a MTS machine. The specimens are clamped-clamped composite beams and were loaded in the center with a 5/8-in. diameter steel cylinder. The MTS controller was used to apply displacement loading to the specimen at a constant rate of 0.02 in./min. A 5,000-lb load cell was used to measure the force. The sensitivity of the load cell was set to 100 lbs/V. The MTS machine has an output range of ± 10 V giving a measurable force range of $\pm$ 1,000 lbs. A LVDT with a sensitivity of 0.25 in./V was used to measure the displacement/ output voltages from the MTS controller. The data were recorded every 0.25 seconds on a PC using ACQPLOT. These voltages were then converted into force and displacement with their respective sensitivities in MATLAB for Windows. The data were also adjusted for any DC offset that may have been present. In all cases, at least half of the full-scale range was used. The steel cylinder was loaded on the composite beam until the specimen completely failed. The load-deflection curve to the complete failure of the beam was obtained.

Experimental Observations and Results

The clamped composite beam underwent a large deformation before its complete failure. No slippage between the beam and grips was found. Matrix cracking and delamination rere found on the beam. The beam finally failed along the loading line, which is underneath the steel cylinder due to the fiber breakage. Fiber pull-out was found. Fibers failing due to tension is the major failure mode in the final stage. After the beam

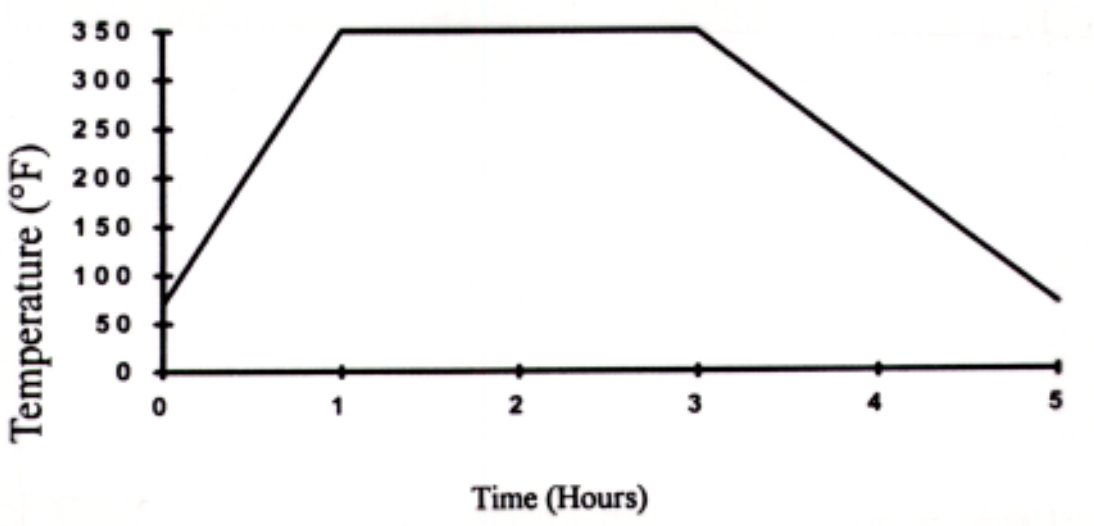

Figure 5.2 Cure cycle for composites [98].

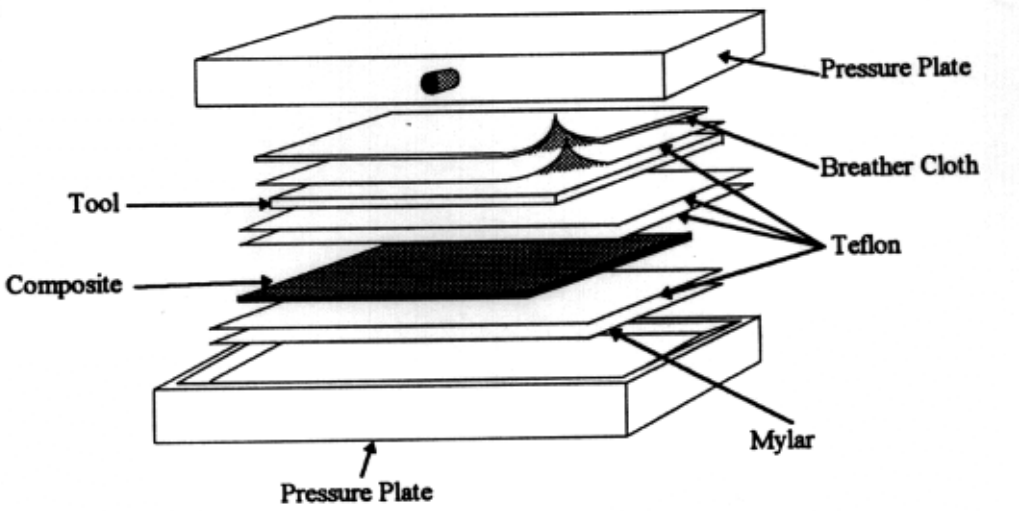

Figure 5.3 Configuration used to cure the composite specimen [98].

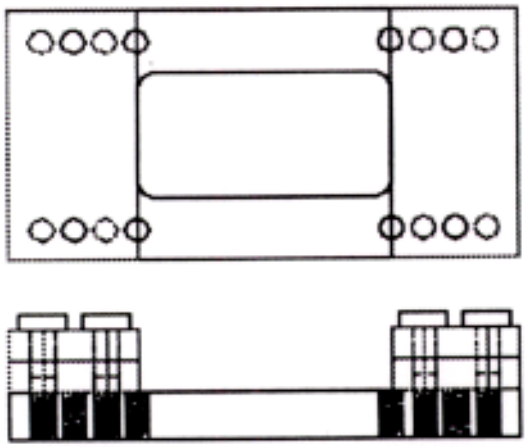

Figure 5.4 The steel fixture [98].

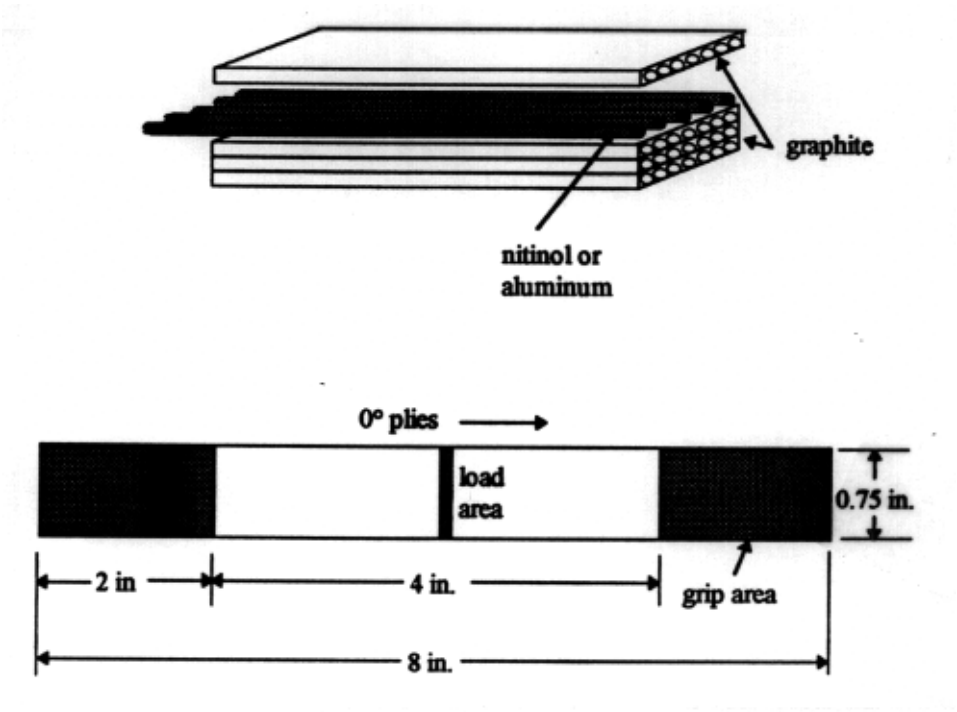

Figure 5.5 SMA composite lay-up [98]

completely fails, the middle line of the beam behaves as a hinge. Its displacement is not certain.

The results are significantly different after the graphite fiber fail under the cylinder. Fig. 5.6 shows that the SMA fibers only significantly affect the composite after fibers fail under the cylinder. Note that the beam was unloaded before failure at the clamps occured. The SMA remains intact after the graphite failure due to its high strain-to-failure.

5.4 The Models Developed by Researchers

Before we proceed to present our analysis and modeling of this problem, which is strongly nonlinear in both geometry (very large deflection) and materials (severe material degradation), a specific review of related literature is given to report up-to-date development in this specific area.

The composite beam loaded at the mid-span by a cylinder can be classified into two categories.

The First Category:

The composite beams do not completely fail. The deflection of the beam is small, and linear theory can be used. The major damage is the matrix cracking and delamination.

The plates or beams retain their integrity during the low-velocity impact or indentation. Therefore, linear plate or beam theories are readily used with the appropriate failure criteria to predict the stresses in the composite and damage area. These kinds of problems can be solved using conventional methods. Choi, et al. [11, 12] present a model to analyze the damage induced by line loading during the low velocity impact. They used linear finite element analysis with the contact law for line loading to predict the initial damage on the plate. In order to solve the equations, they proposed an empirical relation of the ply transverse tensile strength within a laminate as a function of the laminate

thickness and stacking sequence. Due to the complexity of the problem and the lack of analytical solution to the inter-laminar shear strength distribution within a laminated composite, a relation was also proposed to estimate the *in situ* ply shear strength distribution. They also made assumptions that the damaged element cannot sustain any additional transverse tensile stress and out-of-plane shear stress due to the presence of the crack. Although the assumptions are not very precise, it is one of the ways to consider the damage mechanism in modeling the low-velocity impact on composites. The model they developed can be used to predict the impact load needed to initiate the damage in composite plates. However, The model cannot be used to study the damage growth after the initial damage occurs in the composites.

Liu, et al. [99] studied the composites under line loading (quasi-static) using nonlinear plate theory, finite element analysis, and the strain energy release rate approach. They also considered only the damage initiation, such as matrix cracking and delamination. Lo, et al [100] used a similar approach to study the delamination of composite beams under quasi-static or low-velocity impact. Liu and Lo neglected the free edge effect. They assumed the cracks initiate and develop uniformly across the width of the plate or beam. During the initial stage of the loading, this assumption is acceptable; however, it is not true when the impact or quasi-static loads continue to exert on the composites and the composite undergoes substantial matrix cracking and delamaintion.

The above models cannot be used to study the damage growth after the initial damage occurs in the composites, which is strongly nonlinear in both geometry (very large deflection) and materials (severe material degradation).

<u>The Second Category:</u>

The low-velocity impact or quasi-static load continue to exert on the composite after the first damage is initiated in the composite, and the composite undergoes substantial damage growth, such as matrix cracking, delamination, and fiber breakage. The damage or failure modes are successive during the loading process, and composites

finally completely fail under the loading. During this process, the composites usually go through very large deflection, severe material degradation, and discontinuity in geometry.

It is a strongly nonlinear problem and cannot be treated by using the theories in the weakly nonlinear mechanics.

The characteristics of the successive damage growth is the load-deflection curve recorded in the experiment. In order to understand the damage mechanism during this process, researchers have been developing methods and models to predict such load-deflection curves of composites. These problems are significantly different from the problems in the first category, since the composite undergoes a large deflection, usually several times of the magnitude of sample's thickness, and the composite has severe progressive damage, such as multiple matrix cracking, delamination and, finally, fiber breakage. The difficulty of modeling this process is modeling degradation of the material properties and handling the discontinuity of the composites near their final failure. Many researchers have proposed several approaches. However, these approaches are based on the conventional strength, stress failure criteria. Also, the models and methods developed are not sufficiently good to capture the behavior of composites near their final stage of failure, due to the lack of an appropriate approach to account for the material degradation mechanism. During the final stage of failure, the composite experiences severe damage and most of its integrity is lost, and so the conventional plate or beam theory are not applicable.

Due to the complexity of the problem, very little reported research is found in this specific area. Successive failure modes in graphite/epoxy laminated composite beams was studied by Greif, et al. [25]. Two failure theories, the maximum stress and the Tsai-Wu failure, are used. The analysis is based on the laminated plate theory. They assumed that once a ply fails in a laminate, it cannot carry any more load, and its elastic properties are set to zero. The failure analysis is then repeated with the modified laminate based on updated stiffness matrices [A], [B], [D] until the next failure point is reached. A comparison of the theoretical and experimental results shows that failure predicted by

these two failure theories occurs at substantially lower loads than that for the actual failure. Thus, these two failure theories, based on the stresses in the composites and reduction mechanism of damage by setting the stiffness of the failed ply to zero, are not sufficiently accurate to predict the damage growth in composite during the failure process.

Kim, et al. [26] improved the method proposed by Greif, et al. Instead of the total-ply discount approach, they focused on increasing the accuracy for predicting the post first-ply-failure behavior of composites. They implemented a material-degradation approach for predicting the composite beam failure in bending. They proposed some material degradation factors to treat this problem. They assumed the material is linear elastic up to ultimate failure. They used linear beam theory since the load deflection curve is almost linear before the final failure of the composite. They did not consider the contact between the loading and the beam. The stiffness of a damaged layer over a discrete length is replaced by a homogeneous degraded layer whose material properties are a constant multiple of original properties. Constant material degradation factors are used to define a percentage of the stiffness retained in a ply after damage has occurred. Degradation factors are used to globally adjust the local stiffness degradation of a ply discount. Since a degradation level depends among other factors on crack density and lamination sequence, as observed in an experimental evaluation of cross-ply laminates under uniaxial tension by Reifsinider [101], the mechanism of degradation factors during the contact or impact loading is even more complex than that in uniaxial tension and is not available in the literature. Their results showed that the prediction of the maximum load with sufficient accuracy. However, their predicted maximum displacement varies as much as 30 % away from the experimental results. The discrepancy between the predicted value and the experimental data is due to their assumptions that the material degradation factors are constants, uniform cracking across the width of beam, and no consideration of effective thickness.

5.5 Objectives of the Research

From the above review, we can see that in order to analyze this problem, even for plain composite beams without SMA, we need to propose a new method that is able to model the strong nonlinearity in both geometry (very large deflection) and materials (severe material degradation). Thus, based on the development in Chapters 2, 3, and 4, we will develop a model and a new method to account for large deflection, severe material degradation, discontinuity in beam geometry before failure, stress-induced martensite phase transformation, and contact loading for SMA composite beam under quasi-static loading up to complete failure. By applying this model and method to the problem, the characteristics of SMA composite beam during this process, that is the load-deflection curve, will be predicted.

5.6 Assumptions Based on the Experimental Observations

The beam has geometric nonlinearity due to the large deflection, so the nonlinear strain-displacement relations are used. Due to the large deflection, tension dominates, instead of bending. Multiple cracks in the matrix, delamination between the plies, higher crack density along the edges than in the central part contribute to the stiffness degradation in the beam. The deflection of the middle line of the beam is the global parameter which is related to crack density and material degradation. The concept of effective thickness and width of a composite beam with severe material degradation is proposed. Maximum strain failure is adopted to be the criteria for the final failure. Limit analysis from civil engineering is introduced in the failure analysis of composite beams.

5.7 The Major Tasks in the Analysis

The major tasks in the proposed analysis are:

1. Modeling the strong geometric nonlinearity of the composite beam, since the maximum deflection of the beam is more than 6 times of its thickness, and significant membrane effect exists during the loading.
2. Modeling the cylinder contact between the cylinder and the composite.
3. Modeling the discontinuity of the beam at the final failure.

4. Considering severe material degradation of the composite due to the multiple matrix cracking, delamination, and fiber breakage during loading, such as degradation of the Young's modulus, non-uniform matrix cracking, thickness degradation due to the mutilple matrix cracking and delamination.
5. Modeling of stress-induced martensite phase transformation in this process.

5.8 Formulation of the Problem

According to Wen, et al. [86], the problem of a clamped metal beam struck transversely by a heavy mass traveling at a low velocity can be solved by the same deformation mechanism as for the same beam subjected to static load.

Here the loading is quasi-static. We will formulate the problem as follows.

The general governing equations of the composite plates shown in Chapter 2, we can be simplified to the beam case.

The displacement field of the composite beam (as shown in Fig.5.1),

$$u_1 = -zw_x \quad \text{and} \quad u_3 = w, \tag{5.1}$$

where w is the deflection of the middle plane of the composite beam, which is in the z direction. The symbol z represents the coordinate through the thickness of the composite beam, and, u_1 is in longitudinal (x-axis) direction.

The strains and curvature in the mid-plane of the composite beam are

$$\varepsilon_x^0 = \tfrac{1}{2}(w,_x)^2 \quad \text{and} \quad k_x = -w,_{xx} \quad . \tag{5.2}$$

The nonlinearity is due to the large deformation of the beam, which contributes to the higher-order term of strain in the beam.

The Strain field of the beam is

$$\varepsilon_x = \varepsilon_x^0 + zk_x \quad . \tag{5.3}$$

Following the same procedure as in Chapter 2, strain energy of the beam can be written

$$U^* = \frac{1}{2}\int_0^a\int_0^b [\{\varepsilon^0\}^T [A]\{\varepsilon^0\} + 2\{\varepsilon^0\}^T [B]\{k\} + \{k\}^T [D]\{k\}]dxdy \ . \tag{5.4}$$

The resultant forces {N} and {M} in the composite beam are then

$$\begin{Bmatrix} N \\ M \end{Bmatrix} = \begin{bmatrix} A & B \\ B & D \end{bmatrix} \begin{Bmatrix} \varepsilon^0 \\ k \end{Bmatrix}. \tag{5.5}$$

In equation 5.5, the {N} are in-plane resultant forces, the {M} are resultant moments, and [A], [B] and [D] are the stiffness matrices, given by

$$\left(A_{ij}, B_{ij}, D_{ij}\right) = \int_{-h/2}^{h/2} (1, z, z^2) Q_{ij} dz, \ (i, j = 1, 2, 6) \ . \tag{5.6}$$

For a symmetric laminated composite beam, such as Graphite/Bismaleimide, the stiffness matrices are reduced as

$$[A] = \begin{bmatrix} A_{11} & A_{12} & 0 \\ A_{12} & A_{22} & 0 \\ 0 & 0 & A_{66} \end{bmatrix}; \qquad [B] = 0 \ ; \qquad [D] = \begin{bmatrix} D_{11} & D_{12} & 0 \\ D_{12} & D_{22} & 0 \\ 0 & 0 & D_{66} \end{bmatrix} \ . \tag{5.7}$$

For SMA Graphite/Bismaleimide beams, because of SMA/Bismaleimide lamina, the coupling of stiffness matrices are

$$[B] = \begin{bmatrix} B_{11} & B_{12} & 0 \\ B_{12} & B_{22} & 0 \\ 0 & 0 & B_{66} \end{bmatrix} \ . \tag{5.8}$$

Potential energy of the beam is

$$V^* = -Pw_0 \quad , \tag{5.9}$$

where $w_0 = w + \Delta$, is the total displacement of the middle line on the beam, w is the deflection of the middle line on the beam , Δ is the indentation due to contact, and P is the impact force.

The Hertzian contact law is adopted to describe the contact load distribution. The contact load distribution f for a line-loading impact is related to the indentation depth α by [102], [11,12]

$$\Delta = f(\delta_s + \delta_p)\{1 - \ln[fr(\delta_s + \delta_p)]\} \quad . \tag{5.10}$$

The quantity α is defined as the change in the distance between the center of the impactor nose and the mid-plane of beam. That is, $\alpha = u_s - u_p$, where u_s is the impactor displacement, u_p is the beam displacement measured from the center of the mid-plane of the beam, which is opposite to the impactor's surface. The quantity f in equation 5.10 is the contact load distribution, and the quantities δ_s and δ_p are the constants defined

$$\delta_s = \frac{1 - \upsilon_s^2}{\pi E_s} \tag{5.11}$$

and

$$\delta_P = \frac{1}{\pi E_{yy}} \quad . \tag{5.12}$$

The quantities r, υ_s, and E_s are the local radius, the Poisson's ratio, and the Young's modulus of the impactor, respectively. The quantity E_{yy}, which is equal to E_{zz}, is the modulus of elasticity of the impacted composite ply in the direction transverse to the ñ ñ

Total potential energy of the beam is

$$\Pi = U^* + V^* , \tag{5.13}$$

and the virtual work is

$$\delta\Pi = 0. \tag{5.14}$$

Analysis

Displacement Function

In order to solve the problem and get the load deflection curve, the displacement function of the longitudinal coordinate x must be obtained. The beam undergoes a large deformation before it fails completely. From the experiment, we can see that the displacement of the middle line of the beam is more than 6 times the thickness of the beam. The membrane tension is the primary effect and bending is secondary. Also the beam is not the ideal "clamped-clamped" beam anymore. The displacements in the z direction at the clamped ends are zero; however, the slopes at these ends are not zero because of the large deflection and the matrix cracking in the beam.

Wen, et al. [86] studied a clamped metal beam struck transversely by a heavy mass traveling at a low velocity. The beam undergoes a large deflection, then fails at the middle point. Because of the large deflection and discontinuity due to the formation of plastic hinges, the conventional nonlinear clamped-clamped beam theory cannot be used. As an alternative they proposed a displacement function. They assumed that the two parts of the beam between the hinges rotate as rigid bodies around the supports and that the displacement profile can be written

$$W = W_0(1+\frac{X}{L_1}) \qquad -L_1 \le x \le 0; \tag{5.15}$$

and

$$W = W_0(1-\frac{X}{L_2}) \qquad 0 \le x \le L_2, \tag{5.16}$$

where W_0 is the displacement at the loading point.

With this displacement profile, the slope of the beam is

$$\frac{\partial W}{\partial x} = \frac{W_0}{L_1} \qquad -L_1 \le x \le 0; \tag{5.17}$$

and

$$\frac{\partial W}{\partial x} = -\frac{W_0}{L_2} \qquad 0 \le x \le L_2 \ , \tag{5.18}$$

and curvature of the beam is $\frac{\partial^2 W}{\partial x^2} = 0, \quad -L_1 < x < 0; \quad 0 < x < L_2.$

So the bending effect is neglected, and the membrane force N_x is constant throughout the beam. A clamped rigid-plastic beam may enter a fully plastic membrane state when the transverse deflection becomes larger than the beam thickness. So, if interest is confined to large plastic deformations, it is reasonable to assume the membrane force is constant in the beam. Good agreement was obtained between the prediction and experiment results.

The similar approaches of displacement function are also used by researchers in modeling impact on composites resulting in complete failure. Because the target undergoes a large deflection, multi-mode damage with severe geometric discontinuity, and changing (degrading) material properties during this process, it is impossible to use the conventional solution procedure for plate or beam theory with the boundary conditions to obtain the solution for the displacement field of the target. Thus, in modeling the composite under impact or quasi-static loading resulting in complete failure, it is common to assume the displacement function of the target during impact or quasi-static loading. Zhu, et al. [18], assumed the deflection function of the sublaminate with the elliptical delamination in large deflection. Ursenbach,, et al. [103], assumed a quadratic function for the displacement field of the undamaged part of the plate, and a series function of the radius of the damage zone for the displacement field of the damaged part of the plate to deal with the non-homogeneous boundary conditions. Sun, et al. [23], also assumed a displacement function with the lateral displacement and rotation for the circular plate under impact.

With the above discussion, also considering the membrane effect and the bending effect, together with the experimental observation, we assume the form of displacement functions for the composite beam

$$w(x) = -\frac{w_0}{C_2}[(\frac{x}{L})^3 - C_1(\frac{x}{L}) - C_2], \quad -L \le x \le 0,$$

and

$$w(x) = -\frac{w_0}{C_2}[-(\frac{x}{L})^3 + C_1(\frac{x}{L}) - C_2], \quad 0 \le x \le L, \tag{5.19}$$

where w_0 is the total displacement of the middle line on the beam, C_1 and C_2 are the constants which need to be determined, and L is the half-length of the beam. The shape of the deflection of the beam is symmetric about the middle line of the beam.

Slope discontinuity of the beam occurs at the loading point (x = 0), and at the supports (x = -L and x = L), after the initial damage occurs in the beam, and finally the hinges form at these discontinuities when the composite reaches its maximum load and completely fails.

Failure Criteria

We need to apply a failure criterion to the composites to predict the load-carrying capability. The strength theories of composite materials were first investigated by Tsai [104], [105]. Among these theories, Tsai-Hill and Tsai-Wu theories have been widely used for many years. Many researchers then followed these theories and proposed some new failure criteria for predicting the strength and failure of composite structures in various applications.

For impact problems with complete failure or penetration of composite structures, some criteria are more suitable than others. It is demonstrated by many researchers that the maximum strain failure criteria is more suitable than the failure criteria based on stresses in modeling the complete failure (quasi-static punchthrough, low-velocity impact, and high-velocity penetration) of the composites.

Sun, et al. [23], used maximum strain and maximum deflection as the critical parameter for failure criteria in analysis of quasi-static and high velocity impact. Ursenbach, et al. [103] used maximum strain as the failure criteria in analysis of quasi-static penetration of CFRP composite plates. Vinson, et al. [106] first proposed the maximum strain as failure criteria in modeling ballistic impact of textile composites. Zhu, et al. [18] also used maximum strain as penetration criteria.

Based on above discussion, we chose the maximum strain as the failure criteria to analyze the composite beam under cylinder loading.

We notice that for the left half of the beam

$$\text{At } x=-L,\ w(-L)=0;$$

and

$$\text{At } x=0,\quad w(0)= w_0 . \tag{5.20}$$

Applying equation 5.20 to the displacement function, equation 5.19, we have

$$C_1 - C_2 = 1 \quad . \tag{5.21}$$

Applying maximum strain failure criteria, we have

$$\varepsilon_{(x=0)} = \varepsilon_{\max} \quad . \tag{5.22}$$

From equations 5.19, 5.20, and 5.22, we have

$$\frac{C_1}{C_2} = \frac{L\sqrt{2\varepsilon_{\max}}}{w_{0\max}} \quad . \tag{5.23}$$

Thus, C_1 and C_2 can be determined from equations 5.21 and 5.23.

Limit Analysis

When a composite beam completely fails under the cylinder loading, from experimental observation, the beam becomes two halves at the loading point. Also, two ruptures occur at the clamped ends. The beam behaves as two pieces of beam connected with hinges, its displacement at the loading point is not a definite value.

This phenomenon reminds us of the limit analysis of structures in civil engineering. It is very common in the civil engineering community to do the limit analysis on steel and concrete structures to achieve the maximum load-carrying capacity of the structures. However, we have not found the limit analysis in impact or quasi-static loading of composite structures. In order to illustrate the limit analysis methodology in this study, we will briefly discuss limit analysis in civil engineering here. Principles and applications of limit analysis in concrete plasticity can be found in Nielsen's book [107]. There is also an excellent book by Kamenjarzh [108], which illustrates the mathematical foundation of the limit analysis in solids and structures. The book is one of a series of books in applied mathematics and mechanical engineering published by CRC Press. This book covers the concepts, basic ideas, and theorems for limit analysis in solid mechanics with applications to rigid-perfect plastic problems. The limit analysis is rooted in plasticity theory in structures. According the limit analysis in plasticity, there are two important theorems [107].

Lower bound theory: if the load has such a magnitude that it is possible to find a stress distribution corresponding to stresses within the yield surface and satisfying the equilibrium conditions and the static boundary conditions for the actual load, then this load will not be able to cause collapse of the body. This is the statics method.

The upper bound theorem: if various geometrically possible strain fields are considered, the work equation can be used to find values of the load-carrying capacity that are greater than or equal to the true one. This is the kinematics method.

Thus, although it is impractical to determine the maximum deflection of the composite beam by using stress analysis and static approach, it is possible to find the upper bound value of maximum deflection of the beam at its final failure by applying the

kinematics concept in the limit analysis. We introduce limit analysis to this research as follows.

As the load from the cylinder increases, the beam deflection becomes large and undergoes matrix cracking and delamination. Finally the beam fails at the middle due to the fiber breakage. Then the beam becomes a two-piece beam connected by a hinge at the middle. When the load further increases, the displacement of the beam is not a certain value due to the rigid body motion of the hinge. Based on this kinematics concept, a limit analysis method is proposed here. Limit analysis can be performed at the moment that the hinge forms, or at the moment the beam completely fails due to the fiber breakage under the cylinder.

That "the displacement is not a certain value" means that the displacement function w(x) does not have definite values when the beam completely fails. This happens when $w_0 = w_{0\max}$. Thus, this happens when both C_1 and C_2 are approaching infinity in equation 5.15. Solving for C_1, C_2, and imposing these conditions on them, we have the upper bond limit deflection of the composite beam as 0.35665 in. This is the limit deflection of the middle line of the beam which can be reached before it completely fails. This value is the limit case, and will define the upper bond of the maximum deflection of the beam. The measured deflection from experiment should be less than this value. The value of measured displacement from experiment is 0.33333 inches. The difference between the predicted value and experimental result is 7%. This is of significantly improved over that of the analysis done by Kim, et al. [26], in which they reported 30% difference on maximum deflection of Graphite/Epoxy and Glulam-GFRP beams.

Minimum Energy Principle

The displacement function can be determined by obtaining the values of C_1 and C_2. Substituting the maximum deflection into the equations obtained from the boundary condition and maximum strain failure criteria, we can determine the parameters of C_1 and C_2.

With $w_{0\max}$=0.33333 in., corresponding to maximum strain-to-failure of 1.59%, and equations 5.21, 5.23, we have C_1=15.3 and C_2=14.3.

Substituting these displacement functions into the strain-displacement relation and strain energy equation, and applying the minimum energy principle, we have

$$P = 4g_1 w_0^3 + 2g_2 w_0^2 + 2g_3 w_0 \quad , \tag{5.24}$$

where $$g_1 = \frac{bA_{11}}{4C_2^4 L^3}[9 - \frac{108C_1}{7} + \frac{54C_1^2}{5} - 4C_1^3 + C_1^4],$$

$$g_2 = \frac{3bB_{11}}{C_2^3 L^3}[3C_1 - 3 - C_1^2],$$

and

$$g_3 = \frac{12bD_{11}}{C_2^2 L^3}.$$

Stiffness Degradation

One of major differences between the composite laminates and the conventional structural materials, such as aluminum and steel, is that the damage in the composite structure is much more complex. Stiffness of composites degrades due to the matrix cracking and delamination. This phenomenon was first observed experimentally by Reifsnider and his co-workers in early 1980's. A shear lag model was also developed by Reifsnider and his co-workers [101]. The relationship between the stiffness and crack density in the tensile specimen has been established. Many researchers then followed this model and proposed many models to predict the stiffness degradation with the increase in the crack density in the composite specimen under tension. Among these, Talreja developed stiffness-damage relationships based on the continuum mechanics and internal variables [95]. Hashin used variational principles [109]. Laws, et al. [110] used statistical fracture mechanics. Because analytical solutions can be obtained, the stiffness degradation of composite laminate under in-plane loading are well understood.

However, the stiffness degradation in composites due to the transverse loading, such as low-velocity impact or quasi-static loading is not yet well understood. Due to matrix cracking and delamination, stiffness of the composites changes dramatically. The composite undergoes multiple matrix cracking, delamination and fiber breakage, then finally fails under the impact or quasi-static loading. This is a very complex process.

Because there is no analytical solution for these cases, predicting the stiffness degradation of composites during the low-velocity impact, or quasi-static loading, remains a challenging task to researchers. No analytical model has been found in the literature so far.

It is shown by some researchers that strength theory based on the stress failure criteria cannot predict the behavior of the composite with severe damage [25]. Researchers have been proposing approaches to account for material degradation in composites during impact. The approaches proposed are empirical and based on some assumptions. The approaches proposed are quite diverse and are also problem dependent.

In analysis of a rectangular CFRP composite plate under a quasi-static punch, Ursenbach, et al. [103], assumed the damage zone to be an isotropic circular area surrounded by an undamaged circular plate instead of the rectangular plate. They also assumed a fixed-size damage zone. These assumptions significantly reduced the complexity of the problem and still captured the essence of the problem, and made it solvable. With two concentric circular plates, they need use only one variable in the equation to solve this axially symmetric problem. Also, the material degradation is the stiffness of the isotropic damaged circular plate, which can be treated analytically. Their predictions are in quite good agreement with experimental data.

Kim, et al. [26], used constant degradation factors to account for the stiffness degradation due to the damage in composite as follows. For failure related to normal stress in the fiber direction, they used

$$E_1^d = (DF_f)E_1^0,$$

for failure related to normal stress in the transverse direction, they used

$$E_2^d = (DF_m)E_2^0,$$

and for failure related to shear stress, they used

$$G_{12}^d = (DF_m)G_{12}^0,$$

where E_1^d, E_2^d, G_{12}^d are degraded stiffness, E_1^0, E_2^0, G_{12}^0 are original stiffness, DF_f, DF_m are degradation factors in the fiber and in perpendicular fiber directions, respectively. They also did a parametric study of choosing the degradation factors by comparing the predicted ultimate failure loads with the experimental data. By comparison, they chose all of the degradation factors which gave the closest prediction of the failure load, which are 0.25, 0.005.

Sun, et al. [23] proposed a simple model for thick composite laminates subjected to high velocity impact. They modeled the damaged material in a global sense to reproduce the load-displacement curve during quasi-static penetration, since a detailed modeling of delaminated plates is very difficult and impractical. First of all, they used effective laminate elastic properties for quasi-isotropic lay-up of $[0/90/\pm 45]_{s,n}$. Since the major damage to the material before plug formation consists of matrix cracks and delamination, the global modeling of damage was achieved by reducing the effective shear modulus of the laminate to a degraded value. The effective in-plane modulus was assumed to remain the same as the undamaged value since there is no major fiber breakage in the material until the plug is formed. The effective shear modulus was degraded uniformly from the center to the boundary of the plate. Instead of using constant degradation factors as used by Kim, et al.; Sun used five steps (piece-wise linear elastic approach) to account for the reduction of stiffness. For each of these load steps, a value of the reduced shear modulus was determined that would give a close approximation to the average slope of the load-displacement curve.

Jenq, et al. [111] used a similar approach to model the degradation of the material of woven glass/epoxy laminate impacted by a hemisphere impactor. They modeled the degraded material in the delamination zone by reducing the apparent transverse shear modulus uniformly in the delamination zone. The results were determined numerically based on a semi-empirical exercises to fit the load-deflection curve.

The above approaches did not give the analytical solution for material degradation in the composite because of the complexity of the impact problem.

When a composite beam is under cylinder loading in large deflection, the tensile (membrane) stress generated in the beam is predominant, and the bending stress is secondary. Part of the stiffness degradation of the beam is due to the tensile stress in the beam generated by cylinder. Thus, we could use the knowledge of stiffness degradation from a beam under tension in this research.

Also, due to the bending of the beam, the mutliple matrix cracking is more severe than that of beam under uniaxial tension loading. The top and bottom plies of the beam have the most matrix cracking, and at the final stage of the loading, these two plies suffer substantial cracking and delamination from the inner plies. We propose the effective thickness of the beam to account for the damage in the top and bottom plies.

Another factor, the free-edge effect along the two sides of the beam length, is important. According to the experiment and analysis done by Johnson, et al. [112] in 1996, the international damage modes in composite laminates under tension to their final failure could be classified into four modes: matrix cracking, matrix-crack-induced microcracks, matrix-crack-induced delamination, and fiber breakage.Their analysis accounts for the edge effect caused by matrix-crack-induced microcracks and matrix-crack-induced delamination which usually occur on the specimen's free edges. The combination of tension and bending makes matrix-crack-induced microcracks propagate and induce more delamination. Because of this effect, the cracks across the width of the beam are not uniform. The edges have denser cracks than in the central part across the width. Also, delamination in the beam contributes to the damage. Thus we introduce the effective width of the beam to account for these damages.

Based on the approaches proposed by other researchers, and the loading condition of present research, we propose a new approach to account for the material degradation of composite beams under cylinder loading.

In order to predict the stiffness degradation of the beam here, the relationship between the stiffness degradation and the parameter which is related to the loading in the impact process has to be established. Based on the experimental data and many approaches developed by other researchers, a new relationship for describing the stiffness degradation in the beam under cylinder impact is proposed here. Since the membrane tension dominates the deformation of the beam, it is proposed that the crack density is proportional to the displacement of the middle line on the beam. Thus the stiffness degradation is directly related to the deflection of the middle line on the beam.

Instead of assuming the constant degradation factors or piece-wise linear degradation relation, we propose that stiffness degrades nonlinearly to half of its original value until the cracks saturate; that is, when the beam finally fails. This is according to the observation that tension dominates in the beam and it is analogous to the composite under tension. Then the stiffness degradation with the deflection of the middle line of the beam is

$$E_1 = \frac{E_1^0}{1 + \frac{w_0}{w_{0\max}}} \quad , \tag{5.25}$$

where E_1 is the degraded Young's modulus and E_1^0 is the original undamaged Young's modulus. The multiple cracks that are predominantly perpendicular to the fiber direction are taken account in the stiffness degradation by equation 5.21.

Delamination also occurs between the layers and provoke debonding between the fibers and matrix edge cracks along the two longitudinal edges of the beam. Because of these delaminations and debonds, the effective thickness and width of the beam to withstand the impact load decreases during the process of the cylinder loading. These effects must be considered to accurately predict the mechanical behavior of the beam

during the loading. Without including these factors, the prediction will less accurate [26]. Based on the above discussion, two more relationships are proposed here.

Due to the tension and bending, severe damage occurs at the top and bottom plies, and they virtually contribute very little to the thickness when the deflection reaches the maximum value (more that 6 times of the thickness of the beam), or when the beam completely fails. The effective thickness of the beam decreases linearly with the increase of the deflection of the middle line of the beam. This expressed by

$$T_e = -\frac{w_0 T_d}{w_{0\max}} + T_0 \quad , \tag{5.26}$$

where T_d is the final degraded thickness of the beam and T_0 is the original thickness of the beam.

Due to tension, bending and the edge effect, cracks have higher density along the two edges than at the central part across the width of the beam. Delamination also contributes to the degradation of the width. The effective width of the beam decreases linearly with the increase of the deflection of the middle line of the beam, as expressed by

$$b_e = -\frac{w_0}{w_{0\max}}(b_0 - b_d) + b_0 \ , \tag{5.27}$$

where b_d is the final degraded width of the beam andb_0 is the original width of the beam.

Equations 5.24 through 5.27 give the final load-deflection relationship of the composite beam. For graphite/bismaleimide composite beams without SMA fibers, the load-deflection relation can be easily computed from equations 5.24 through 5.27 with symmetric lay-up. For graphite/bismaleimide composite beams with SMA fibers, stress/strain-induced martensite transformation depends on the contact load. When the contact load reaches a certain value, SMA fibers start the phase transformation from austenite to martensite at the loading line. The phase front then propagates to the two

ends of the composite beam. Due to this transformation, the stiffness of SMA/ bismaleimide lamina is changing along the length of the beam during the loading. Figs. 5.6 (a-d) shows schematically the loading process from the beginning to the failure of the SMA beam with the growth of the stress/strain induced martensite phase transformation along the beam. An algorithm for computing the critical parameters and simulating this phase transformation and loading process is developed. The algorithm is also coded in Virtual C++ 4.0. The codes are included in Appendices A and B. The material properties and parameters are given in Table 5.1.

Table 5.1 Properties of SMA composite beam and parameters.

Length of beam	4 in.	Strain to initiate M transformation	0.0065
Width of beam	0.75 in.	Strain-to-failure of composite	1.59%
Thickness of beam	0.048 in.	Width degradation factor	0.3
Volume fraction of SMA Ksma	0.138	Young's modulus of composite E1	23.8 ksi
Young's modulus of matrix Em	0.5 ksi	Parameter for effective thickness	0.018
Young's modulus of SMA E1sma	11.85928 ksi	Constant C1	15.3
Young's modulus of SMA E2sma	0.16008 ksi	Constant C2	14.3

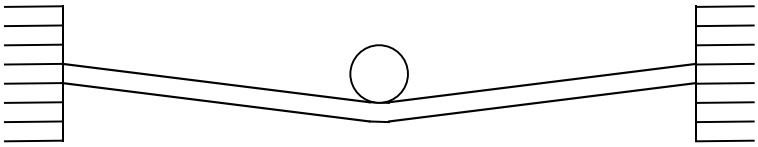

Figure 5.6 (a) Stage one: SMA fibers are in austenite phase during the initial contact loading (SMA composite beam under cylinder loading, schematically).

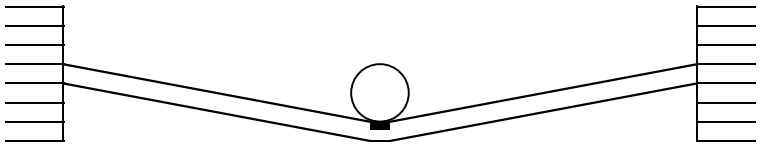

Figure 5.6 (b) Stage two: Martensite phase transformation starts at the middle of the beam at the loading point (SMA composite beam under cylinder loading, schematically).

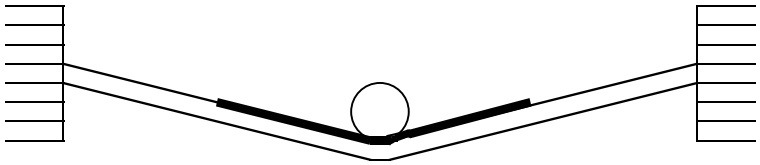

Figure 5.6 (c) Stage three: Martensite phase transformation proceeds along the beam when the cylinder continues to load (SMA composite beam under cylinder loading, schematically).

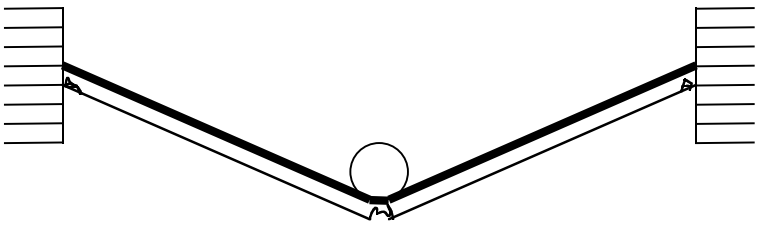

Figure 5.6 (d) Stage four: Martensite phase transformation propagates out along the beam and reaches two ends of the beam with varying transformation fraction along the beam. The loading point has the highest transformation fraction, and the two ends have the lowest value. The composite beam fails at the loading point while SMA fibers are not broken (SMA composite beam under cylinder loading, schematically).

5.10 Results

The predicted load-deflection curve and experimental measured data for load-deflection are shown in Fig. 5.7. The dotted line is the experimental data of SMA composite beam. Bold solid line is the prediction by the model. Solid line is the experimental data of plain composite beam. The two most important parameters are the maximum deflection and maximum load. The predicted maximum deflection (upper bond limit value) is 0.35665 in., compared with 0.33333 in. from experiment, the error is 7 %. The error is calculated by using the formula, error (percentage) = (predicted value-experimental value)/experimental value, throughout this chapter. The predicted maximum load of SMA composite beam (with width degradation factor 0.3) is 710.3 lbs, while the experimental value is 710 lbs. A sensitivity study of the width degradation factor is performed. It was found that the width degradation factors from 0.27 to 0.33 give the predicted maximum load of SMA composite beam with error less than 4.2 %. It was also found that width degradation factors from 0.28 to 0.34 provide the predicted maximum load of plain composite beam with error less than 4.88 %. These results are listed in the Appendix C. Also, we can see from the load-deflection curves, the model captures the highly nonlinear characteristics of SMA composite beam during the failure process. The model simulates the stress/strain induced martensite phase transformation along the beam during the loading. It starts at the center of the beam underneath the loading point, proceeds towards the two ends of the beam. The C++ code in Appendix A simulates the front of martensite phase transformation in the x coordinate as shown in the output file in Appendix D. Non-uniform distribution of martensite phase transformation is due to the non-uniform distribution of strain along the beam. The center part, the loading point has the highest strain, and finally breaks first, while the two ends have the lowest values of strain. Also, the bottom has larger strain than that of the corresponding point on the top of the beam. These are shown in Figs. 5.8 and 5.9.

Fig. 5.10 shows that the difference between the strain distributions along the top ply when martensite starts underneath the loading point and at the moment the beam finally fails. The counter part for the bottom ply is shown in Fig. 5.11. As we can see,

substantial increase in strains between these two stages, which is the characteristics of large deformation problem.

The model also can be used to study the effect of different lay-up of SMA fibers on the maximum load, as shown in Fig. 5.12. Two sets of SMA fibers embedded on top and bottom layers will significantly increase the maximum load-carrying capability of the beam.

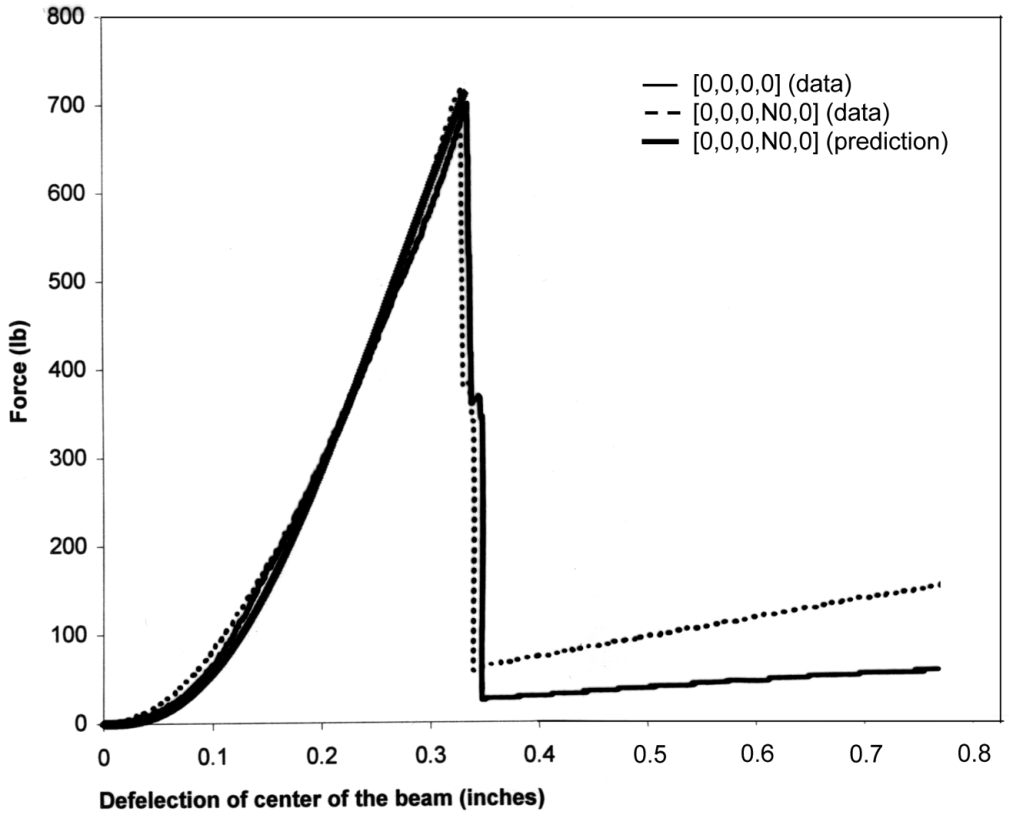

Figure 5.7 Prediction by the model and experimental data [98].

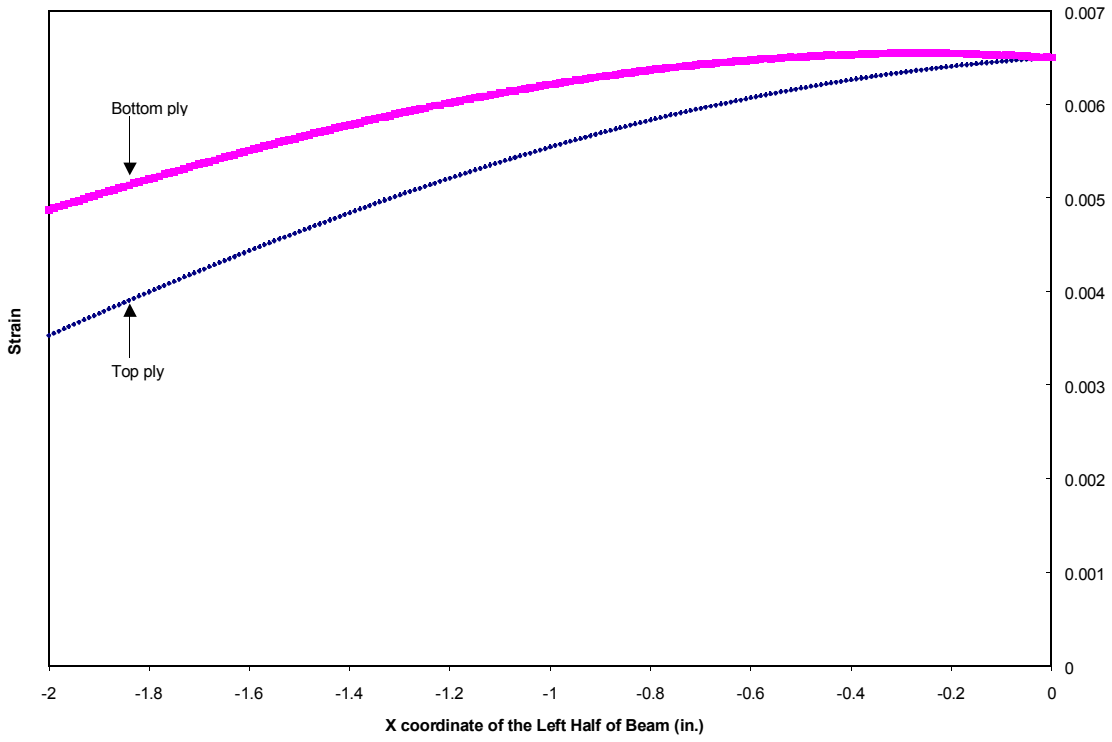

Figure 5.8 Strain distributions on the top and the bottom plies of the beam (Initial stage).

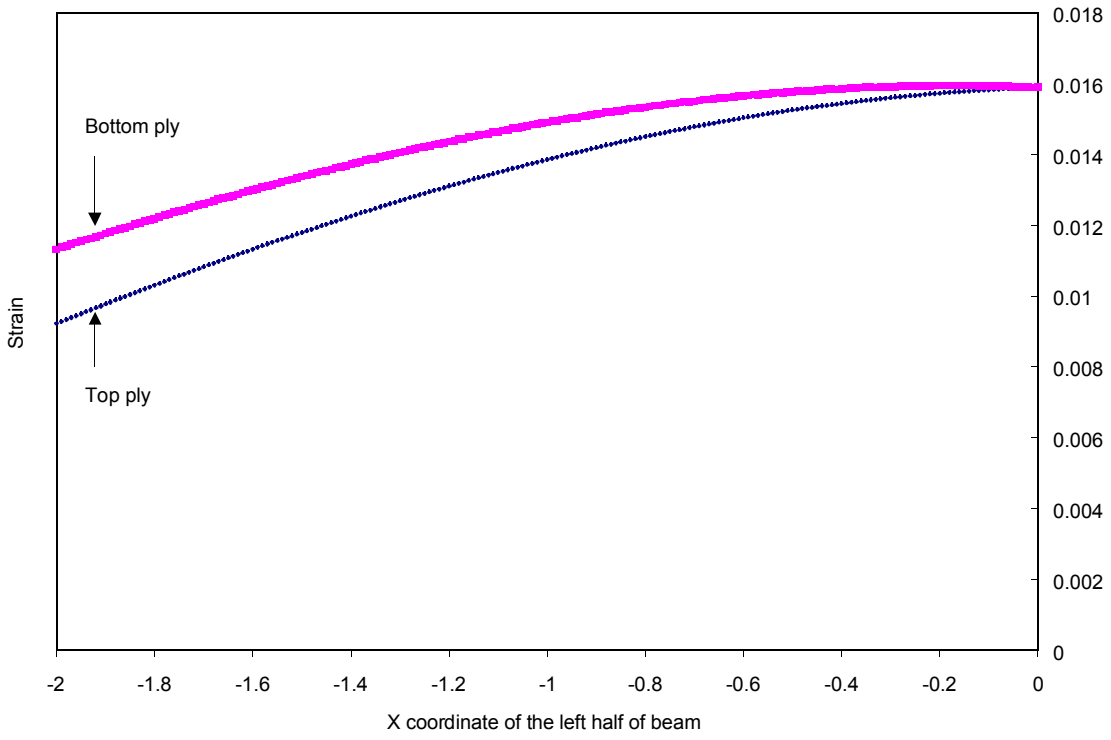

Figure 5.9 Strain distributions on the top and the bottom plies of the beam (Final Stage).

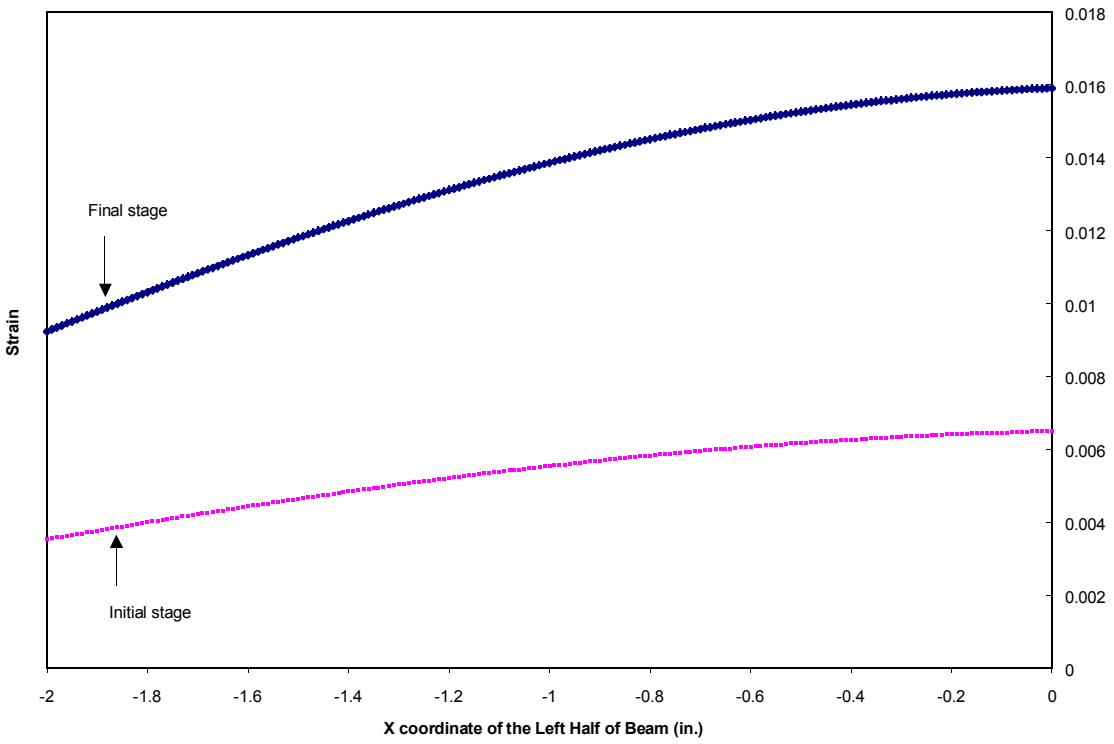

Figure 5.10 The strain distributions on top ply of the beam.

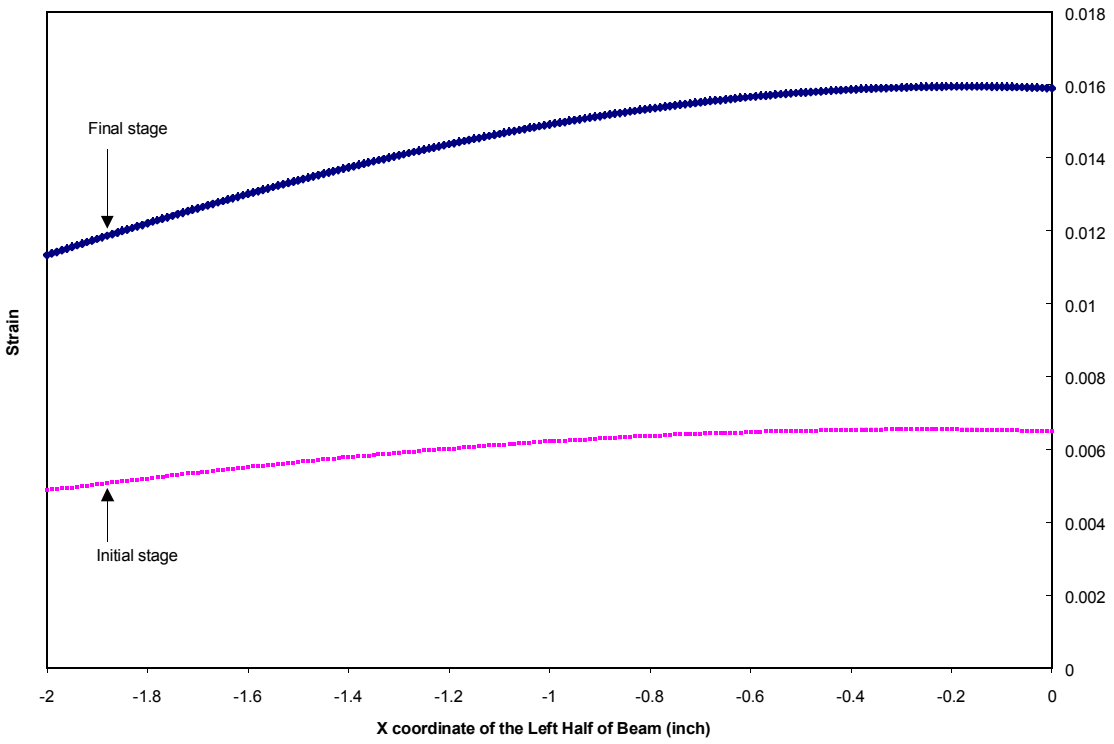

Figure 5.11 The strain distributions on bottom ply of the beam.

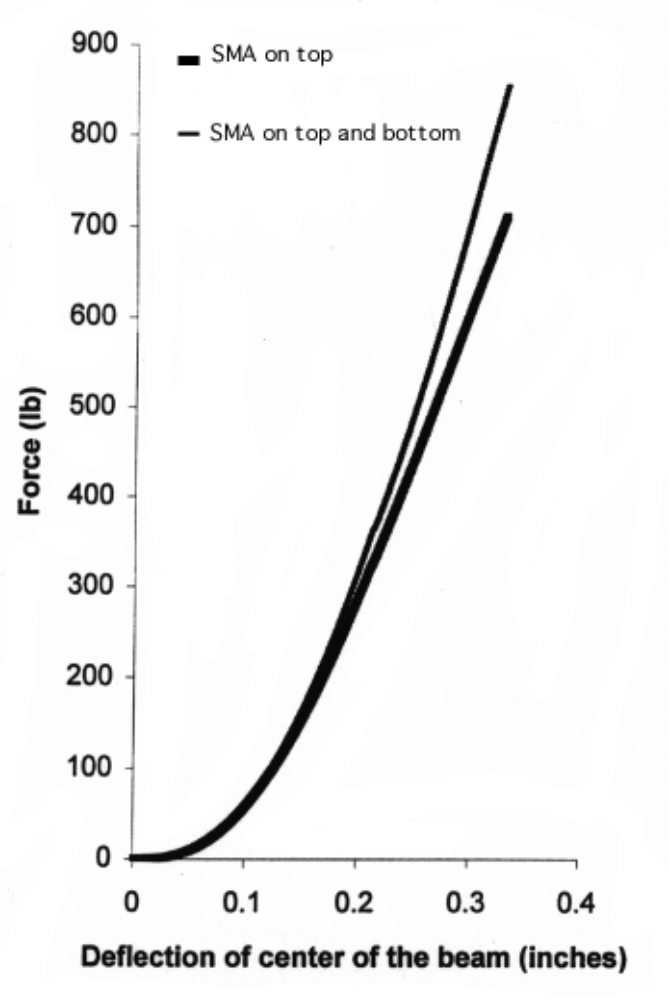

Figure 5.12 The effect of SMA fiber lay up on the maximum load.

5.11 Conclusions and Summary

A nonlinear beam model and a new failure analysis method have been developed to predict the load-deflection characteristics of a Graphite/Bismaleimide composite beam under the quasi-static by a steel cylinder. The model considers the large deflection of the beam, contact deformation of the beam, stiffness degradation due to the matrix cracks, delamination, and fiber breakage. The model captures the characteristics of SMA composite beam with strong nonlinearity in geometry and materials. The model also simulates the stress/strain induced martensite phase transformation during this failure process. This is the fist reported research in modeling SMA composite under low velocity impact and quasi-static loading resulting in the complete failure. Thus, it is the contribution to the literature. The model and the understanding developed here can be used for further study and design of SMA composites for low velocity impact or quasi-static loading in failure process.

Chapter Six

Conclusions and Future Work

This research studied some basic issues of strain energy absorption of shape memory alloys, and their applications in SMA hybrid composites for damage resistance under low-velocity impact and quasi-static loading. New models are proposed for strain energy absorption of shape memory alloys, SMA hybrid composite plates and beams under impact. New failure analysis method is proposed for analyzing the failure process of SMA hybrid composite beam with strong geometric and material nonlinearities. The conclusions and summary are:

1. The strain energy absorption of shape memory alloy bars and beams under tension and bending loading was studied. This theoretical model gives quantitative relations between the martensite fraction, the applied load, and the strain energy absorbed in the SMA. The theoretical relations are only valid in the elastic range, stopping at the end of the martensitic phase transformation where the plastic deformation begins. As expected, the super-elastic SMA has demonstrated a high strain energy absorption capability. Also, the SMA shows a highly nonlinear relation between the martensite fraction, the applied load, and the strain energy absorbed in the SMA. The closed form solution of the strain energy absorption capability of SMA bars is a simple and useful tool in the design of energy absorption applications of super-elastic SMA. The model also gives, the threshold load for initiating and completing the martensitic phase transformation both for tension and bending loading. The advantage of using super-elastic SMA to absorb strain energy compared to martensitic SMA was demonstrated numerically.

2. The nonlinear equations for SMA hybrid composite plate, which can be used for low-velocity impact or quasi-static contact loading, are derived. The governing equations include the transverse shear deformation to the first order, large deformation of the plates,

and SMA/matrix lamina. The equations are derived in the general form with general boundary conditions, general stack of angle ply. The equations can be simplified to special forms in the specific applications.

3. A theoretical study of the impact force and the strain energy absorption of an SMA/graphite/epoxy composite beam under a low-velocity impact has been performed. The contact deformation, the global bending deformation, the transverse shear deformation, and the martensitic phase transformation of the super-elastic SMA fibers are studied. Then, the energy absorbed by the SMA hybrid composite was calculated for each of the absorption mechanisms: contact deformation, global bending deformation, and transverse shear deformation. The basic relationship between the energy absorption mechanisms and the extent of martensitic phase transformation is obtained. It was found numerically that the total strain energy absorption of the SMA hybrid composite beam increases when the martensitic fraction of SMA increases. This observation agrees with the conclusions drawn from previous experiments. This is an important numerical observation, which has built the basis for further study of SMA composite under impact. This is the first effort to perform the analysis on the impact of SMA hybrid composite, and the results are enable us to go further and study the modeling of damage and failure of SMA composite in low velocity impact or quasi-static contact loading

4. A nonlinear beam model and a new failure analysis method have been developed to predict the load-deflection characteristics of a Graphite/Bismaleimide composite beam under the quasi-static load by a steel cylinder. The model considers the large deflection of the beam, contact deformation of the beam, stiffness degradation due to the matrix cracks, delamination, and fiber breakage. The model captures the characteristics of SMA composite beam with strong nonlinearities in both geometry and materials. The model also simulates the stress/strain-induced martensite phase transformation during this failure process. The model and the method developed here can be used for further study and

design of SMA composites for low-velocity impact or quasi-static loading in failure process.

5. This research is the first reported research in the analysis and modeling of strain energy absorption of super-elastic SMA, and SMA hybrid composites for damage resistance.

The models, method and conclusions developed in this research provide some basis and tools for future research and design of SMA hybrid composites for energy absorption and damage resistance.

While this research has shown the great promise of SMA hybrid composites, there is still much future work to be done to utilize its potential .

It was found that due to the martensite transformation, super-elastic SMA can withstand the load after the host composites fail. Thus, it has more energy absorption capability. However, the martensite transformation has not been utilized to its full potential in SMA Graphite/Bis composites since the degree of the phase transformation is small when the beam fails. Thus, in order to use SMA's potential, more compatible materials with the strain-to-failure larger than that of graphite composites are needed to hold the super-elastic SMA to make them more compatible. Such as thermoplastic layers could provide this functionality and could be used together with SMA and graphite composites. Experimental investigations are needed for this purposes.

Since this study here is the first effort to model and analyze the SMA composites under low-velocity impact and quasi-static loading in the failure process, there are tasks need to be done to improve the models proposed here and enhance our understanding about the failure process of SMA composites. Micromechanical models will give us in depth understanding of multiple cracks, delamination, and material degradation of SMA hybrid composites during the quasi-static contact loading or low-velocity impact. Although it looks forbidden to develop such micromechanical models for impact and failure process, it worthies trying, since we cannot fully understand the failure process until we know it in micro-scale.

References

[1] Tracy, J. J., Dimas, D. J., and Pardoen, G. C., "The effect of impact damage on the dynamic properties of laminated composite plates," Proceedings of 5th International Conference on Composite Materials, ICCM-V, San Diego CA, July 29-August 1, 1985, pp.111-125.

[2] Wang, C. Y. and Yew C. H., "Impact damage in composite laminates," *Computer and Structures*, Vol. 37 (6), 1990, pp.967-982.

[3] Sun, C. T. and Chattopadhyay, S., "Dynamic response of anisotropic plates under initial stress due to impact of a mass," *Journal of Applied Mechanics*, Vol. 42, 1975, pp. 693-698.

[4] Caprino, G., Crivelli-Visconti, I., and Di Ilio, A., "Elastic behavior of composite structures under low velocity impact," *Composites,* Vol.15(3), 1984, pp. 231-234.

[5] Sjoblom, P., Hartness, J., and Cordell, T. , "On low-velocity impact of composite materials," *Journal of Composite Materials*, Vol.22 (1), 1988, pp. 30-52.

[6] Shivakumar, K. N., Elber, W. and Illg, W., "Prediction of impact force and duration due to low-velocity impact on circular composite laminates," *Journal of Applied Mechanics*, Vol. 52, September 1985, pp. 674-680.

[7] Wu, H. Y. and Springer, G. S., "Measurements of matrix cracking and delamination cause by impact on composite plates," *Journal of Composite Materials*, Vol. 22 (1988), pp.518-532.

[8] Elber, W., "Effect of matrix and fiber properties on impact resistance," *Tough Composite Materials: Recent developments*, Noyes, Park Ridge, NJ, 1985, pp. 89-110.

[9] Sierakowski, R. L., and Chaturvedi, S. C., "Dynamic Loading and Characterization of Fiber-Reinforced Composites", John Wiley & Sons, Inc., 1997.

[10] Matsumoto, H., Ogwa, Y. and Adchi, T., "Stress analysis of an orthotropic

laminated slab to transverse load," *JSME International Journal Series*, I, Vol.35(2), 1992, pp.165-169.

[11, 12] Choi, H.Y., Downs, R. J., and Chang, F. K., "A new approach toward understanding damage mechanisms and mechanics of laminated composites due to low-velocity impact: Part I- experiments, Part II- Analysis," *Journal of Composite Materials*, Vol.25, (1991), pp. 992-1038.

[13] Choi, H.Y. and Chang, F. K., "A model for predicting damage in graphite/epoxy laminated composites resulting from low-velocity point impact," *Journal of Composite Materials*, Vol. 26, No. 14, (1992), pp. 2134-2169.

[14] Sun, C. T. and Jih, C. J., "A quasi-static treatment of delaminatioin crack propagation in laminates subjected to low velocity impact," Proceedings of 7th Technical Conference of ASC, Pennsylvania State University, October 13-15, pp. 949-961.

[15] Cantwell, W. J. and Morton, J., "Comparison of the low and high velocity impact response of CFRP," *Composites,* Vol. 20(6), (1989), pp. 545-551.

[16] Cantwell, W. J. and Morton, J., "The influence of varying projectile mass on the impact response of CFRP," *Composite Structures*, Vol.13, (1989), pp. 101-104.

[17] Cantwell, W. J. and Morton, J., "Impact perforation of carbon fibre reinforced plastic," *Composite Science and Technology*, Vol. 38, (1990), pp. 119-141.

[18] Zhu, G., Goldsmith, W., and Dharan, C. K. H., "Penetration of laminated kevlar by projectiles- I. Experimental investigation," *International Journal of Solids and Structures*, Vol. 29 (1992), pp. 421-436.

[19] Lee, S. W. R. and Sun, C. T., "Dynamic penetration of graphite/epoxy laminates impacted by a blunt- ended projectile," *Composite Science and Technology*, Vol.49 (1993), pp. 369-380.

[20] Wu, E., Tsai, C. Z. and Chen, Y. C., "Pentration of glass/epoxy composite laminates," *Journal of Composite Materials*, Vol.28, (1994), pp. 1783-1802.

[21] Abrate, S., "Impact on laminated composites: recent advances," *Applied Mechanics Reviews*, Vol. 47, No. 11 (1994), pp.517-544.

[22] Goldsmith, W., Dharan, C. K. H., and Chang, H., "Quasi-static and ballistic perforation of carbon fiber laminates," *International Journal of Solids and Structures*, Vol. 32, No.1 (1995), pp. 89-103.

[23] Sun, C. T. and Potti, S. V., "A simple model to predict residual velocity of thick composite laminated subjected to high velocity impact," *Internal Journal of Impact Engineering*, Vol.18, No.3 (1996), pp. 339-353.

[24] Lee, S. W. R. and Sun, C. T., "A quasi-static penetration model for composite laminates," *Journal of Composite Materials*, Vol.27 (1993), pp. 251-271.

[25] Greif, R. and Chapon, E, "Investigation of successive failure modes in graphite epoxy laminated composite beams," *Journal of Reinforced Plastics and Composites*, Vol. 12 (1993), pp. 602-620.

[26] Kim, Y., Davalos, J. F. and Barbero, E. J., "Progressive failure analysis of laminated composite beams," *Journal of Composite Materials*, Vol.30, No.5 (1996), pp. 536-560.

[27] Abrate, S. "Impact on laminated composite materials," *Applied Mechanics Review*, Vol. 44, No. 4 (1991), pp. 155-190.

[28] Cantwell, W. J., Curtis, P. T., and Morton, J., 1986, "An assessment of the impact performance of CFRP with high strain carbon fibers", *Composites Science and Technology*, Vol. 25 (1986), pp. 133-148.

[29] Cantwell, W. J., Curtis, P. T., and Morton, J., "Low velocity impact damage tolerance in CFRP laminates containing woven and non-woven layers", *Composites*, Vol. 14 (1983), pp. 301-305.

[30] Jang, B. Z., Chen, L. C., Wang, C. Z., Lin, H. T., and Zee, R. H., "Impact resistance and energy absorption mechanisms in hybrid composites", *Composites Science and Technology*, Vol. 34 (1989), pp. 305-335.

[31] Wang, C. J. and Jang, B. Z., "Deformation and fracture mechanisms of advanced

polymer composites under impact loading," *Journal of Thermoplastic Composite Materials,* Vol.4 (1991), pp. 140-172.

[32] Paine, J. S. N., and Rogers, C. A., "The response of SMA hybrid composite materials to low velocity impact", *Journal of Intelligent Material Systems and Structures*, Vol. 5 (1994), pp. 530-535.

[33] Paine, J. S. N., and Rogers, C. A., "Observations of the drop-weight impact response of composites with surface bonded nitinol layers", *Proceedings, Durability and Damage Tolerance of Composites Symposium, ASME IMEC&E*, San Francisco, CA, November. 12-18, 1995.

[34] Kiesling, T.C., Chaudhry, Z., Paine, J.S.N., and Rogers, C.A., 1996, "Impact Failure Modes of Thin Graphite Epoxy Composites Embedded with Superelastic Nitinol", *Proceedings, 37th AIAA/ASME/ASCE/AHS/ASC Structures, Structural Dynamics, and Materials Conference*, Salt Lake City, Utah, 15-17 April 1996, pp. 1448-1457.

[35] Ellis, R., Lalande, F., Jia, H., and Rogers, C. A., "An investigation into the energy absorbed during ballistic impact of shape memory alloy and SPECTRA hybrid composites", 38th AIAA/ASME/ASCE/AHS/ASC Structures, Structural Dynamics, and Materials Conference, pp.906-916, April 7-10, 1997, Orlando, Florida.

[36] Buehler, W. J., and Wiley, R. C., Nickle-based alloys, (1965) *US Patent 3,174,851*.

[37] Buehler, W. J. and Cross, W. R., *Wire Journal*, Vol. 2, (1969), pp. 41.

[38] Harrison, J. D. and Hodgson, D. E., Shape memory effects in alloys (1975), pp.517, Plenum.

[39] Liang, C. and Rogers, C. A., "A multi-dimensional constitutive model for shape memory alloys," *Journal of Engineering Mathematics,* Vol. 26 (1992), pp. 429-443.

[40] Paine, J. S. N. and Rogers, C. A., "Review of multi- functional SMA hybrid composite materials and their applications," *Proceedings, Adaptive Structures and Material Systems,* No. 1. (1994) AD-45, ASME, Chicago, IL.

[41] Liang, C., "The constitutive modeling of shape memory alloys," Ph.D. Dissertation (1990), Virginia Tech.

[42] Cross, W. B., Kariotis, A. H. and Stimler, F. J., "Nitinol Characterization Study," Goodyear Aerospace Corporation Report No. Ger 14188, (NASA CR-1433) (1970), Akron, Ohio.

[43] Jia, H, Lalande, F. and Rogers, C. A., "Review of constitutive modeling of shape memory alloys," *International Mechanical Engineering Congress and Exposition,* Nov. 17-22, (1996), Atlanta, GA, Vol. AD-52, pp. 585-591.

[44] Müller, I., "A model for a body with shape memory," *Arch. Rational Mech. Anal*., Vol.70 (1979), pp. 61-77.

[45] Müller, I. and Wilmanski, K., "A model for phase transformation in pseudoelastic bodies," I1 *Nuovo Cimento*, Vol. 57B (1980), pp. 238-318.

[46] Müller, I., "On the size of the hysteresis in pseudoelasticity," *Continuum Mechanics, Thermodynamics*, Vol. 1 (1989), pp.125-142.

[47] Müller, I. and Xu, H., "On the pseudo-elastic hysteresis,"*Acta Metallurgy Materials*., Vol.39 (1991), pp. 263-271.

[48] Falk, F., "Model free energy, mechanics, and thermodynamics of shape memory alloys," *Acta Metallurgical*, Vol. 28 (1980), pp. 1773-1780.

[49] Hoffmann, K. H. and Zheng, S. M., "Uniqueness for nonlinear coupled equations arising from alloy mechanism," Preprint No.118 (1986), Inst. fur Mathe, Uni. Augsburg.

[50] Hoffmann, K. H. and Sprekels, J., "Phase transformation in shape memory alloys I: stability and optimal control," Preprint No. 136 (1987), Inst. fur Mathe, Uni. Augsburg.

[51] Liang, C. and Rogers, C. A., "One-dimensional thermomechanical constitutive relations for shape memory materials," *Journal of Intelligent Material Systems and Structures*, Vol.1 (1990), pp. 207-234.

[52] Tanaka, K. and Nagaki, S., "A thermomechanical description of materials with internal variables in the process of phase transformation," *Ingenieur-Archiv*, Vol.51

(1982), pp. 287-299.

[53] Tanaka, K. and Iwasaki, R., "A phenomechanical theory of transformation superplasticity," *Engineering Fracture Mechanics*, Vol. 21, No. 4 (1985), pp. 709-720.

[54] Tanaka, K., "A thermomechanical sketch of shape memory effect: one-dimensional tensile behavior," *Res. Mechanica*, Vol.18 (1986), pp. 251-263.

[55] Tanaka, K. and Fischer, F. D., "Deformation analysis of shape memory alloys during thermomechanical processes," *Mechanics of Materials* -VI, Vol. 3 (1991), Jono, M. and Inoue, T., eds., New York: Pergamon Press, pp. 249-254.

[56] Tanaka, K., Nishimura, F. and Tobushi, H., "Phenomenological analysis on subloops in shape memory alloys due to incomplete transformations," *Journal of Intelligent Material Systems and Structures*, Vol.5 (1994), pp. 487-493.

[57] Tanaka, K.,Oberaigner, E. R., and Fischer, F. D., "A unified theory on thermomechanical mesoscopic behavior of alloy materials in the process of martensitic transformation," *Mechanics of Phase Transformations and Shape Memory Alloys*, AMD-Vol. 189/PVP-Vol. 292 (1994), pp.151-157.

[58] Zhang, X. D., Rogers, C. A. and Liang, C., "Modeling of the two-way shape memory effect," *Philosophical Magazine A*, Vol. 65, No. 5 (1992), pp.1199-1215.

[59] Brinson, L.C. , "One-dimensional constitutive behavior of shape memory alloys: thermomechanical derivation with non-constant material functions and redefined martensite internal variable," *Journal of Intelligent Material Systems and Structures*, Vol. 4 (1993), pp. 229-242.

[60] Brinson, L. C., and Lammering, R., "Development and application of one-dimensional truss finite elements for shape memory alloys," *Adaptive Structures and Material Systems*, AD-Vol. 35 (1993), ASME, pp.1-10.

[61] Brinson, L. C., and Lammering, R., "Finite element analysis of the behavior of shape memory alloys and their applications," *International Journal of Solids and*

Structures, Vol. 30, No. 23 (1993), pp.3261-3280.

[62] Barret, D. J., "A one-dimensional constitutive model for shape memory alloys," *Journal of Intelligent Material Systems and Structures*, Vol.6 (1995), pp. 329-337.

[63] Barret, D. J. and Sullivan, B. J., "A three-dimensional phase transformation model for shape memory alloys," *Proceedings of the SES Symposium on Active Materials and Smart Structures* (1994), pp.246-259.

[64] Boyd, J. G. and Lagoudas, D. C., "A constitutive model for simultaneous transformation and reorientation in memory materials," *Mechanics of Phase Transformations and Shape Memory Alloys*, AMD-Vol. 189/PVP-Vol. 292 (1994), pp. 159-172. ASME .

[65] Bo, Z. and Lagoudas, D.C., "Comparison of different thermomechanical models for shape memory alloys," *Adaptive Structures and Composite Materials: Analysis and Application*, AD-Vol. 45/MD-Vol. 54 (1994), pp. 9-19, ASME.

[66] Kafka, V., "Shape memory: a new concept of explanation and of mathematical modeling. part I: micromechanical explanation of the causality in the SM processes," *Journal of Intelligent Material Systems and Structures*, Vol.5 (1994), pp. 809-814.

[67] Kafka, V., "Shape Mmmory: a new concept of explanation and of mathematical modeling. part II: mathematical modeling of the SM effect and of pseudoelasticity, " *Journal of Intelligent Material Systems and Structures*, Vol.5 (1994), pp. 815-824.

[68] Kafka, V., *Inelastic Mesomechanics*, Singapore, New Jersey, Hong Kong: World Scientific Publ. Co., (1987).

[69] Brandon, D. and Rogers, R. C., "Constitutive laws for pseudo-elastic materials," *Journal of Intelligent Material Systems and Structures*, Vol. 3 (1992), pp. 255-267.

[70] Graesser, E. J., "Multi-dimensional modeling of hysteretic materials including shape memory alloys: theory and experiment," Ph.D. dissertation (1990), State University of New York at Buffalo, NY.

[71] Graesser, E. J. and Cozzarelli, F. A., "Shape memory alloys as new materials for

seismic isolation," *Journal of Engineering Mechanics*, Vol.117, No. 11 (1991), pp. 2590-2608.

[72] Graesser, E. J. and Cozzarelli, F. A., "A proposed three-dimensional constitutive model for shape memory alloys," *Journal of Intelligent Material Systems and Structures*, Vol.5 (1994), pp. 78-89.

[73] Ivshin, Y. and Pence, T. J., "A thermomechanical model for a one variant shape memory material," *Journal of Intelligent Material Systems and Structures*, Vol.5 (1994), pp. 455-473.

[74] Pence, T. J. and Grummon, D. S. and Ivshin, Y., "A macroscopic model for thermoelastic hysteresis in shape-memory materials," *Mechanics of Phase Transformations and Shape Memory Alloys*, AMD-Vol. 189/PVP-Vol. 292 (1994), pp. 45-58 , ASME.

[75] Abeyaratne, R., Kim, S. J. and Knowles, J. K., "Continuum modeling of shape memory alloys," AMD-Vol. 189/PVP-Vol. 292 (1994), *Mechanics of Phase Transformations and Shape Memory Alloys*, pp. 59-69, ASME.

[76] Boyd, J. G. and Lagoudas, D. C., "Thermomechanical response of shape memory composites," *Journal of Intelligent Material Systems and Structures*, Vol.5 (1994), pp. 333-346.

[77] Rogers, C. A., and Robertshaw, H. H, "Shape memory alloy reinforced composites", *Engineering Science Preprints* 25, ESP25.88027, Society of Engineering Sciences, (1988).

[78] Sunders, W. R., Robertshaw, H. H, and Rogers, C. A., "Structural acoustic control of a shape memory alloy composite beam", *Journal of Intelligent Material Systems and Structures*, Vol. 2 (1991), pp. 508-527.

[79] Ro, J., and Baz, A., "Nitinol-reinforced plates: part I. thermal characteristics," *Composite Engineering*, Vol.5, No.1 (1995), pp. 61-75.

[80] Saravanos, D. A., Birman, V., and Hopkins, D. A., "Micromechanics and stress

analysis of composites with shape memory alloy fibers in uniform thermal fields," *AIAA-95-1210-CP* (1995), pp. 433-443.

[81] Jia, J., and Rogers, C. A., " Formulation of a laminated shell theory incorporating embedded distributed actuators," *Journal of Mechanical Design*, Vol. 112 (1990), pp. 596-604.

[82] Chia , C. Y., "*Nonlinear Analysis of Plates*," McGraww-Hill, Inc., (1980).

[83] Whitney, J. M., "*Structural Analysis of Laminated Anisotropic Plates*," Technomic, Lancaster, PA, (1987).

[84] Reddy, J. N., "Geometrically nolinear transient analysis of laminated composite plates," *AIAA Journal*, V. 21, No. 12 (1983), pp. 621-629.

[85] Reddy, J. N., "A simple higher-order theory for laminated composite plates," *Journal of Applied Mechanics*, Vol. 51 (1984), pp.745-752.

[86] Wen, H. M., Reddy, T. Y., and Reid, S. R., "Deformation and failure of clamped beams under low speed impact loading," *International Journal of Impact Engineering*, V.16, No. 3 (1995), pp. 435-454.

[87] Jones, R. M., *Mechanics of Composite Materials*, Hemisphere Publishing Co. (1975)

[88] Jia, H., Lalande, F., Ellis, R., and Rogers, C. A., "Impact energy absorption of shape memory alloy hybrid composite beams", 38th AIAA/ASME/ASCE/AHS/ASC Structures, Structural Dynamics, and Materials Conference, pp.917-926, April 7-10, 1997, Orlando, Florida.

[89] Timoshenko, S. P. and Gere J. M., "*Mechanics of Materials*," D. Van Nostrand Company (1972).

[90] Wang, C. M., "Timoshenko beam-bending solutions in terms of Euler-Bernoulli solutions," *Journal of Engineering Mechanics*, June (1995), pp. 763-765.

[91] Zukas, J. A., Nicholas, T., Swift, H. F., Greszczuk, L. B. and Curran, D. R., "*Impact Dynamics*," John Wiley & Sons (1982).

[92] Shivakumar, K. N., and Elber, W., and Illg, W., "Prediction of impact force and

duration due to low-velocity impact on circular composite laminates," *Journal of Applied Mechanics*, Vol. 52, September (1985), pp. 674-680.

[93] Cantwell, W. J. and Morton, J., "The impact resistance of composite materials-A review," *Composites*, V.22, No.5 (1991), pp.347-362.

[94] Lagace, P. A. and Wolf, E., "Impact damage resistance of several laminated material systems," *Proceedings of the Structural Dynamics and Materials Conference*, AIAA-93-1524-cp (1993), pp. 1863-1872.

[95] Talreja, R., "Transverse cracking and stiffness reduction in composite laminates," *Journal of Composite Materials*, V. 19 (1985), pp.355-375.

[96] Williams, J. G., and Rhodes, M. D., "Effects of resins on impact damage tolerance of graphite/epoxy laminates", *ASTM STP 787* (1982), 450.

[97] Jia, H, Lalande, F., and Rogers, C. A., " Failure analysis of graphite/bismaleimide composite beam under impact by a steel cylinder", Presented in The 3rd Army Research Office Workshop on Smart Structures, August 27-29, 1997, Blacksburg, Virginia.

[98] Kiesling, T. C., "Impact failure modes of graphite epoxy composites with embedded superelastic Nitinol," Master Thesis, Virginia Tech, 1995.

[99] Liu, S., Kutlu, Z., and Chang, F. K., "Matrix cracking and delamination in lamianted polymeric composite resulting from transversely concentrated loadings," *Proceedings of the 1st International Conference on Deformation and Fracture of Composites*, Manchester, England, March 25-27, (1991), pp. 30/1-30/7.

[100] Lo, D. C., Costanzo, F., Zocher, M. A, and Allen, D. H., "Modeling of damage evolution in thick laminates subjected to low velocity impact," AMD v. 162, *Mechanics of thick composite*, ASME (1993), pp. 137-150.

[101] Highsmith, A. L. and Reifsnider, K. L., "Stiffness reduction mechanisms in composite laminates," *Damage in Composite Materials*, ASTM STP 775 (1982), ed. by Reifsnider, K. L., American Society for Testing and Materials, pp.103-117.

[102] Goldsmith, W. , *Impact, the Theory and Physical Behavior of Colliding Solids*. London: Edward Arnold Ltd., (1960) pp. 88.

[103] Ursenbach, D. O., Vaziri, R. and Delfosse, D., "An engineering model for deformation of CFRP plates during penetration, " *Composite Structures*, v. 32, n 1-4, (1995), pp. 197-202.

[104] Tsai, S. W., "Strength theories of filamentary structures", in Schwartz, R. T. and Schwart, H. S. (eds.), "Fundamental Aspects of Fiber Reinforced Plastic Composites," Wiley Interscience, New York, 1968, pp. 3-11.

[105] Tsai, S. W., and Wu, E. M., "A general theory of strength for anisotropic materials", Journal of Composite Materials, January, 1971, pp. 58-80.

[106] Vinson, J. R. and Zukas, J. A. , "On the ballistic impact of textile body armor," *Journal of Applied .Mechanics*, June (1975), pp. 263-268.

[107] Nielsen, M.P., *Limit analysis and concrete plasticity*, (1984), Prentice-Hall, Inc.

[108] Kamenjarzh, J. A., "*Limit Analysis of Solids and Structures*," CRC Press (1996).

[109] Hashin, Z., "Analysis of cracked laminates: A variational approach," *Mechanics of Materials*, V.4 (1985), pp. 121-136.

[110] Laws, N. and Dvorak, G. J., "Progressive transverse cracking in composite laminates," *Journal of Composite Materials*, V. 22 (1985), pp. 900-916.

[111] Jenq, S. T., Jing, H. S., and Chang, C, "Predicting the ballistic limit for plain woven glasss/epoxy composite laminate", *International Journal of Impact Engineering*, Vol. 15, No. 4 (1994), pp. 451-464.

[112] Johnson, P., and Chang, F. K., "Accumulated damage and failure of finite-width composite laminates", AIAA-96-1356-CP., pp. 356-365.

APPENDIX A

C++ Code for SMA Graphite/Bis Composite Beam Under Quasi-Static Loading

```
////////////////////////////////////////////////////////////////////////////////
//
// This code for computing the cylinder impact of SMA
// composite with SMA fibers underneath the top ply
// (impacted side).
//
// Comparison with experiment.
//
// Author:  Hongyu Jia
//
// Version: 1.0
//
// Date:    December, 1997.
//
////////////////////////////////////////////////////////////////////////////////


#include <iostream.h>

#include <fstream.h>

#include <math.h>

#include <iomanip.h>


const double C1 = 15.3;

const double C2 = 14.3;

const double L = 2.0;

const double z = 0.024;

const double Ksma = 0.138;

const double Km = 0.862;

const double Em = 0.5e6;

const double Esma_a = 11.85928e6;
```

```
const double Esma_m = 0.16008e6;
double Strain(double, double);
double Force(double, double);
void print(double, double, double, double, ofstream&);
double B_Effect(double);
double A11_a(double);
double F1(double);
double B11_a(double);
double F2(double);
double D11_a(double);
double F3(double);
double A11_m(double);
double B11_m(double);
double D11_m(double);
double Q11_25a(double);
double Q11_1a(double);
double T_Effect(double);
double Q11_25m(double);
double Q11_1m(double);
int main()
{
```

```
ofstream outStream;
outStream.open("Out.File");
double w0;
const double d1 = 0.001;
double Epx;
double x;
w0 = 0;
outStream<<setw(15)<<"w0,Deflection"
                <<setw(15)<<"P,Force"
                        <<setw(15)<<"Epx,Strain"
                        <<setw(15)<<"x,Coordinate"
                        <<endl;

while (w0 <= 0.333)
{
        double P;
  const double d2 = 0.1;
        x=-2.0;
        Epx = Strain(w0,x);
        cout<<"Epx0="<<Epx<<endl;
        while (x < -0.0001 && Epx <= 0.0065)
```

```
        {
                x = x+d2;

                Epx = Strain(w0,x);

           cout<<"Epx="<<Epx<<endl;

        }


        P = Force(w0, x);

        print(w0, P, Epx, x, outStream);

        w0 = w0 + d1;

        cout<<"w0="<<w0<<endl;

   }

  outStream.close();

  return 0;

}


double Strain(double w0, double x)

{
  double S;

  double f1;

  f1 = 3*x*x/(L*L*L)-C1/L;

  S = w0*w0*f1*f1/(2*C2*C2)-z*6*x*w0/(C2*L*L*L);

  return S;

}
```

```
double Force(double w0, double x)
{
  double G;
  double Ga;
  double Gm;
  Ga = -B_Effect(w0)*w0*w0*w0*A11_a(w0)*(F1(-L)-F1(x))
            /pow(C2,4)+3*B_Effect(w0)*w0*w0*B11_a(w0)*
            (F2(-L)-F2(x))/pow(C2,3)-2*B_Effect(w0)*w0*w0*
            D11_a(w0)*(F3(-L)-F3(x))/(C2*C2);
  Gm = -B_Effect(w0)*w0*w0*w0*A11_m(w0)*(F1(x)-F1(0))
            /pow(C2,4)+3*B_Effect(w0)*w0*w0*B11_m(w0)*
            (F2(x)-F2(0))/(C2*C2*C2)-2*B_Effect(w0)*w0*w0*
            D11_m(w0)*(F3(x)-F3(0))/(C2*C2);
  G = Ga+Gm;
  return G;
}

double B_Effect(double w0)
{
  double B;
  const double b0 = 0.75;
  const double w0_max = 0.333;
```

```
 B = -w0*0.3*b0/w0_max + b0;
 return B;
}

double A11_a(double w0)
{
 double Aa;
 Aa = (4*Q11_25a(w0)+Q11_1a(w0))*T_Effect(w0)/5.0;
 return Aa;
}
double F1(double x)
{
 double G1;
 G1 = 9*pow(x/L, 9)/pow(L, 3)+36*C1*C1*pow(x/L, 5)/
          (5*pow(L,3))+pow(C1/L,4)*x-108*C1*pow(x/L,7)/
          (7*pow(L,3))+18*C1*C1*pow(x/L,5)/(5*pow(L,3))
          -4*pow(C1/L,3)*pow(x/L,3);
 return G1;
}

double B11_a(double w0)
{
```

```
 double Ba;
 Ba = (Q11_25a(w0)-Q11_1a(w0))*pow(T_Effect(w0)/5, 2);
 return Ba;
}

double F2(double x)
{
 double G2;
 G2 = 6*(3*pow(x/L,6)/2-3*C1*pow(x/L,4)/2+C1*C1*
        pow(x/L,2)/2)/(pow(L,3));
 return G2;
}

double D11_a(double w0)
{
 double Da;
 Da = (28*Q11_25a(w0)+3.25*Q11_1a(w0))*
        pow(T_Effect(w0)/5,3)/3;
 return Da;
}

double F3(double x)
{
 double G3;
```

```
  G3 = 12*x*x*x/pow(L,6);
  return G3;
}

double A11_m(double w0)
{
  double Am;
  Am = (4*Q11_25m(w0)+Q11_1m(w0))*T_Effect(w0)/5;
  return Am;
}

double B11_m(double w0)
{
  double Bm;
  Bm = (Q11_25m(w0)-Q11_1m(w0))*pow(T_Effect(w0)/5,2);
return Bm;
}

double D11_m(double w0)
{
  double Dm;
  Dm = (28*Q11_25m(w0)+3.25*Q11_1m(w0))*pow(T_Effect(w0)
            /5, 3)/3;
return Dm;
```

```
}

double Q11_25a(double w0)

{
 double Q25a;

 const double E1_0 = 23.8e6;

 const double C = -3.0;

 Q25a = E1_0/(1-C*w0);

return Q25a;

}

double Q11_1a (double w0)

{

 double Q1a;

 const double C = -3.0;

 const double Ksma = 0.138;

 const double Km = 0.862;

 const double Em = 0.5e6;

 const double Esma_a = 11.85928e6;

 Q1a = (Ksma*Esma_a+Km*Em)/(1-C*w0);

 return Q1a;

}
```

```
double T_Effect(double w0)
{
  double T;
  const double w0_max = 0.333;

  T = -0.018*w0/w0_max+ 0.048;
  return T;
}

double Q11_25m(double w0)
{
  double Q25m;
  const double E1_0 = 23.8e6;
  const double C = -3.0;
  Q25m = E1_0/(1-C*w0);
  return Q25m;
}

double Q11_1m(double w0)
{
  double Q1m;
  const double C = -3.0;
  const double Ksma = 0.138;
```

```
  const double Km = 0.862;
  const double Em = 0.5e6;
  const double Esma_m = 0.16008e6;
  Q1m = (Ksma*Esma_m+Km*Em)/(1-C*w0);
  return Q1m;
}

void print (double w0,
                        double P,
                        double Epx,
                        double x,
                        ofstream& outStream)
{
        outStream<<setw(15)<<setprecision(4)<<w0
                    <<setw(15)<<setprecision(4)<<P
         <<setw(15)<<setprecision(4)<<Epx;
                        if(x > -1.0e-010){
                                x = 0;
                        }
         outStream << setw(15) << setprecision(4) << x << endl;
  }
```

APPENDIX B

C++ Code for Graphite/Bis Composite Beam Under Quasi-Static Loading

```
////////////////////////////////////////////////////////////////////////////
//
// This code for computing the cylinder impact of
// composite without SMA fibers.
//
// Comparison with experiment.
//
// Author:  Hongyu Jia
//
// Version: 1.0
//
// Date:    September, 1997.
////////////////////////////////////////////////////////////////////////////


#include <iostream.h>

#include <fstream.h>

#include <math.h>

#include <iomanip.h>


const double C1 = 15.3;

const double C2 = 14.3;

const double L = 2.0;

const double z = 0.024;

double Strain(double, double);

double Force(double, double);

void print(double, double, double, double, ofstream&);

double B_Effect(double);

double A11_a(double);
```

```
double F1(double);
double B11_a(double);
double F2(double);
double D11_a(double);
double F3(double);
double A11_m(double);
double B11_m(double);
double D11_m(double);
double Q11_25a(double);
double T_Effect(double);
double Q11_25m(double);

int main()
{
  ofstream outStream;
  outStream.open("Out.File");
  double w0;
  const double d1 = 0.001;
  double Epx;
  double x;
  w0 = 0;
```

```
outStream<<setw(15)<<"w0,Deflection"
                <<setw(15)<<"P,Force"
                        <<endl;

while (w0 <= 0.333)
{
        double P;
 const double d2 = 0.1;
        x=-2.0;
        Epx = Strain(w0,x);
        cout<<"Epx0="<<Epx<<endl;
        while (x < -0.0001 && Epx <= 0.0065)
        {
                x = x+d2;
                Epx = Strain(w0,x);
           cout<<"Epx="<<Epx<<endl;
        }

         P = Force(w0, x);
         print(w0, P, Epx, x, outStream);
         w0 = w0 + d1;
         cout<<"w0="<<w0<<endl;
 }
```

```
 outStream.close();
 return 0;
}


double Strain(double w0, double x)
{
 double S;
 double f1;
 f1 = 3*x*x/(L*L*L)-C1/L;
 S = w0*w0*f1*f1/(2*C2*C2)-z*6*x*w0/(C2*L*L*L);
 return S;
}


double Force(double w0, double x)
{
 double G;
 double Ga;
 double Gm;
 Ga = -B_Effect(w0)*w0*w0*w0*A11_a(w0)*(F1(-L)-F1(x))
          /pow(C2,4)+3*B_Effect(w0)*w0*w0*B11_a(w0)*
          (F2(-L)-F2(x))/pow(C2,3)-2*B_Effect(w0)*w0*w0*
```

```
            D11_a(w0)*(F3(-L)-F3(x))/(C2*C2);
  Gm = -B_Effect(w0)*w0*w0*w0*A11_m(w0)*(F1(x)-F1(0))
            /pow(C2,4)+3*B_Effect(w0)*w0*w0*B11_m(w0)*
            (F2(x)-F2(0))/(C2*C2*C2)-2*B_Effect(w0)*w0*w0*
            D11_m(w0)*(F3(x)-F3(0))/(C2*C2);
  G = Ga+Gm;
  return G;
}
double B_Effect(double w0)
{
  double B;
  const double b0 = 0.75;
  const double w0_max = 0.333;

  B = -w0*0.3*b0/w0_max + b0;
  return B;
}

double A11_a(double w0)
{
  double Aa;
  Aa = (4*Q11_25a(w0))*T_Effect(w0)/4.0;
```

```
 return Aa;
}

double F1(double x)
{
 double G1;
 G1 = 9*pow(x/L, 9)/pow(L, 3)+36*C1*C1*pow(x/L, 5)/
          (5*pow(L,3))+pow(C1/L,4)*x-108*C1*pow(x/L,7)/
          (7*pow(L,3))+18*C1*C1*pow(x/L,5)/(5*pow(L,3))
          -4*pow(C1/L,3)*pow(x/L,3);
 return G1;
}

double B11_a(double w0)
{
 double Ba;
 Ba = 0;
 return Ba;
}

double F2(double x)
{
```

```
 double G2;
 G2 = 6*(3*pow(x/L,6)/2-3*C1*pow(x/L,4)/2+C1*C1*
          pow(x/L,2)/2)/(pow(L,3));
 return G2;
}

double D11_a(double w0)
{
 double Da;
 Da = (16*Q11_25a(w0))*
          pow(T_Effect(w0)/4,3)/3;
 return Da;
}

double F3(double x)
{
 double G3;
 G3 = 12*x*x*x/pow(L,6);
 return G3;
}

double A11_m(double w0)
```

```
{
 double Am;

 Am = (4*Q11_25m(w0))*T_Effect(w0)/4;

 return Am;

}


double B11_m(double w0)

{
 double Bm;

 Bm = 0;

return Bm;

}


double D11_m(double w0)

{
 double Dm;

 Dm = (16*Q11_25m(w0))*pow(T_Effect(w0)

          /4, 3)/3;

return Dm;

}


double Q11_25a(double w0)
```

```
{
 double Q25a;
 const double E1_0 = 23.8e6;
 const double C = -3.0;
 Q25a = E1_0/(1-C*w0);
return Q25a;
}

double T_Effect(double w0)
{
 double T;
 const double w0_max = 0.333;

 T = -2*0.012*w0/w0_max+ 0.048;
 return T;
}

double Q11_25m(double w0)
{
 double Q25m;
 const double E1_0 = 23.8e6;
 const double C = -3.0;
```

```
  Q25m = E1_0/(1-C*w0);
  return Q25m;
}


void print (double w0,
                        double P,
                        double Epx,
                        double x,
                        ofstream& outStream)
{
        outStream<<setw(15)<<setprecision(4)<<w0
                <<setw(15)<<setprecision(4)<<P << endl;


}
```

APPENDIX C

Sensitivity Study of Width Degradation Factor

Graphite/Bis composite beam under cylinder loading
Sensitivity study of width degradation factor

Degradation factor	Maxim load (lb)	Error (%)
0.35	655.8	-6.3
0.34	665.8	-4.8
0.33	675.9	-3.4
0.32	685.9	-2
0.31	696	-0.5
0.3	706	0.8
0.29	716	2.3
0.28	726.1	3.7
0.27	736.1	5.2
0.26	746.2	6.6

SMA graphite/Bis composite beam under cylinder loading
Sensitivity study of width degradation factor

Degradation factor	Maxim load (lb)	Error (%)
0.28	730.5	2.9
0.29	720.4	1.7
0.3	710.3	0.04
0.31	700.2	-1.4
0.32	690.1	-2.8
0.33	680	-4.2
0.34	669.9	-5.6
0.35	659.8	-7.1

APPENDIX D

Output File of SMA Graphite/Bis Composite Beam Under Quasi-Static Loading

w0,Deflection	P,Force	Epx,Strain	x,Coordinate
0	0	0	0
0.001	0.0002011	1.431e-007	0
0.002	0.001154	5.724e-007	0
0.003	0.003377	1.288e-006	0
0.004	0.007376	2.29e-006	0
0.005	0.01365	3.577e-006	0
0.006	0.02268	5.151e-006	0
0.007	0.03494	7.012e-006	0
0.008	0.05091	9.158e-006	0
0.009	0.07104	1.159e-005	0
0.01	0.09578	1.431e-005	0
0.011	0.1256	1.731e-005	0
0.012	0.1608	2.061e-005	0
0.013	0.202	2.418e-005	0
0.014	0.2494	2.805e-005	0
0.015	0.3036	3.22e-005	0
0.016	0.3649	3.663e-005	0
0.017	0.4336	4.135e-005	0
0.018	0.5102	4.636e-005	0
0.019	0.5951	5.166e-005	0
0.02	0.6886	5.724e-005	0
0.021	0.791	6.31e-005	0
0.022	0.9026	6.926e-005	0
0.023	1.024	7.57e-005	0
0.024	1.155	8.242e-005	0
0.025	1.297	8.943e-005	0
0.026	1.449	9.673e-005	0
0.027	1.612	0.0001043	0
0.028	1.786	0.0001122	0
0.029	1.972	0.0001203	0
0.03	2.17	0.0001288	0
0.031	2.379	0.0001375	0
0.032	2.601	0.0001465	0
0.033	2.836	0.0001558	0
0.034	3.083	0.0001654	0
0.035	3.344	0.0001753	0
0.036	3.618	0.0001854	0
0.037	3.905	0.0001959	0
0.038	4.206	0.0002066	0
0.039	4.522	0.0002176	0
0.04	4.852	0.000229	0
0.041	5.196	0.0002405	0
0.042	5.555	0.0002524	0
0.043	5.929	0.0002646	0
0.044	6.318	0.000277	0
0.045	6.722	0.0002898	0
0.046	7.142	0.0003028	0
0.047	7.577	0.0003161	0
0.048	8.028	0.0003297	0
0.049	8.496	0.0003436	0
0.05	8.979	0.0003577	0
0.051	9.479	0.0003722	0
0.052	9.996	0.0003869	0
0.053	10.53	0.000402	0
0.054	11.08	0.0004173	0
0.055	11.65	0.0004329	0

0.056	12.23	0.0004487	0
0.057	12.83	0.0004649	0
0.058	13.45	0.0004814	0
0.059	14.09	0.0004981	0
0.06	14.74	0.0005151	0
0.061	15.41	0.0005325	0
0.062	16.1	0.0005501	0
0.063	16.81	0.0005679	0
0.064	17.53	0.0005861	0
0.065	18.28	0.0006046	0
0.066	19.04	0.0006233	0
0.067	19.82	0.0006423	0
0.068	20.62	0.0006617	0
0.069	21.43	0.0006813	0
0.07	22.27	0.0007012	0
0.071	23.12	0.0007213	0
0.072	24	0.0007418	0
0.073	24.89	0.0007625	0
0.074	25.8	0.0007836	0
0.075	26.73	0.0008049	0
0.076	27.68	0.0008265	0
0.077	28.65	0.0008484	0
0.078	29.63	0.0008706	0
0.079	30.64	0.000893	0
0.08	31.66	0.0009158	0
0.081	32.71	0.0009388	0
0.082	33.77	0.0009622	0
0.083	34.85	0.0009858	0
0.084	35.96	0.00101	0
0.085	37.08	0.001034	0
0.086	38.22	0.001058	0
0.087	39.38	0.001083	0
0.088	40.56	0.001108	0
0.089	41.76	0.001133	0
0.09	42.98	0.001159	0
0.091	44.22	0.001185	0
0.092	45.47	0.001211	0
0.093	46.75	0.001238	0
0.094	48.05	0.001264	0
0.095	49.36	0.001291	0
0.096	50.7	0.001319	0
0.097	52.05	0.001346	0
0.098	53.43	0.001374	0
0.099	54.82	0.001402	0
0.1	56.24	0.001431	0
0.101	57.67	0.00146	0
0.102	59.12	0.001489	0
0.103	60.59	0.001518	0
0.104	62.08	0.001548	0
0.105	63.6	0.001578	0
0.106	65.13	0.001608	0
0.107	66.67	0.001638	0
0.108	68.24	0.001669	0
0.109	69.83	0.0017	0
0.11	71.44	0.001731	0
0.111	73.06	0.001763	0
0.112	74.71	0.001795	0

0.113	76.37	0.001827	0
0.114	78.06	0.00186	0
0.115	79.76	0.001892	0
0.116	81.48	0.001925	0
0.117	83.22	0.001959	0
0.118	84.98	0.001992	0
0.119	86.76	0.002026	0
0.12	88.55	0.002061	0
0.121	90.37	0.002095	0
0.122	92.2	0.00213	0
0.123	94.06	0.002165	0
0.124	95.93	0.0022	0
0.125	97.82	0.002236	0
0.126	99.73	0.002272	0
0.127	101.7	0.002308	0
0.128	103.6	0.002344	0
0.129	105.6	0.002381	0
0.13	107.5	0.002418	0
0.131	109.5	0.002456	0
0.132	111.6	0.002493	0
0.133	113.6	0.002531	0
0.134	115.6	0.002569	0
0.135	117.7	0.002608	0
0.136	119.8	0.002647	0
0.137	121.9	0.002686	0
0.138	124	0.002725	0
0.139	126.2	0.002765	0
0.14	128.3	0.002805	0
0.141	130.5	0.002845	0
0.142	132.7	0.002885	0
0.143	134.9	0.002926	0
0.144	137.1	0.002967	0
0.145	139.4	0.003009	0
0.146	141.6	0.00305	0
0.147	143.9	0.003092	0
0.148	146.2	0.003134	0
0.149	148.5	0.003177	0
0.15	150.8	0.00322	0
0.151	153.2	0.003263	0
0.152	155.6	0.003306	0
0.153	157.9	0.00335	0
0.154	160.3	0.003394	0
0.155	162.7	0.003438	0
0.156	165.1	0.003482	0
0.157	167.6	0.003527	0
0.158	170	0.003572	0
0.159	172.5	0.003618	0
0.16	175	0.003663	0
0.161	177.5	0.003709	0
0.162	180	0.003755	0
0.163	182.5	0.003802	0
0.164	185.1	0.003849	0
0.165	187.7	0.003896	0
0.166	190.2	0.003943	0
0.167	192.8	0.003991	0
0.168	195.4	0.004039	0
0.169	198	0.004087	0

0.17	200.7	0.004135	0
0.171	203.3	0.004184	0
0.172	206	0.004233	0
0.173	208.7	0.004283	0
0.174	211.4	0.004332	0
0.175	214.1	0.004382	0
0.176	216.8	0.004432	0
0.177	219.5	0.004483	0
0.178	222.3	0.004534	0
0.179	225	0.004585	0
0.18	227.8	0.004636	0
0.181	230.6	0.004688	0
0.182	233.4	0.00474	0
0.183	236.2	0.004792	0
0.184	239	0.004845	0
0.185	241.8	0.004897	0
0.186	244.7	0.00495	0
0.187	247.5	0.005004	0
0.188	250.4	0.005058	0
0.189	253.3	0.005111	0
0.19	256.2	0.005166	0
0.191	259.1	0.00522	0
0.192	262	0.005275	0
0.193	264.9	0.00533	0
0.194	267.9	0.005385	0
0.195	270.8	0.005441	0
0.196	273.8	0.005497	0
0.197	276.8	0.005553	0
0.198	279.8	0.00561	0
0.199	282.8	0.005667	0
0.2	285.8	0.005724	0
0.201	288.8	0.005781	0
0.202	291.8	0.005839	0
0.203	294.8	0.005897	0
0.204	297.9	0.005955	0
0.205	300.9	0.006014	0
0.206	304	0.006072	0
0.207	307.1	0.006131	0
0.208	310.2	0.006191	0
0.209	313.3	0.00625	0
0.21	316.4	0.00631	0
0.211	319.5	0.006371	0
0.212	322.6	0.006431	0
0.213	324.7	0.006515	-0.3
0.214	327.2	0.006528	-0.5
0.215	330	0.006545	-0.6
0.216	332.8	0.00655	-0.7
0.217	335.6	0.006541	-0.8
0.218	338.5	0.006518	-0.9
0.219	341.6	0.006577	-0.9
0.22	344.5	0.00654	-1
0.221	347.7	0.006599	-1
0.222	350.5	0.006548	-1.1
0.223	353.7	0.006606	-1.1
0.224	356.6	0.00654	-1.2
0.225	359.8	0.006597	-1.2
0.226	362.7	0.006518	-1.3

0.227	365.9	0.006574	-1.3
0.228	369.2	0.00663	-1.3
0.229	372.1	0.006535	-1.4
0.23	375.3	0.00659	-1.4
0.231	378.5	0.006646	-1.4
0.232	381.5	0.006535	-1.5
0.233	384.8	0.006589	-1.5
0.234	388	0.006644	-1.5
0.235	391	0.006517	-1.6
0.236	394.3	0.00657	-1.6
0.237	397.5	0.006624	-1.6
0.238	400.8	0.006678	-1.6
0.239	403.8	0.006533	-1.7
0.24	407.1	0.006586	-1.7
0.241	410.3	0.006639	-1.7
0.242	413.6	0.006692	-1.7
0.243	416.7	0.006529	-1.8
0.244	420	0.006581	-1.8
0.245	423.3	0.006633	-1.8
0.246	426.6	0.006685	-1.8
0.247	429.7	0.006504	-1.9
0.248	433	0.006555	-1.9
0.249	436.3	0.006605	-1.9
0.25	439.6	0.006656	-1.9
0.251	442.9	0.006707	-1.9
0.252	446	0.006507	-2
0.253	449.3	0.006556	-2
0.254	452.6	0.006606	-2
0.255	456	0.006655	-2
0.256	459.3	0.006705	-2
0.257	462.6	0.006755	-2
0.258	466	0.006805	-2
0.259	469.3	0.006856	-2
0.26	472.6	0.006906	-2
0.261	476	0.006957	-2
0.262	479.3	0.007008	-2
0.263	482.7	0.007059	-2
0.264	486	0.00711	-2
0.265	489.3	0.007162	-2
0.266	492.7	0.007213	-2
0.267	496	0.007265	-2
0.268	499.4	0.007317	-2
0.269	502.7	0.007369	-2
0.27	506.1	0.007422	-2
0.271	509.5	0.007474	-2
0.272	512.8	0.007527	-2
0.273	516.2	0.00758	-2
0.274	519.5	0.007633	-2
0.275	522.9	0.007686	-2
0.276	526.2	0.00774	-2
0.277	529.6	0.007793	-2
0.278	532.9	0.007847	-2
0.279	536.3	0.007901	-2
0.28	539.7	0.007955	-2
0.281	543	0.00801	-2
0.282	546.4	0.008064	-2
0.283	549.7	0.008119	-2

0.284	553.1	0.008174	-2
0.285	556.4	0.008229	-2
0.286	559.8	0.008285	-2
0.287	563.1	0.00834	-2
0.288	566.5	0.008396	-2
0.289	569.8	0.008452	-2
0.29	573.2	0.008508	-2
0.291	576.5	0.008564	-2
0.292	579.8	0.00862	-2
0.293	583.2	0.008677	-2
0.294	586.5	0.008734	-2
0.295	589.8	0.008791	-2
0.296	593.2	0.008848	-2
0.297	596.5	0.008905	-2
0.298	599.8	0.008963	-2
0.299	603.1	0.009021	-2
0.3	606.5	0.009078	-2
0.301	609.8	0.009137	-2
0.302	613.1	0.009195	-2
0.303	616.4	0.009253	-2
0.304	619.7	0.009312	-2
0.305	623	0.009371	-2
0.306	626.3	0.00943	-2
0.307	629.6	0.009489	-2
0.308	632.9	0.009548	-2
0.309	636.2	0.009608	-2
0.31	639.5	0.009668	-2
0.311	642.7	0.009728	-2
0.312	646	0.009788	-2
0.313	649.3	0.009848	-2
0.314	652.5	0.009909	-2
0.315	655.8	0.009969	-2
0.316	659.1	0.01003	-2
0.317	662.3	0.01009	-2
0.318	665.6	0.01015	-2
0.319	668.8	0.01021	-2
0.32	672	0.01028	-2
0.321	675.2	0.01034	-2
0.322	678.5	0.0104	-2
0.323	681.7	0.01046	-2
0.324	684.9	0.01052	-2
0.325	688.1	0.01059	-2
0.326	691.3	0.01065	-2
0.327	694.5	0.01071	-2
0.328	697.7	0.01078	-2
0.329	700.8	0.01084	-2
0.33	704	0.0109	-2
0.331	707.2	0.01097	-2
0.332	710.3	0.01103	-2

VITA

Hongyu Jia was born in Jinna, Shandong, China on April 9, 1963. He graduated from the First High School in Xiangfan, Hubei in 1981. He graduated in 1985 with a BS degree in Railway Vehicle Manufacturing from Dalian Institute of Railway Technology in Dalian, Liaoning. In 1988, he obtained his MS degree in Solid Mechanics from Dalian University of Technology with research area in Mechanics of Composite Materials. His Master Thesis was "Analysis of Nonlinear Dynamic Buckling of Composite Plates". Upon his graduation, he began his career at the Institute of Computer Science and Mechanics in Mechanical Engineering Department, Dalian University. As a lecturer, he taught undergraduate classes and supervised senior undergraduate design projects. He participated in the research in nonlinear buckling of composite shell structures and offshore oil pipelines. At the beginning of 1992, he started to pursue his Ph.D. study at University of Central Florida in the United States. In 1995, he decided to pursue his Ph.D. study in novel area of smart materials and composites. After obtaining admissions to Pennsylvania State University, Rensselaer Polytechnic Institute, Stanford University, and Virginia Polytechnic Institute and State University (Virginia Tech), he decided to study smart materials and composite structures in Mechanical Engineering Department at Virginia Tech in August, 1995. He obtained a Ph.D. in Mechanical Engineering in May, 1998.